BRNO UNIVERSITY OF TECHNOLOGY

VYSOKÉ UČENÍ TECHNICKÉ V BRNĚ

FACULTY OF MECHANICAL ENGINEERING

FAKULTA STROJNÍHO INŽENÝRSTVÍ

INSTITUTE OF SOLID MECHANICS, MECHATRONICS AND BIOMECHANICS

ÚSTAV MECHANIKY TĚLES, MECHATRONIKY A BIOMECHANIKY

ANALYSIS OF INFLUENCE OF BLOOD FLOW AND ARTERIAL GEOMETRY ON PATHOLOGICAL PROCESSES IN ARTERIES

ANALÝZA VLIVU PROUDĚNÍ KRVE A GEOMETRICKÉHO USPOŘÁDÁNÍ NA PATOLOGICKÉ PROCESY V TEPNÁCH

DOCTORAL THESIS

DIZERTAČNÍ PRÁCE

AUTHOR — Ing. Jiří Jagoš

AUTOR PRÁCE

SUPERVISOR — prof. Ing. Jiří Burša, Ph.D.

ŠKOLITEL

BRNO 2023

Abstract

An occurrence of cardiovascular diseases is rising together with increasing average life expectancy as well as to an unhealthy lifestyle. Since the most of these diseases are asymptomatic, a great effort has been devoted to early detection of these diseases because if they are detected in early phase, a conservative treatment can be an option. If not, a highly invasive and risky surgery is usually the only option. We can still observe a very large portion of patients in the risk group to whom the disease does not develop, and, on the contrary, in many patients who are not in the risk group, it does. Computational modelling of cardiovascular system is one of the options, which can help with stratification of the patients that are at risk of developing cardiovascular diseases.

Firstly, a successful validation of the numerical model of pulsatile flow in the rigid and compliant tubes via velocity profiles was performed. Experiment circuit was arranged to correspond conditions in the human aorta.

Next part is devoted to proper treatment of boundary conditions (BCs) for numerical model of pulsatile flow in human arteries. The first approach works with pulse wave velocity which needs to be computed first. Then, a shift between input and outputs BCs can be determined easily. Nevertheless, we have to prescribe also flow or pressure waveforms for each inlet and outlet. Thus, the predictive capabilities of this approach are significantly limited. Its next disadvantage is applicability only for simulations considering compliance of the vessel wall. We used this approach in fluid-structure interaction simulations to check the potential risk factor of the aorto-iliac angle on development of an aneurysm in the abdominal aorta (AAA). It has been shown that the pressure increases due to a large (but still physiological) span of the aorto-iliac angles is negligible. We also investigated the influence of the area ratio on pressure in the abdominal aorta. The results of this computational study show a substantial increase in pressure as the ratio decreases and confirms clinical observations showing significantly elevated risk of AAA in patients with lower limp amputation or those with iliac artery stenosis.

In the final part we have investigated the effect of a flow waveform shape in the human carotid artery on the risk of atherosclerosis. The five geometrically different geometries of the carotid bifurcation from “healthy” old individuals were reconstructed. The representative input flow BCs in the common carotid artery for the young and old individual were adopted from a literature. The outputs BCs for the internal and external carotid artery were represented by three-element Windkessel model. The parameters of the Windkessel model were iteratively tuned to reach flow waveform shape in internal carotid artery according to literature. These BCs represent the behaviour of the periphery very reliably. Moreover, the predictive capabilities and numerical stability of this approach are much better than the first approach. The results show that the time average wall shear stress decreases significantly in case of healthy elderly subjects in comparison to young ones which indicates elevated risk of atherosclerosis. The results are in agreement with clinical observations and further extend the existing knowledge with a much deeper analysis of this trend. The final discussion is devoted to a potential benefits of an antihypertensives and regular physical activity.

Keywords

Computational fluid dynamics, Fluid-structure interaction, Blood flow in arteries, Risk factors, Atherosclerosis, Aneurysms

Abstrakt

Se zvyšující se průměrnou délkou života a nezdravým životním stylem se velmi úzce pojí zvýšený výskyt kardiovaskulárních chorob. Většina z těchto nemocí je asymptomatických. Je zde tedy velká snaha rozpoznat tato onemocnění časně, dokud je možné je léčit konzervativně pomocí změny životního stylu či různých léků. Pokud se nemoc objeví až v pozdním stádiu, je nutná často velmi riziková operace. Stále se velmi často stává, že u pacienta v rizikové skupině se kardiovaskulární choroba nerozvine, a naopak u toho, který v rizikové skupině dle stávajících kritérií není, ano. Výpočtové modelování kardiovaskulárního systému je jedním z mnoha způsobů, které mohou pomoci se sofistikovanější indikací osob, u kterých je zvýšené riziko vývoje těchto chorob.

V práci byly nejprve úspěšně validovány výsledky numerického modelu pulzujícího proudění v tuhé a elastické trubici skrze rychlostní profily. Podmínky experimentu byly záměrně voleny tak, aby byly blízké podmínkám v lidské aortě.

Další část práce je věnována výběru a implementaci okrajových podmínek pro numerické modely pulzujícího proudění v lidských tepnách. První přístup pomocí určení rychlosti šíření pulzní vlny v tepně a následné časové korekci mezi vstupní a výstupní okrajovou podmínkou je poměrně jednoduchý, nicméně přímo předepisuje tvaru tlakové nebo průtokové vlny pro každý vstup a výstup z modelu a jeho prediktivní vlastnosti jsou tímto výrazně omezené. Jeho další nevýhodou je aplikovatelnost pouze pro simulace proudění, které uvažují poddajnost stěny. V případě simulace proudění s tuhou stěnou časovou korekci vstupní a výstupní okrajové podmínky nelze provést. Zde v práci byl tento přístup využitý v simulacích, které uvažují vzájemnou interakci stěny tepny s kapalinou, při prověřování potenciálního rizikového faktoru úhlu ilických tepen na rozvoj aneurysmatu abdominální aorty (AAA). Ukázalo se, že pro velký (ale stále fyziologický) rozsah úhlu ilických tepen nedochází ke zvýšení tlaku v aortě. Dále byl prověřen vliv poměru průřezů ilických tepen vůči průřezu aorty, u kterého se prokázal výrazný vliv na zvýšení tlaku v aortě. Výsledky jsou v souladu s klinickým pozorováním, které ukazují, že lidé po amputaci dolní končetiny, nebo lidé se stenózou v ilické tepně mají významně zvýšené riziko vzniku AAA.

V závěrečné části byl zkoumán vliv tvaru průtokové vlny v lidské karotidě na vznik aterosklerózy. Bylo zrekonstruováno pět geometricky odlišných karotických bifurkací ze „zdravých“ starších pacientů. Reprezentativní vstupní okrajové podmínky průtoků pro staršího i mladého jedince byly převzaty z literatury. Výstupní okrajové podmínky pro interní a externí karotidu byly reprezentovány tří parametrickým Windkessel modelem. Parametry Windkessel modelu byly iteračním postupem odladěny tak, aby průběh průtokové vlny v interně byl v souladu s průběhem v literatuře. Tyto okrajové podmínky vystihují chování periferie velmi věrohodně. Navíc vykazují výrazně vyšší numerickou stabilitu a predikční vlastnosti než prvně zmíněný přístup. Analýzou výsledků bylo zjištěno že proudění v karotidě u zdravé starší osoby vykazuje výrazné snížení časově průměrovaného smykového napětí na stěně tepny vůči osobě mladé, což indikuje zvýšené riziko vzniku aterosklerózy. Výsledky jsou v souladu s klinickým pozorováním a rozšiřují dosavadní znalosti o mnohem hlubší analýzu. Je zde také diskutován případný přínos antihypertenziv a pravidelného cvičení.

Klíčová slova

Výpočtová dynamika tekutin, Interakce těles s tekutinou, Proudění krve v tepnách, Rizikové faktory, Ateroskleróza, Aneurysma

JAGOŠ, Jiří. *Analýza vlivu proudění krve a geometrického uspořádání na patologické procesy v tepnách* [online]. Brno, 2023 [cit. 2023-07-25].
Dostupné z: https://www.vut.cz/studenti/zav-prace/detail/146611. Dizertační práce. Vysoké učení technické v Brně, Fakulta strojního inženýrství, Ústav mechaniky těles, mechatroniky a biomechaniky. Vedoucí práce Jiří Burša.

Prohlašuji, že jsem disertační práci *Analýza vlivu proudění krve a geometrického uspořádání na patologické procesy v tepnách* vypracoval samostatně pod vedením prof. Ing. Jiřího Burši, Ph.D., s použitím materiálů uvedených v seznamu literatury. Práce je psána v anglickém jazyce.

Ing. Jiří Jagoš

Rád bych poděkoval svému školiteli prof. Ing. Jiřímu Buršovi, Ph.D.za odborné vedení, rady a profesionální přístup během mého postgraduálního studia. Děkuji také lékařům z II. chirurgické kliniky bez jejichž pomoci by tato práce nebyla možná. Dále děkuji kolegům jak z ústavu mechaniky, tak z ústavu fluidního inženýrství, za odborné diskuze a rady.
Velmi děkuji svým rodičům za jejich podporu během studia a také mé ženě Barboře, která mi byla po celou dobu oporou.
Tato práce vznikla za podpory projektů Grantové Agentury České Republiky 18-13663S a 21-21935S.

Ing. Jiří Jagoš

Contents

List of abbreviations and symbols

a [-]	Womersley number
AA	Abdominal aorta
AAA	Abdominal aortic aneurysm
AR [-]	Aortic ratio
BC	Boundary condition
BL	Boundary layer
BMT	Best medical treatment
BP [mmHg]	Blood pressure
CA	Cerebral aneurysm
cBP [mmHg]	Central aortic blood pressure
CCA	Common carotid artery
CFD	Computational Fluid Dynamics
CLI	Critical limb ischemia
CVD	Cardiovascular disease
cfPWV [$m.s^{-1}$]	Carotid-femoral pulse wave velocity
CTA	Computed tomography angiography
DBP [mmHg]	Diastolic blood pressure
E_{inc} [Pa]	Incremental Young´s modulus of elasticity
ECA	External carotid artery
ECAP [Pa^{-1}]	Endothelial cell activation potential
ESC	European Society of Cardiology
EU	European union
FFR [-]	Flow fractional reserve
FSI	Fluid-Structure Interaction
MRI	Magnetic Resonance Imaging
ICA	Internal carotid artery
ISHY	Isolated systolic hypertension
ITKE [$m^2.s^{-2}$]	Integrated turbulent kinetic energy
n [-]	Power law index
OSI [-]	Oscillatory shear index
PDMS	Polydimethylsiloxane
PS	patient-specific
PIV	Particle image velocimetry
PWV [$m.s^{-1}$]	Pulse wave velocity
Re [-]	Reynolds number
RRT [Pa^{-1}]	Relative residence time
LDL	Low-density lipoproteins
SAH	subarachnoid hemorrhage
SBP [mmHg]	Systolic blood pressure
STL	stereolithography
t_0 [s]	Time constant
TKE [$m^2.s^{-2}$]	Turbulent kinetic energy
TAWSS [Pa]	Time-averaged wall shear stress
US	United States
WSS [Pa]	Wall shear stress
WSSG [$Pa.m^{-1}$]	Wall shear stress gradient
WHO	World health organization
μ [-]	Poisson number
η_0 [Pa.s]	Shear viscosities at zero strain rate
η_{inf} [Pa.s]	Shear viscosities at infinity strain rate
R_{CC} [$N.s.m^{-5}$]	resistance of the CCA segment
R_{IC} [$N.s.m^{-5}$]	resistance of the ICA segment
R_{EC} [$N.s.m^{-5}$]	resistance of the ECA segment
R_p^{IC} [$N.s.m^{-5}$]	characteristic impedance or proximal resistance at the ICA
R_p^{EC} [$N.s.m^{-5}$]	characteristic impedance or proximal resistance at the ECA
C_a^{IC} [$N^{-1}.m^5$]	compliance of a periphery downstream the ICA
C_a^{EC} [$N^{-1}.m^5$]	compliance of a periphery downstream the ECA
R_d^{IC} [$N.s.m^{-5}$]	resistance of a periphery downstream the ICA
R_d^{EC} [$N.s.m^{-5}$]	resistance of a periphery downstream the ECA
L_{CC} [$kg.m^{-4}$]	inductance represents the inertia of a blood within the CCA
L_{IC} [$kg.m^{-4}$]	inductance represents the inertia of a blood within the ICA
L_{EC} [$kg.m^{-4}$]	inductance represents the inertia of a blood within the ECA
2WK	Two-element Windkessel
3WK	Three-element Windkessel

1. Introduction - motivation of the research

... at the beginning a disease is easy to cure but difficult to diagnose; but as time passes, not having been treated or recognized at the outset, it becomes easy to diagnose but difficult to cure ...

Niccolo Machiavelli, *II Principe*, 1513

The first citation comes from a famous Italian philosopher, writer and especially a politician. Although it is several hundred years old, unfortunately, it is still true. Even in such fast-growing field as a medicine. Notwithstanding that humanity has almost eradicated some deadly diseases, others have arrived. Our body has a tremendous complexity together with a great subject-to-subject variability. Probably for these reasons, we have not been able to understand and consequently prevent all of the diseases yet. And in my opinion, it will be never possible. However, we can try to minimize their incidence, mortality or severity of their consequences and to prolong thus a life expectancy but, mainly, to ensure a dignified and active aging. According to a quite optimistic book written by a leading researcher in the field of aging, David A. Sinclair, we are going to reach the point in near future when not only life expectancy will be much longer, but also our good health will follow this trend [1]. This view can be supported by a fact that life expectancy has more than doubled in the last one hundred and fifty years [2]. However, this argument is misleading. When we take a closer look at the numbers, it can be seen that the main reason is not that a man has longer life but due to significantly lowered infant mortality during this period [3]. Finally, it should not be forgotten that we have the greatest degree of responsibility for our bodies.

A man is as old as his arteries.

Thomas Sydenham

The second quotation is from a prominent English physician from the second half of the 17th century and also very actual today. Life expectancy has more than doubled in the last one hundred and fifty years and the most common causes of death are so-called diseases of old age, *i.e.*, cardiovascular diseases [2][4]. Although the occurrence of these diseases is largely conditioned by genetics (*i.e.*, family history) and age, development of diseases of civilization (atherosclerosis, hypertension, overweight, diabetes mellitus, cancer, etc.) occurs often within individuals under 40 years of age. This assures us that we can largely contribute to the possible emergence or suppression of the development of the disease by ourselves. Most of these diseases of civilization, if not being directly cardiovascular diseases, represent their significant risk factors. A common feature of both types of these diseases is they have a significant effect on the degradation of arterial structure (either as a consequence or as a cause) and are often referred to as accelerated aging. On the other hand, regular exercise, healthy food without excessive salt and alcohol consumption and smoking cessation act as an effective prevention against these diseases. It is also interesting that obesity and diabetes used to be exclusively the disease of rich people whereas today these diseases are more frequent in the lower socio-economic class. It is often referred as "modern famine".

I am optimistic, but everything that requires an effort on the side of an individual often does not win over a solution that does not. For this reason, one of the main goals of this work is to

strengthen the set of risk factors for cardiovascular diseases, on the basis of which it is possible to identify a high-risk patient, send him to in-depth examination where a particular disease is confirmed or refuted. Early identification of the disease will significantly increase the chances of its suppression. To be more precise, this work focuses on an occlusive disease of the arteries (*i.e.*, atherosclerosis) and, conversely, a disease causing artery dilation, an aneurysm. Both diseases are very dangerous, mainly because they are mostly asymptomatic for a very long time. Moreover, they have some mechanisms in common and, they were even considered in the past to be one and the same disease with different external manifestations. In case of the worst scenarios, the former ends with a myocardial infarction or stroke while the latter may result in a massive internal bleeding which is usually fatal or at least, the subject becomes functionally dependent. An aneurysm is most often found in intracranial arteries or within the infrarenal aorta. For instance, the aneurysm in the infrarenal aorta, if ruptured, has the highest mortality of all, reaching up to 90% [5].

Aneurysms and atherosclerosis occur mostly in the population above 55 years and are mostly asymptomatic [6,7], hence, not easily detectable without ultrasound, computer tomography or magnetic resonance imaging. Of course it is not possible to scan regularly all this population in order to monitor if the aneurysms and/or atherosclerosis are developing or not. Therefore, a large effort has been done to identify patients at enhanced risk of developing these diseases. During last decades, the most relevant risk factors were identified: male sex, age, smoking status, hypertension and family history. These factors can be easily identified without any additional examination and patients with high risk score can be further examined (preferentially using ultrasound). Nevertheless, in case of the atherosclerosis, most heart attacks and strokes occur at people at averaged risk-factor level who are classified as low or intermediate risk according to traditional risk factor scoring [8]. Similar findings can be found in retrospective study [9] of small aneurysms (*i.e.*, ranked as low-risk) with subarachnoid hemorrhage (SAH). For this reason, there is still a need of further refinement of the risk factors to decrease a rate of these misclassification.

1.1. Goals of the thesis

- Creation of a credible computational model of pulsatile blood flow in arteries, including its BCs, and its validation with experiments.
- Design and creation of an experimental circuit simulating pulse wave propagation (PWV) in a compliant tube.
- Exploitation of the created model for FSI analyses of human aortic tree and evaluation of impact of some of its geometrical parameters on the risk of development of aneurysms and atheromas in critical regions.
- Creation of a 3D CFD PS model of human carotid arteries with lumped parameters BCs. Analysis of influence of diastolic phase length on hemodynamic parameters.

2. Innovation and invention

What is the innovation? Innovation is related to, but not the same as invention. Main difference is that an invention creates an ability, but innovation takes that ability and allows it to scale and create impact in a market or society [10]. Moreover, very interesting description of a process of innovation can be found in the book [11]: „The process of innovation consists of a number of individual inventions, followed by incremental improvements, which together utilize the full potential of the initial invention ". Thus, not all innovations require invention. According to [11], an innovation usually arises via combining already existing technologies and procedures. Some of the recent examples are:

- World wide web (WWW) was developed based on combination of existing protocol TCP/IP; HTML language and existing application called "browser "
- Nobelist Karl Mullins (who invented the method for replication of the DNA segments) said during his Nobel prize speech: "It was too easy, there was no unknown in this scheme "
- Waze (navigation), which uses user´s smartphones as sensors.

This work utilizes a state-of-art methodology to create a high-fidelity numerical model of human arteries and uses it to strengthen or dispute previously stated hypothesis, which are, from our point of view, weakly supported by evidence. I believe that this is an innovation by its definition.

3. Research background

3.1. Cardiovascular system hemodynamics

Cardiovascular system consists of the heart, blood and network of blood vessels, namely arteries, arterioles, capillaries, capillary beds, venules and veins. Its crucial function is to maintain homeostasis and favourable cellular environment via circulation of blood. One of the most fascinating examples of maintaining the homeostasis is organ called brain. Blood flow into the brain is maintained almost constant over a range ± 50% change from baseline in arterial blood pressure [12]. The homeostasis, *i.e.*, autoregulation, is simply controlled through changes in vessel radius since the resistance of the blood vessel is inversely proportional to its radius by power of four. Consequently, the constriction or dilatation of vessels is realized via smooth muscle cells (mainly made up of myosin and actin) by regulation of its vascular tone [12]. The second crucial function of the circulatory system is to move an oxygenated blood away from heart via arteries provide required amount of nutrients and oxygen for all vital organs. Simultaneously, carbon dioxide, waste product and de-oxygenated blood are removed and transported through the venules and veins towards the heart and other organs where they are cleaned up [13,14]. This exchange is done within the microcirculation, the most peripherical part of the system. Microcirculation consists of arterioles which further branch into capillaries. Capillaries end up in capillary beds which merge into venules that also merge to form small veins [14,15] (see Figure 1).

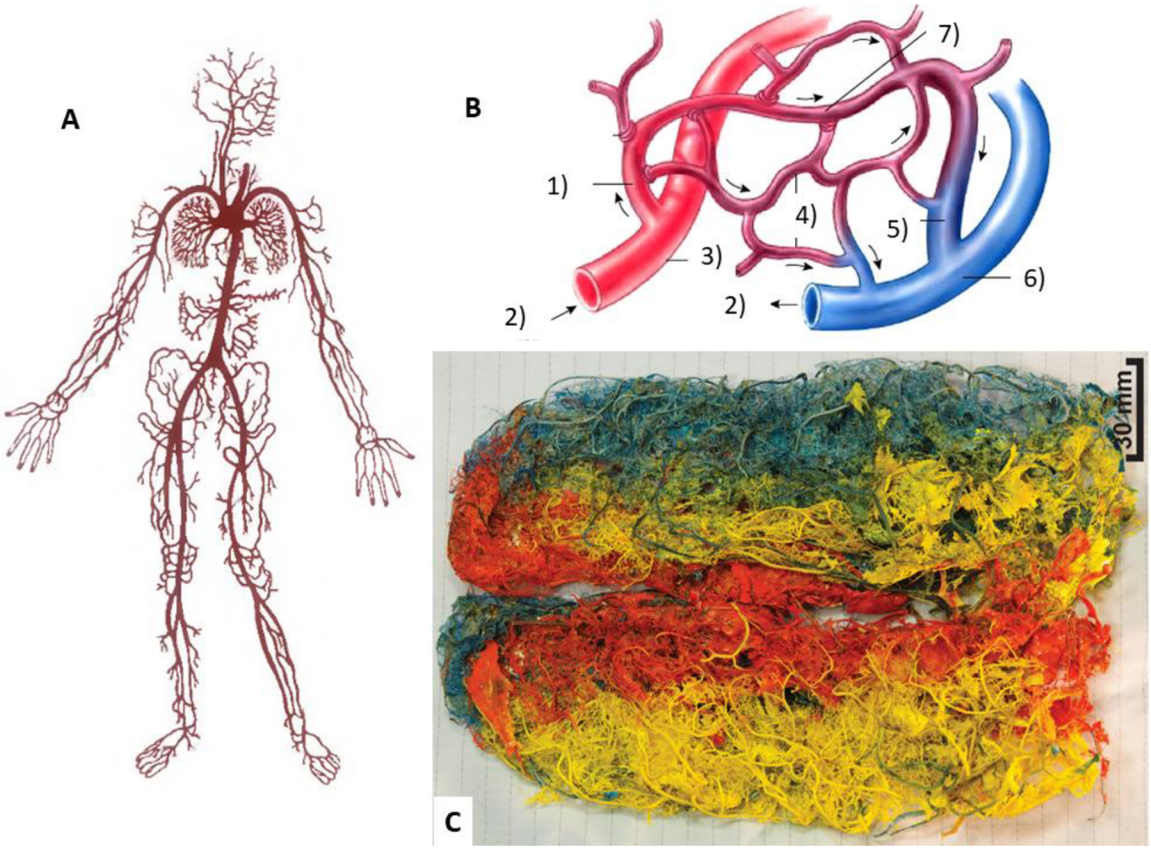

Figure 1 A) – The arterial tree. Adopted from [16]. *B) - Capillary beds: 1) – arteriole; 2) – blood flow; 3) – artery; 4) – capillaries; 5) – venule; 6) – vein and 7) – arteriovenous shunt. Modified from* [16]. *The plastic cast of the full cerebral arterial circulation. The pattern was harvested from a female subject (57 years old without signs of of brain pathology) and casting was performed under pressure to preserve an in vivo dimensions (Modified from* [17]*).*

And finally, the arterial tree, as a part of the cardiovascular system has to transform the highly pulsatile nature of flow generated by ventricular ejection in large vessels (with relatively high mean velocities ~ 20 cm/s) into quasi stationary flow (with mean velocities ~ 0.03 cm/s) at the arteriolar and capillary level (see Figure 2A). This transformation of the flow waveform provides suitable conditions for proper diffusion since the exchange of the oxygen, nutrients and waste products between blood and the surrounding tissue is rather diffusive [13,18]. On the contrary, the pressure wave amplitude (and systolic pressure) and steepness of the front part of the waveform increase as we move towards the periphery within the arterial tree [15,19]. Only a slow decrease in the mean pressure is observed (see Figure 2B) [13,18,19]. Such large changes (of flow and pressure waveforms) are caused by several factors:

- large arteries are highly compliant (e. g. proximal aorta alone represents ~ 60% of the total arterial compliance [20]) and geometrically complex vessels;
- large arteries taper along their length [15];
- arteries become stiffer with smaller radii (*i.e.*, distally from the heart) as the elastin content decreases and the smooth muscle component becomes more prominent [15,16]. For this reason, small arteries/arterioles/capillaries are a main source of the arterial resistance and thus predominantly determine the decrease of mean arterial pressure towards the periphery [13];
- the blood rheology shows great change throughout the tree. It behaves as Newtonian flow in large systemic arteries while ending as a single red blood cell „flow“ which is forced to pass through very small capillaries [18];
- and finally, to cover all organs from a single inlet (heart), the tree must branch in such a way that the capillary density is relatively uniform throughout the organs. This results in a massive expansion of total cross-sectional area of the vessels: while cross-section of the ascending (proximal) aorta is approx 5 cm^2 to reach ~ 400 cm^2 at the arterioles level (with diameters ~ 0.1 mm) [14,19].

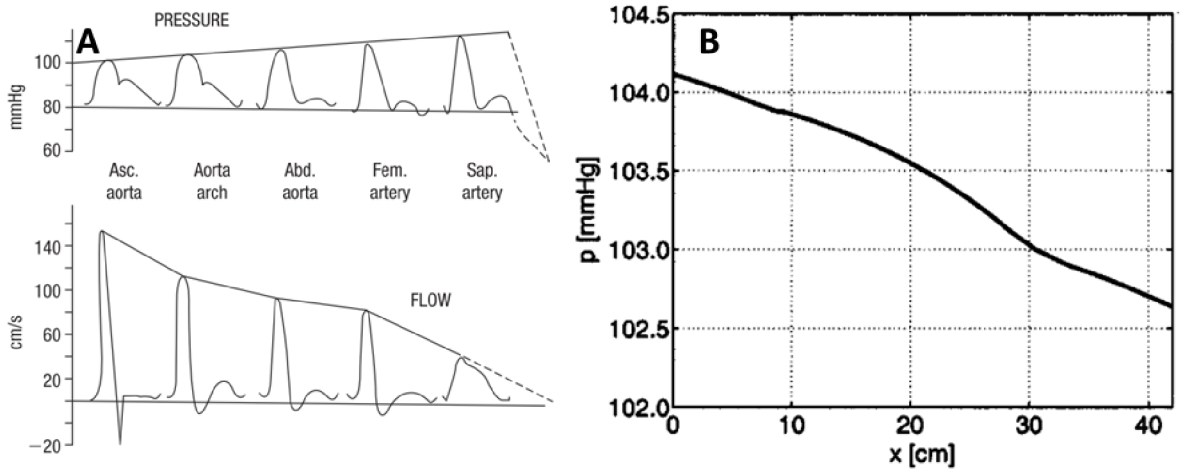

Figure 2 A) – Schematic of pressure and velocity waves as they travel towards the periphery. While the velocity waves are damped out in relative consistent manner, an amplitude of the pressure waves increases up to the saphenous artery and then decreases sharply (see broken line). Adopted from [15]. *B) – Although the amplitude of the pressure waves increases, mean pressure falls slowly (x axis represents a distance from the heart). Adopted from* [19].

The significant compliance of large arteries causes marked two-way interaction between vessel wall and blood flow. Furthermore, the pressure and velocity wave travel with some finite

velocity **c**, *i.e.*, pulse wave velocity (PWV). In contrast to water hammer phenomenon in a rigid piping system where pressure wave velocity is reduced by the compressibility of the fluid (**c** ~ 1500 $m.s^{-1}$ for case of water in a piping system made of steel), in elastic arteries the waves propagate much slower due to compliance of the arteries wall rather than to blood compressibility. PWV observed clinically for a normotensive middle-aged subject increases from 5 $m.s^{-1}$ in the thoracic aorta to 6 $m.s^{-1}$ in the abdominal aorta (AA) and to 9 $m.s^{-1}$ in the iliac and femoral arteries [21]. Moreover, the average increases in the aortic arch PWV due to age-related changes in a cohort of 111 asymptomatic subjects (age range: 20 to 84 years) were $1{,}6 \pm 0{,}3$ $m.s^{-1}$ for each decade of age [22]. Although it is possible to solve the PWV analytically via Moens-Korteweg equation, many assumptions have to be stated such as straight, linear, isotropic, homogeneous and thin-walled circular tube (not the case of arteries) to obtain the solution.

Although a real arterial tree is very complex, some simplifications from the hemodynamics point of view can (or rather have to) be done, without losing its key features. The large arteries can be considered as a source of the capacitance and should by modelled based on their real topology. When we move towards the periphery, the viscosity forces and higher stiffness of vessels cause that the resistance is gaining importance, and thus a frequency dependent impedance seems to be a good approximation for describing the remaining part of the tree [15,19,23]. And this statement is quite a simplified attempt to describe the main concept of multiscale modelling, which will be treated more rigorously later in this work.

3.2. Arterial wall structure

Arteries can be divided into elastic, muscular and intermediate. Main constituents of the artery wall are elastin and collagen (50% of dry weight); the rest consists of smooth muscle cells and non-fibrous matrix [15]. The elastic arteries are located close to heart with elastin as a dominant component of the wall while the muscular arteries are located at the periphery where collagen fibres dominate [15]. Since the elastic modulus of collagen is more than 300 times higher than elastin modulus (~ 100 MPa vs 0.3 MPa), stiffness of arteries increases towards the periphery [15]. The normal arterial wall consists of three concentric layers: tunica intima, t. media and t. adventitia (see Figure 3A, B).

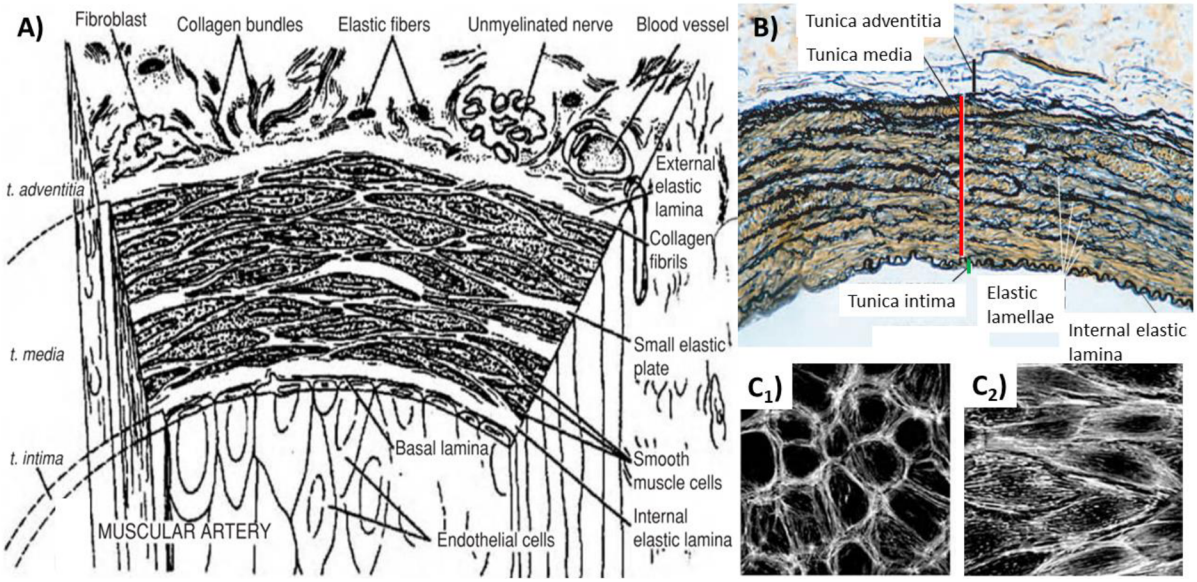

Figure 3 Structure of the multi-layered artery wall. Schematic (A) versus real (B) histological section through an artery wall. Figures (C_{1-2}) showing remodelling of the endothelial cells after being exposed to shear stress of 1.5 Pa for 48 h. Modified from [18].

The innermost (blood-contacting) layer, the intima, is only a few micrometres thick (in a healthy artery) and consists of a monolayer of endothelial cells attached to basal lamina. The basal lamina is composed from collagen, fibronectin and laminin [18,24]. The endothelium monolayer acts as a selectively permeable barrier which regulates the transport of macromolecules between vascular lumen (*i.e.*, blood) and vascular smooth muscle through the muscle cells themselves (in a diffusive manner) or through cell-to-cell junctions [25]. They are subjected to pulsatile wall shear stress from the blood flow and also to a cyclic strain from the pulsatile pressure induced by the heart. The endothelial cells sense these mechanical stimuli and play a significant role in the local regulation of vascular tone via smooth muscle cells to preserve homeostasis [18]. Under physiological conditions, endothelial cells are long flat cells oriented along the vessel axis (see Figure 3C2). This configuration can be characterized as a tight junction [25]. If the process of homeostasis is disrupted and the endothelium is no longer capable to preserve the optimal wall shear stresses and strains, the endothelium cells become rounder with a non-uniform orientation and greater permeability (see Figure 3C1) resulting in conditions which are linked with genesis of some cardiovascular diseases [25–28]. The middle layer (media) is separated from the intima by a thin elastin-rich ring known as the internal elastic lamina (see Figure 3A, B) [18]. Media consists of smooth muscle cells embedded in an extracellular matrix composed of elastin, multiple types of collagen, and proteoglycans [18,24]; finally, the outermost layer (adventitia) consists of a loose connective tissue that contains collagen, nerves, fibroblasts, and some elastin fibers [18,24]. Boundary between the media and adventitia is defined by external elastic lamina (see Figure 3A). The adventitia keeps the arteries attached to the surrounding connective tissue [18].

3.3. The most common cardiovascular causes of death

Cardiovascular diseases (*i.e.*, diseases of the heart and circulatory system) are the most frequent causes of death in the US [29,30] and also in the EU [31] with coronary heart disease ranked as the most frequent one. Stroke (both ischemic and hemorrhagic, *i.e.*, representing two different diseases related to degeneration of blood vessels) was ranked as the fifth most frequent cause of death in the US in 2017 [29] and even second single most common cause of death in the EU [31]. In the view of absolute numbers, heart diseases (I00 – I09; I11; I13; I20 – I51 according to WHO classification) were responsible for almost 615 k and 650 k deaths, cerebrovascular diseases (I60 – 69) for about 130 k and 146 k deaths in the US in 2014 and 2017, respectively [30,32]. Moreover, diseases of heart and stroke together cause 15.2 million deaths wordwide in 2016 (*i.e.*, 27% of total annual deaths) [33].

Atherosclerosis plaque rupture can cause total occlusion of the vessel and consequently, heart attack or stroke [15], depending on the location of the plaque within the arterial tree. Since atherosclerosis preferentially develops at arterial branches and curvatures [28], it can be frequently found at the outer wall along carotid sinus or at the aortic bifurcation. As regard to the latter, here the plaque rupture does not lead to heart attack or stroke whereas resulting in a critical limb ischemia (CLI). In the US, over 1 million patients suffer from CLI every year [34]. Furthermore, CLI is associated with major health complications and may lead up to lower limb amputation.

The same area of arterial tree is also often affected by aortic aneurysms which is responsible for nearly 10 - 11 k deaths (alone in US) every year [5,30,35] and 150 – 200 k worldwide [36], with abdominal aortic aneurysm (AAA) representing a vast majority of them. In case of AAA rupture, the mortality rates reach up to 90% [5]. As regards to aneurysms, they are frequently

found also within intracranial arteries, where they are called cerebral. The cerebral aneurysm (CA) rupture is leading mostly to nontraumatic SAH, an event with high rate of severe morbidity and mortality (*i.e.*, 30 – 50%) [37–39]. Furthermore, 3 of 5 who survive SAH [38] (or more than half [39]) may be functionally dependent. Although preventable, hypertension and hypertensive renal disease remain another major cause of death globally and also in the developed world, with direct risk for cardiovascular diseases (CVDs) [4,15,40,41]. For instance, they were responsible for about 30 k and 35 k deaths in the US in 2014 and 2017, respectively [30,32]. It will be shown that atherosclerosis, aneurysms and hypertension are closely related to each other. Thus, to avoid possible misunderstanding in the causality and consequence between these diseases, we summarize here their main features in detail. Moreover, the distinction from true aging process is pointed out, if necessary.

It should be noted that, besides surgical interventions (*i.e.*, irreversible processes with the risk of associated morbidity or mortality) for aneurysms and atherosclerosis treatment, there are effective non-surgical and non-drug general ways of how to limit CVDs progression (especially at their early phases): a healthy lifestyle (e.g. the mediterranean diet, regular exercise), weight loss, strong emphasis on smoking cessation (for those who smoke), restriction on excessive alcohol consumption, and regularly controlled blood pressure (BP) [15,28,38,39]. This is especially important for aneurysms where no or unclear benefits of drug therapies exist [36]. In case of atherosclerosis, best medical treatment (BMT) already exists and is frequently recommended [42–44]. BMT may differ slightly depending on the stenosis location (*i.e.*, coronary, carotid or peripheral stenosis) but, in general, it consists of lifestyle modifications in parallel with pharmacological proceedings including a medical therapy [42]. Also regarding to hypertension, many successful treatments methods exist for BP-lowering. Available evidence confirms the ability of all five basic groups of antihypertensives (angiotensin-converting enzyme inhibitors–ACEi, angiotensin receptor blockers–ARB, calcium channel blockers–CCB, beta-blockers, and diuretics) to decrease arterial stiffness and consequently the blood pressure in the long-term application [45]. The evidence proves their ability to reduce cardiovascular events, they are similarly effective in overall morbidity and mortality improvement [40]. There are also multiple other groups of antihypertensives used when these basic ones are not sufficient, but their usage is very limited with strict indications and a high risk of adverse effects. Nevertheless, if possible, non-pharmacological ways (e.g., low salt diet, weight loss, regular exercise and alcohol restriction) should be preferred. For instance, intensive regular exercise can decrease systolic (SBP) and diastolic (DBP) blood pressure by ~ 5 and ~ 3 mmHg, respectively [46][40]. Finally, it has to be distinguished between exceptional and regular exercise, since the former can accelerate cardiovascular events whereas the latter prevents against them [15].

3.3.1. Atherosclerosis

Atherosclerosis is localized, obstructive disease and initiated primarily in the intima of major arteries, nevertheless, occasionally may spread into the surrounding media [15]. The disease develops silently over decades, mostly in asymptomatic manner [8,15], unfortunately, and it causes that the arterial blood flow to tissues is limited by a growing plaque (*i.e.*, stenosis, see Figure 4) [15].

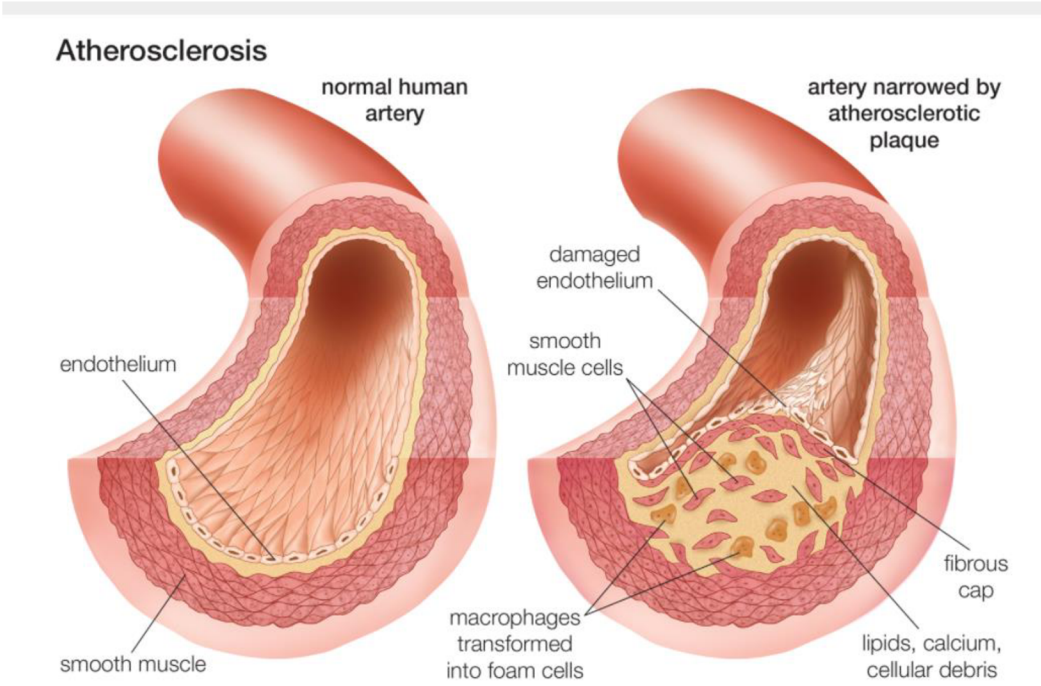

Figure 4 Schematic depiction of differences between a healthy (left) and an atherosclerotic (right) artery. Adopted from: https://www.britannica.com/science/atherosclerotic-plaque.

In contrast to arteriosclerosis which is considered as a degenerative process of arterial aging and hypertension. It has a diffuse character in elastic arteries, located predominantly in media and causes dilatation of the arteries instead of their constriction. Main consequences are microvascular damage in brain and kidney which are the basis of dementia and renal failure, respectively [15].

BMT is recommended for both asymptomatic and symptomatic patients with stenosis, irrespective of the decision whether to undergo an invasive treatment [42–44] such as endarterectomy, stenting, coronary artery bypass surgery etc. A surgical intervention is necessary if the stenosis severity and related risks are too high. Mostly, the severity of stenosis is classified on the basis of the minimum residual luminal diameter [43,47]. For instance, carotid endarterectomy or carotid artery stenting are recommended for symptomatic patients with >50% stenosis or asymtomatic patients with >70% stenosis [43]. Similarly, indication for revascularization of stable coronary artery disease is based mainly on the minimum luminal diameter (50% stenosis with a clinical proof of ischaemia or 70 - 90% stenosis in two angiographic views, depending on the type and location of the atheroma in the coronary artery [44]). This criterion is used despite of several drawbacks: (i) in cases of eccentric stenosis is often difficult or impossible to find true minimum diameter [48]; (ii) it does not provide any information about vessel wall or extravascular structures [15,48,49]; (iii) different reference diameters are used to calculate the degree of diametric stenosis in EU and US [47,48]; (iv) cross-section area criterion correlates much better with the hemodynamic effect of stenosis than luminal diameter and thus, represents a more accurate (but much more time consuming if evaluated manually) way of measuring arterial stenosis [48].

Hovewer, a big progress has been done in the evaluation of stenosis severity in the coronary arteries. Clinically applicable methodology was developed [50] and implemented in the European Society of Cardiology (ESC) guidelines [44] on the basis of the mean arterial pressure, a pressure measured invasively behind the stenosis and from a pressure with closed periphery (the pressure recorded distal to a stenosis while the inflated balloon occludes the coronary artery during angiography [50]). There is a very important assumption for this so

called “flow fractional reserve (FFR)” methodology, namely that the pressures are measured during maximum arteriolar vasodilatation (so called hyperemic conditions, *i.e.*, coronary resistances remain constant and minimal) which causes that the flow in the coronary arteries is fully governed by these pressures and thus, the true functional stenosis severity is determined. Moreover, this methodology was sucesfully validated in humans also for tandem stenosis within one coronary artery by the same authors [51]. Although this criterion shows much better results than luminal stenosis criterion determined from invasive coronary angiography [52,53], it is still underused. This may be due to combination of factors related to practicality, time and cost [54] or due to small cohorts of patients in most clinical studies favouring incorporation of FFR, being thus susceptible for selection bias [55]. However, recent progress in computed tomography angiography (CTA) together with advances in computational fluid dynamics permit to compute FFR in a noninvasive way and without induction of hyperemic condition [53,54,56]. Such methodology is less time-consuming than to make invasive measurements and might result in potentially elevated utilization of FFR in clinical practice in future. More recently, the same noninvasive methodology based on the computed FFR was applied to assess stenosis severity of carotid artery [57]. Hovewer, since the correct drug-dosage in induction of hyperemia in peripheral arteries is not known yet [58], a clinical procedure for the invasive measurement of peripheral FFR has yet to be established to allow consequent validation.

In generall, the most common location of atherosclerosis lesions are at arterial branches or curvatures [28] (on its lateral side away from the bifurcation [15]), sites of dilatation (carotid bulb) and relative constriction (the infrarenal aorta) [15]. Thus, a disturbed flow pattern with recirculation eddies and changes in flow direction with space and time are common features [28]. Interestingly, atheroprone sites with the constriction, which correspond to a relatively straight segment of the infrarenal aorta might look like a paradox because the flow is elevated when a cross section is narrowed; also one may expect a directional flow here. However, during the resting condition, the muscles of leg require only low portion of blood and thus, the peripheral resistance is high [39]. Moreover, renal flow is almost continuous throughout the cardiac cycle [15]. As a consequence, a retrograde and oscillatory flow can be observed within large part of a cardiac cycle along the infrarenal aorta, thus creating a site prone to the atherosclerosis and/or AAA development [15,39]. Since the blood flow to periphery can be elevated during the exercise, its protective function by eliminating the disturbed flow is understandable.

There is a great attention devoted to atherosclerosis and inflammation response (part of a natural healing system) [15,59–61]. Under normal conditions, the endothelial cells of the arterial wall inhibit adhesion and aggregation of leukocytes and promote fibrinolysis [60]. Proper endothelial function could be disrupted by several factors such as its injury, hypertension, smoking, an unhealthy diet, obesity, insulin resistance or inflammation [60,61]. The common feature is an accumulation of the low-density lipoproteins (LDL) within intima, which is believed to be inception of plaque formation [59,61]. Moreover, many in vivo and in vitro observations and experiments show that low and disturbed wall shear stress (WSS) without a preferential direction causes elevated endothelium permeability by increasing turnover rate of endothelial cells [26,27,62]. Consequently, LDL accumulation may be higher in these regions of arterial wall [26–28]. LDL particles are prone to oxidation which causes that endothelial cells express a series of adhesion molecules, chemokines, proinflammatory cytokines and other mediators. Consequently, chemokines provide a chemotactic stimulus that induces migration of adherent monocytes (*i.e.*, large types of leukocyte) into the intima where they interact with modified (*i.e.*, oxidized) LDL to form the foam cells. Moreover, maturated monocytes (*i.e.*, macrophages) can further proliferate within the intima and be responsible for sustaining and amplifying the inflammatory process by releasing several growth factors and cytokines,

including enzymes that can destroy the arterial extracellular matrix (see Figure 5) [60,61]. These immune responses are known to play an important role during all stages of atherosclerosis, from its inception through further progression and the final plaque rupture and thrombosis [60]. On the other hand, high-density lipoproteins can transport some antioxidant enzymes which can break down the oxidized lipids and neutralize their proinflammatory effect [59].

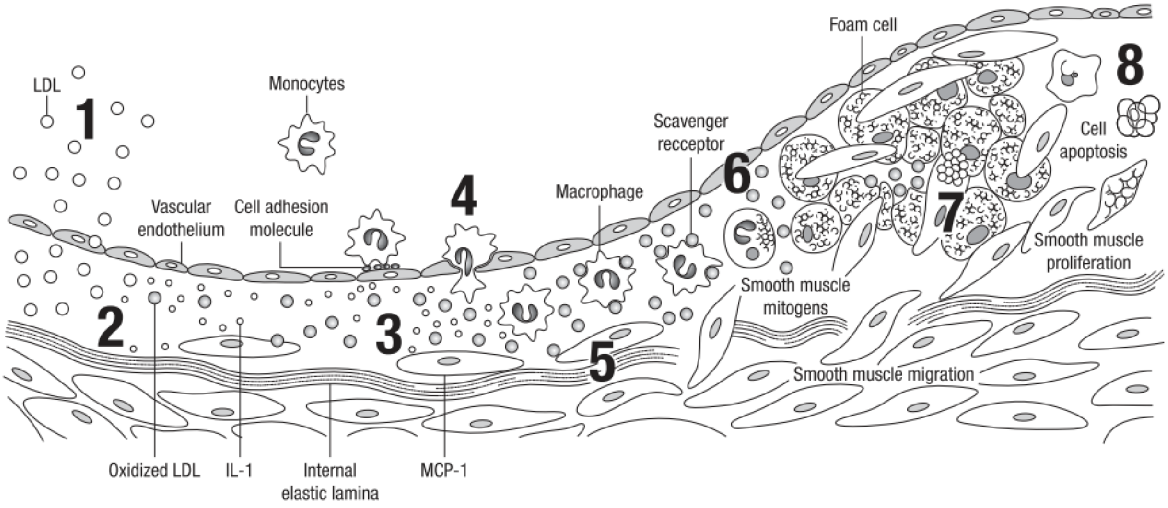

Figure 5 Scheme showing all phases of the inflammatory process. Adopted from [15].

3.3.2. Aneurysms

From a macroscopic view, aneurysm can be defined as a permanent, irreversible localized pathological dilatation of any artery as a result of structural medial changes in the artery wall (*i.e.*, in contrast to atherosclerosis which is primarily an intimal disease) [15,24,36,39,63,64]. Since aneurysms are mostly asymptomatic, their exact prevalence is unknown [37].

Their shape is commonly classified as fusiform or saccular (*i.e.*, berry), see Figure 6. The former develop mostly along the infrarenal aorta with whole circumference involved, whereas the latter arise within the vicinity of the circle of Willis [24,39,63,65] and includes only a part of the artery circumference. Although they may develop elsewhere along the arterial tree, aneurysms of thoracic aorta are ~ 5 times less common than in the infrarenal aorta. Aneurysms are rare in upper splenic or pulmonary arteries or exceedingly rare in the external iliac or upper limb arteries [65].

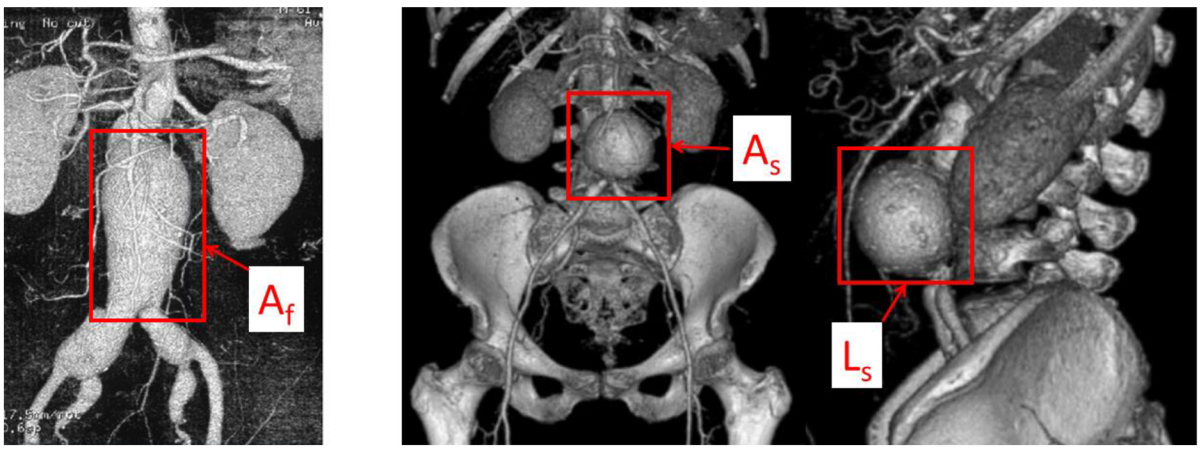

Figure 6 Example of the fusiform aneurysm (on the left within the red rectangle A_f) and the saccular aneurysm (in the middle within the red rectangle A_s) from the anterior view. The same saccular aneurysm is shown on the right, however from lateral view (within red rectangle L_s). Modified from [65].

An AAA is regarded as small when its diameter is below a threshold value of 50 mm for women and 55 mm for men [36]. If the small AAAs are also asymptomatic, conservative management (through periodic screening of AAA diameter and symptoms) is usually recommended [36]. Since up to now, nonsurgical options have not shown convincing arguments to demonstrate ability to limit the AAA growth or rupture [5,36], once the AAA diameter exceeds this threshold or becomes symptomatic, the patient should be considered for elective repair [5,36,64]. Current deficiency in management of a small AAA is a serious issue because it was estimated the 28 % of men with AAAs diameter in range of 25 – 29 mm develop AAAs of > 55 mm within 15 years [36]. Furthermore, the tissue damage is less severe at this early phases bringing thus an opportunity for drug therapies to stop AAA progression effectively [36]. In case of the CA, patients with aneurysm size < 7 mm, without SAH or a symptomatic aneurysm in his/her family history and over 60 years of age are recommended for routine periodic follow-up imaging with Magnetic Resonance Imaging (MRI) or CTA [38]. The surgical procedure is recommended for those with CA size larger than 12 mm and aged over 60 years [38]. Unfortunately, similarly to AAAs, a proper management of small unruptured cerebral aneurysms remains unclear [38].

It is interesting that CAs and AAAs have many common risk factors and reveal similar pathological pathways despite of their different morphologies in different types of arteries and, consequently, under different hemodynamic conditions [36,39,65]. Both, CAs and AAAs are associated with older age, smoking, hypertension and genetic predisposition. They share endothelial cell damage and loss of elastin in the early phase, with a subsequent decrease in smooth muscle cells proliferation, their increased apoptosis, media thinning and initial bulge formation [24,37,39]. Whereas the media attenuates and an initial bulge starts to form in the wall, the thickness of the adventitia is gradually elevated via a turnover of fibrillar collagen, *i.e.*, the main reinforcing component in the arterial wall [24,64]. As a result, the aneurysm increases to a degree that is clinically detectable [24,39]. If the aneurysms are left untreated, they may grow till rupture; this process is believed as a consequence of imbalance between degradation of old collagen and cross-linking and synthesizing the new one [24,37,63]. An imbalance from physiological collagen content to higher or lower values was found within aneurysms while the higher content occurrs probably at the late phase and the lower during the earlier phase [64]. However, the role of inflammation process differs probably between the saccular cerebral and fusiform aortic aneurysms. Recent studies [36,39,64] show that inflammation is critical in pathogenesis of the aortic aneurysms in contrast to strong evidence that inflammatory cells are missing during the CA pathogenesis [37,39]. Different hemodynamics between these aneurysms may shed some light here. Despite of a poor understanding the etiology of aneurysms is [24,39,63,64], there is a growing evidence supporting the role of disturbed hemodynamics in the pathogenesis of aneurysms [37,39,65]. This hypothesis was further confirmed by studies with animal models because the process of aneurysm development starts only when disrupted hemodynamic was also applied [37]. More specifically, the saccular CAs are prone to development under sustained high WSS and high wall shear stress gradient (WSSG) while aortic aneurysms preferentially arise under condition of sustained low WSS and high WSSG. The circulating inflammatory cells require sufficient residence time and elevated endothelium permeability to be able to infiltrate into the vessel wall [26,27,37,39,62] These conditions correspond to AAs [39] or also some saccular CAs after their enlargement (*i.e.*, recirculating zone formation in the sac) [37] and thus elucidate the distinct timing of the inflammation process in the aneurysms development. On the other hand, in the healthy intracranial artery or in some CAs where impinging flow persist either after aneurysm enlargement, different pathways of aneurysm pathogenesis and progression develop [37]. This case corresponds to high WSS and WSSG which is linked with mural-cell-mediated destructive

remodeling rather than to the previously described inflammatory-cell-mediated destructive remodeling [37].

3.3.3. Hypertension

Hypertension is defined as chronically increased BP above 140/90 mmHg with overall prevalence in adults ranging from 30 – 45% [40,66]. It is also a leading risk factor for major CVDs, such as heart attack, stroke, chronic kidney disease, heart failure, cognitive impairment and dementia [15,66]. The hypertension is related to the increase in peripheral resistance and decrease in arterial distensibility. Consequently, the arterial tree is exposed to increased pulsatile stress [46] in the load-bearing media within large elastic arteries. As result, the pulsatile stress is transferred from hyperelastic elastin fibres to much stiffer collagen fibres due to successive decrease of elastin content and loose of its loadbearing capacity. In addition, the significant nonlinearity of the stress-strain curve of arteries (due to recruitment of the stiffer collagen fibers at higher stresses) causes further progressive stiffening of the central elastic arteries as the BP is elevated [15]. This stiffening causes further an abnormal blood flow, endothelial dysfunction (similarly to the atherosclerosis [15,46], increase in PWV and thus an elevated amplitude of the initial pressure wave with earlier return of the reflected one [15]. Furthermore, target-end organs damage (*i.e.*, left ventricular hypertrophy, chronical kidney disease, microalbuminuria) occur frequently in early phase of the hypertensive disease (*i.e.*, prehypertension) and thus hypertension is further accelerated [15,46].

The hypertensive arterial disease has many similarities to the aging, and thus it can be considered as a type of accelerated aging [15]. However, we have to distinguish between natural aging and hypertension. The former process shows lower cardiac output and only modestly elevated mean arterial pressure, the latter demonstrates normal or even initially elevated cardiac output and a substantial increase in the mean arterial pressure [15]. Two main problems are related to hypertension in clinical practice:

(i) First is its rather confusing classification based on systolic, diastolic, or systolic plus diastolic cut-off BP values [15]. In recents guidelines [40], the cut-off BP values for treatment and in final targets were slightly lowered because epidemiological associations between cardiovascular risk and BP have been found even for very low levels (*i.e.*, SBP > 115 mmHg). Since the benefits of treatments (either with lifestyle interventions or drugs) have to clearly outweigh the risk of treatment [40], further substantial lowering of the thresholds and targets seems limited.

(ii) Second is related to location where the pressure is usually measured. Measurement of BP is typically performed via sphygmomanometer in peripheral (brachial) artery despite of clear evidence that arterial pulse is amplified here to a variable degree (compared to central aortic blood pressure (cBP), see Figure 7) [15] with the greatest discrepancies, *i.e.*, amplification, in people with healthy compliant arteries (*i.e.*, adolescent and younger people, mainly men) [40,46]. Since only increase in the cBP is linked with CV risk and end-organ damage [15,41], this rather artificial amplification can cause that such subjects are diagnosed with "isolated" or spurious systolic hypertension (ISHY). In the most recent review [41], three studies suggested ISHY is spurious while a nearly equal number of studies suggested that ISHY represents a similar risk to that of high-normal BP. They conclude that such ambiguity could be caused by existence of two distinct cohorts within subjects with ISHY. The first (unhealthy cohort) can be characterized as being current smokers, of lower socioeconomic status, decreased physical activity and increased BMI. The second (healthy) cohort is clearly depicted as being taller, more physically active, younger, non-smoker and with lower blood cholesterol levels. Subjects within the first group

mostly have normal or low cBP whereas those in the second group are associated with elevated cBP and thus, at increased CV risk and end-organ damage. Hence, to prevent misleading diagnosis of ISHY and consequent unnecessary treatment, new clinical management plan was proposed in [41] for these subjects suspected with ISHY. The finding about presence of spurious ISHY in taller young subjects are also in accordance with [15].

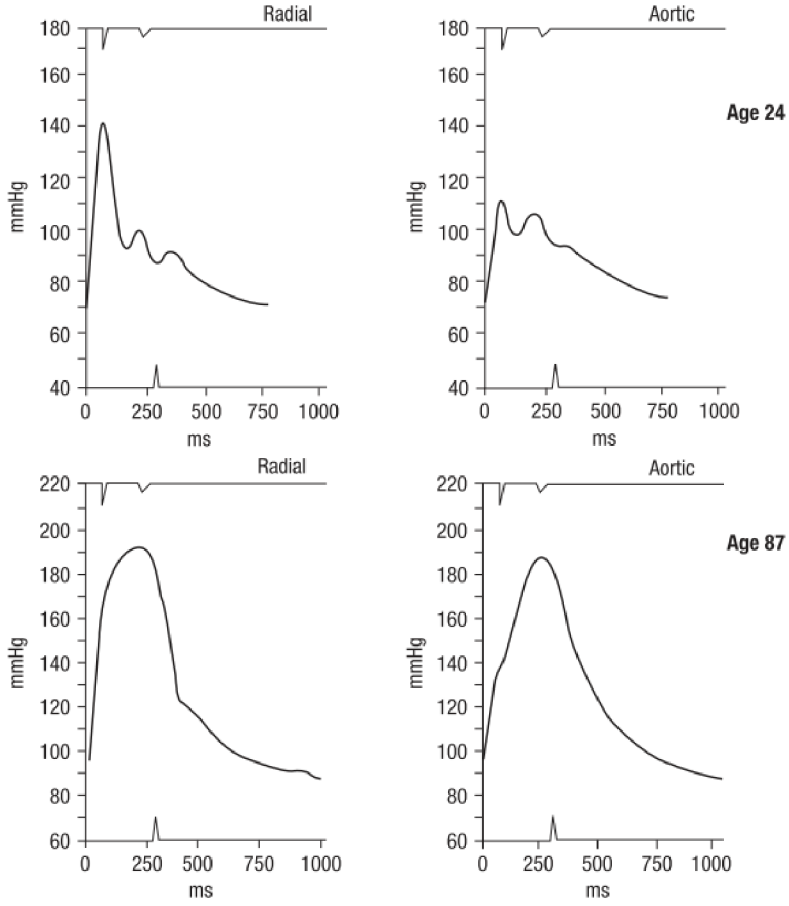

Figure 7 Example of isolated systolic hypertension in a 24-year-old man (top) in comparison with the hypertension in an 84-year-old woman (bottom). Adopted from [15].

3.3.4. Relation between atherosclerosis, aneurysm and hypertension

Except for uncommon causes such as infection or congenital disorders of connective tissue, aortic aneurysm have originally been understood as result of atherosclerosis [67]. However, this concept was challenged when some clinical studies [68–70] brought an evidence, that presence of atherosclerosis in aneurysms might be only incidental, because many patients with advanced atherosclerosis do not show developed aneurysm and vice versa. Nowadays, it is generally accepted that aneurysm and atherosclerosis are two different diseases [71,72]. Both of them are polygenic, multifactorial and share most of the risk factors [72,73], nevertheless, aneurysm is not a clear manifestation of atherosclerosis [72]. More probable, atherosclerosis develops in parallel with or secondary to aneurismal dilatation [71]. On the contrary, some aneurysms may develop as a result of excessive positive arterial remodelling in response to arterial narrowing related to atherosclerosis in some cases [36]. Anyway, the atherosclerosis still remains a significant independent risk factor for aneurysm development [5,72].

Recent meta-analysis [74] found a 66% higher risk of AAA in hypertensive patients compared to non-hypertensive patients. Study also reveals a strong and nonlinear dose-response

relationship between DBP and risk of developing AAA (risk increases with a higher level of DBP) and weak to moderate dose-response relationship between SBP and AAA. When we look at it from opposite side, the hypertension was diagnosed in 81% of patients (n = 211) with AAA in the retrospective study [73]. It is worth noting that the main benefit of hypertension treatment is reduction in the related morbidity and mortality. Typical cardiovascular events related to hypertension include hemorrhagic stroke, ischemic stroke, myocardial infarction, sudden death, heart failure, peripheral artery disease, and end-stage renal disease [75]. Some new evidence shows that increased vascular stiffness might be a predictor of cardiovascular events and all-cause mortality independent of traditional cardiovascular risk factors [76–78].

Hypertension is evidently a significant risk factor for inception of both atherosclerosis [79] and aneurysms [80], but the mechanisms are poorly understood. It is generally accepted that antihypertensive drugs (ARBs, CCBs, and ACEIs) can improve endothelial function in patients with CVD. Although the effect is partially related to the decrease of angiotensin II levels and angiotensin II receptor signaling. But many other mechanisms were described [81]. The new generation of beta-blockers might have a positive influence on endothelial dysfunction [82] as well as some diuretics [83]. All these effects might at least partially slow down the process of atherosclerosis. Moreover, it is broadly recognized that the age-related elevation of arterial stiffness changes the blood flow rate dynamics in a similar manner as arterial hypertension [15,84,85]. Since elevated pressure and abrupt hemodynamics play crucial role in genesis of these diseases (as described in chapters 3.3.1 and 3.3.2) or [25–28,37,39,79,80], it may explain a much higher incidence of aneurysms and atherosclerosis in hypertensive patients.

According to World health organization (WHO), the cause of death is based solely on the underlying disease which is defined by WHO as “the disease or injury which initiated the train of morbid events leading directly to death, or the circumstances of the accident or violence which produced the fatal injury” [35]. It was shown that all the mentioned diseases are closely related, and one can accelerate or initiate development of the another. Thus, focus only on the disease being the most frequent cause of death and underestimation of the others could be misleading.

3.4. Numerical modelling of blood flow in arteries

Cardiovascular modelling based on mathematical representation has a long history. Lumped models (also referred as 0D or Windkessel among the literature) are the simplest and the oldest ones and typically represent electrical networks. The utilization of these models in cardiovascular modelling was started by Otto Frank in 1899 [23], who set up an analogy between electrical networks and cardiovascular system. The first model was the two-element Windkessel (2WK) consisting of a compliance C of a part of arterial tree represented by a capacitor whereas their resistance R is described by a resistor. As the simultaneous measurement of the flow and pressure waveforms together with progress in computing capabilities that allow Fourier analysis became possible in living being, validation of the 2WK has been feasible not only via pressure waveform, but also by input impedance (*i.e.*, frequently dependent resistance computed from the flow and pressure signals). It was found that the 2WK is not able to capture the input impedance, especially at higher frequencies (see Figure 8) [23].

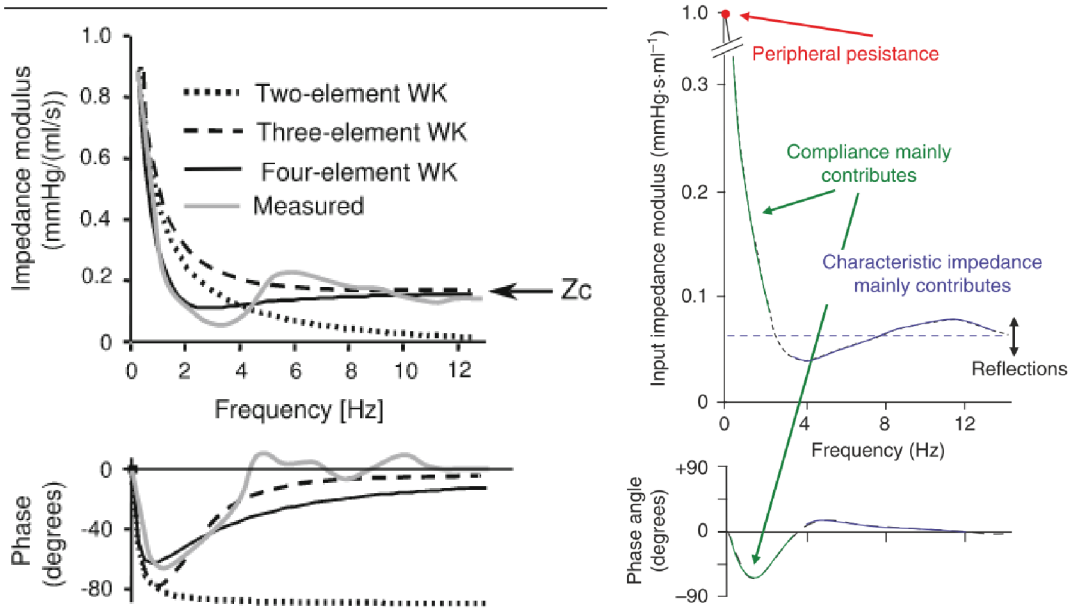

Figure 8 An example of measured aortic input impedance depicted together with impedances predicted by two, three and four-element Windkessel (Adapted from [23] and from [86] – page 195)

This shortcoming was partly offset by adding another element which represents characteristic impedance Z (also referred as R_p) to form three-element Windkessel (3WK) – see Figure 8. The characteristic impedance Z (or R_p) in the three-element Windkessel, can be seen as a link between the lumped Windkessel model and wave travel aspects of the arterial system since characteristic impedance equals wave speed times blood density divided by (aortic) cross-sectional area [23]. The 3WK shows no fluctuation of modulus, nor of phase compared to measured input impedance, because such models cannot capture a wave travel or reflection phenomenon in the model (*i.e.*, it is 0D model – discrete approach). Nevertheless, in overall, the input impedance of the whole systemic tree is sufficiently approximated by the 3WK with this improvement. To overcome partly the issue with discrete approximation of the continuous arterial system with a Windkessel approach, Noordergraaf and co-workers [87] designed and constructed a model of the human systemic tree with distributed properties based on Windkessel principle. The model consists of all major vessels (over one hundred segments in total) which were represented by combination of serial-parallel connections of a 2WKs and 3WKs models. Several distributed models based on this prototype had been designed but I will only mention that one developed by Westerhof et al. [88], because their proposed changes greatly improved the model performance compared to [87] and complied very well with its real counterpart. Also, four-parameter Windkessel has been proposed by adding a term L, representing an arterial inertance. Thus, the model consists of 3WK plus arterial inertance L [23]. Moreover, different variants (*i.e.*, with linear or non-linear resistance R and capacitance C) of WK have been proposed, nevertheless, it seems that benefits do not outweigh drawbacks [23,89]. The biggest drawback of these more sophisticated models lays in the consequent estimation procedure which is needed for parameters determination. I will address this issue in detail at the end of this chapter.

Regardless of the success and simplicity of a 0D approach, another approach started to develop nearly in parallel. Its foundation was set by Taylor during 1950s, who designed and constructed

simple tubular model with fluid oscillation in an elastic pipe based on Womersley solution [15]. Main advantage was this approach was continuous (*i.e.*, 1D) where the wave propagation and reflection were considered. This methodology has been developed into a sophisticated 1D structural model of the whole arterial tree using non-invasive measurements of flow waveform which serves as input boundary condition (BC) together with considering patient-specific (PS) dimensions of most of the larger vessels in humans (e.g., [19]). In general, they divided the arterial tree into two 1D models: a non-linear model of the aortic tree with large arteries (up to the second branches from aorta) and a linear structured tree model for its peripheral parts, which supplies the aortic model with impedance-based BCs. Model was further improved by considering viscoelastic constitutive law for the arterial wall and coupled with the left ventricle which was modelled using the varying elastance model [90]. Moreover, a linear structured tree model for peripheral parts was replaced by 3WK model and the model was also extensively validated against the PS *in-vivo* data [91]. It is worth noting that coupling between 1D (continuous) and 0D (discrete) models had to be done. This is called as multiscale modelling and can be used between different levels of models (e.g., 3D-1D; 3D-0D; 3D-1D-0D) [92].

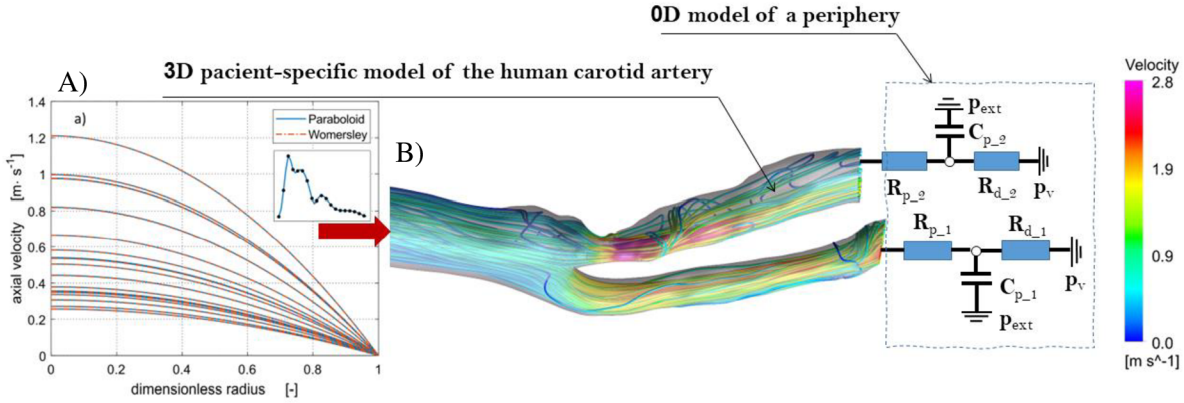

Figure 9 Example of multiscale model. A) 3D paraboloidal velocity profile used as an input boundary condition. B) A three-element Windkessel model coupled to the 3D model.

Neither 0D nor 1D models solve detailed flow patterns. To overcome this, a 1D model of larger arteries, for example carotid artery can be replaced with a 3D PS geometry and coupled with 1D or 0D models for its peripheral sites (see Figure 9). A 1D or 0D model of peripheral and venous part of the circulatory system is necessary here due to its excessive complexity for 3D modelling. Such form of simplification is needed not only due to high computational cost (despite of a great progress in this field) which would be the case of 3D PS models of arterial tree considering most larger arteries, but also due to the time necessary for their reconstruction and convergence issues.

On the basis of a review performed on multiscale modelling approaches in the blood flow modelling in large vessels, I can point out that the 3WK model for a periphery (specifically RCR configuration) has become a standard among the most fidelity models [57,93,94]. It has to be emphasized that estimating of parameters for 3WK is crucial for reaching appropriate PS BCs which represent the remaining circulation. Specifically, we are facing a problem with three unknown parameters per each outlet for the 3WK RCR (R_p – characteristic impedance or proximal resistance; C – compliance and R_d – resistance of a periphery). A general methodology (independent of an estimation algorithm, see Figure 10) was proposed by Spilker and Taylor [93] and their variations were successfully utilized by many others (e.g., the most recent works

[57,95] or the older one reviewed in [94]). First, a 0D representation of a real geometry has to be created. Mostly it consists of a network of many serial-parallel WKs. Then, initial parameters are derived based on average geometrical dimensions and steady-state analytical solutions (e.g., Poiseuille profile in a cylindrical artery segment) or using CFD solver to solve steady-state problem on real geometries. Since initial guess based on a steady computation is done, a parameter estimation procedure is used to obtain an estimate on the WK parameters. The clinical measurements of pressure or flow/velocity (or both) waves are needed here along with some other modelling assumptions (e.g., flow split ratio, proximal resistance ratio). For example, Spilker and Taylor in [93] measured the flow waveform Q at the inlet of a common carotid artery segment and reconstructed its shape from the transient Doppler ultrasonology measurement; these results could be used as an input to WK model while the blood pressure range from brachial artery tonometry together with a chosen proximal resistance fraction were provided as measurements (*i.e.*, reference signals). Thereafter, WK parameter estimates were used to start a 3D-0D (*i.e.*, multiscale) simulation. Mostly two to thirteen parameter updates based on the results from 3D simulation are needed to reach agreement between 0D and 3D models. The number of updates depends on multiple factors: (i) quality of the 0D representation of a 3D domain; (ii) complexity of the geometry (e.g., number of outlets) or (iii) the estimation algorithm used [57,93,94]. I note that the same procedure with some minor changes should work for a 1D model. Although both rigid or flexible wall can be considered for a 3D model, one has to keep in mind that the 3D FSI transient simulation will have considerably higher requirements on computational resources, a higher complexity of the model may lead to convergence problems and lastly, reconstruction of a 3D geometry takes more time.

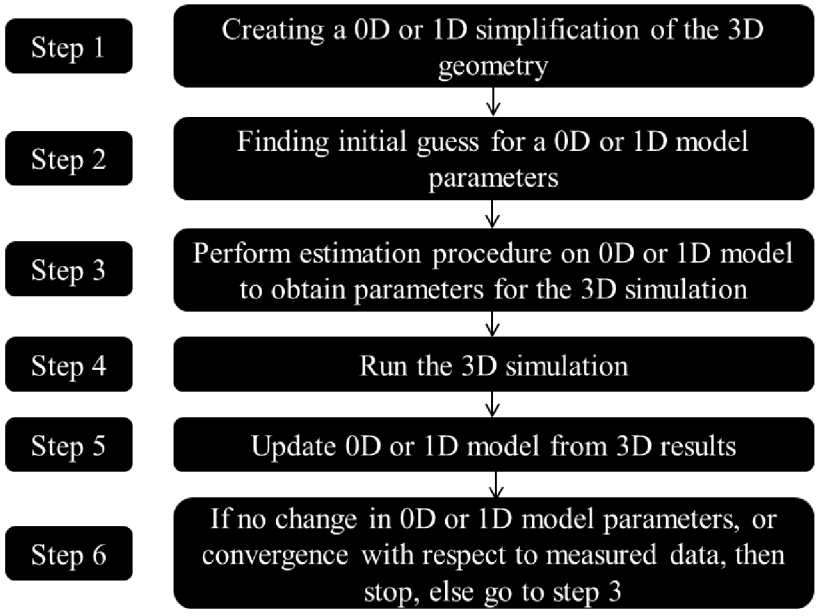

Figure 10 Algorithm for multi-scale simulations using an estimation procedure for finding parameters which represent a periphery (modified from [93,94]*).*

To summarize this chapter, I will answer a crucial and very practical question: Is it worth the effort? Is such sophisticated methodology with multiple steps necessary for obtaining relevant BCs at the outlets? The answer is definitely yes. A frequently used approach, which imposes zero/constant pressure as outlet BCs yields, unsurprisingly, to physiologically unrealistic results ignoring the effect of the downstream circulation. Consequently, the flow split is dictated solely

by the resistance to flow in the vessels which are considered in the computational domain [96]. The results are even worst when model have multiple outlets and/or stenoses [57,97]. Another approach represents periphery as a single straight 1D axisymmetric and elastic tube with some porous zone at the end [98]. Parameters for estimation procedure when downstream compliance is known are: the length of the tube and porous zone and arrival time of the reflected wave. Such approach concentrates the reflection sites into two locations: an interface between 3D-1D model and at the end of the elastic tube. This is not the case of a real periphery, where the reflection sites are spatially distributed as the waves move towards the capillary beds. Moreover, a multiscale approach with 3WK or 1D structured tree as outflow BCs have very good predictive behaviour, in terms of validity over a certain range of physiological conditions, and it is also less constraining the boundary velocities [94]. Finally, it is worth noting that the number of parameters which need to be estimated is lower for 3WK or 1D structured tree.

4. Computational model of a pulsatile flow and its validation

Main goals of these experiments were: (i) validation of the CFD and FSI approaches in the aorta-like tube; (ii) evaluation of the influence of turbulent flow; (iii) assessment of the effect of the wall compliance on the haemodynamic parameters. For a detailed description of such complex flow (pulsatile, transitional), the particle image velocimetry (PIV) measurements across the tube diameter were performed using high-speed camera which enabled us to capture eventual turbulent structures. All experiments were performed by Ing. Michal Kotek, PhD and Ing. Darina Jašíková, PhD from the Czech Technical University of Liberec (Department of Physical Measurement). Postprocessing of the measurement data sets, validation of the performed FSI simulations and further analyses are my own work. Ing. Jiří Kohút (at that time student of master program at the department of fluid engineering of BUT) was involved in the CFD simulations of pulsatile flow in the rigid tube within his master thesis. One of the most important outputs of his work was a choice of the suitable turbulence model for such a complex flow. Since it was successful for rigid tube (CFD) simulations, it was also used for the compliant tube (FSI) simulations. Prof. Jiří Burša, PhD. was responsible for review, editing and formal analysis.

The results of this computational and experimental study have been published in [99] where an information regarding the experimental circuit and numerical simulation can be found in detail.

4.1. Main findings

4.1.1. Validation of the CFD/FSI approach in the aorta-like tube

The overall agreement of the velocity profiles between the experiment and simulation using the turbulent model is very good for both cases. Discrepancies in the near wall region could be caused due to the relatively coarse radial resolution of the camera. Since the dynamic range and spatial resolution of PIV method is limited by the size of the camera's chip (see [99] for detail), higher small-scale resolution is always accompanied by loosing large-scale picture.

4.1.2. Evaluation of the influence of turbulent flow

This work confirms the hypothesis stated in [100] that a longer deceleration phase triggers transition to turbulence while a shorter and more rapid deceleration delayed the transition. In addition, the results are also in accordance with [101] stating that, in a straight rigid tube, turbulent formation takes place in the near wall region and then it diffuses to the core region. In case of the rigid tube, this phenomenon cannot be observed in velocity profiles (see [99]) and neither in peak velocities (see Figure 11A – orange curve representing k-ω SST turbulence model is almost coincident with laminar flow model – blue curve). However, the turbulence is much more significant in the compliant tube, where substantial differences can be observed in both (see [99] for velocity profiles and Figure 11B for peak velocities – blue versus orange curves). Therefore, we put foundations for extension of this hypothesis to compliant tubes while these phenomena were found also here for physiological Reynolds and Womersley numbers. Thus, the length of the deceleration phase should be considered (in addition to the geometry or severity of the stenosis) in decision whether the fluid simulations should be performed with or without the laminar flow assumption. For instance, flow waveforms in carotid bifurcation for old adults (with little or no carotid artery disease) are significantly different compared to young adults [84]. The deceleration phase is longer and two pronounced peaks occur at the systole due to an earlier return of the reflected wave. It would be of interest to evaluate the effect of this age-related change in the flow waveform shape on the turbulence and thus, on the hemodynamic

parameters (*i.e.*, wall shear stress, oscillatory shear index, endothelial cell potential). On the other hand, flow waveforms within the AA of healthy old subjects have rather shorter and more rapid deceleration phase and thus the laminar flow assumption should be acceptable.

4.1.3. Assessment of the effect of the wall compliance on the haemodynamic parameters

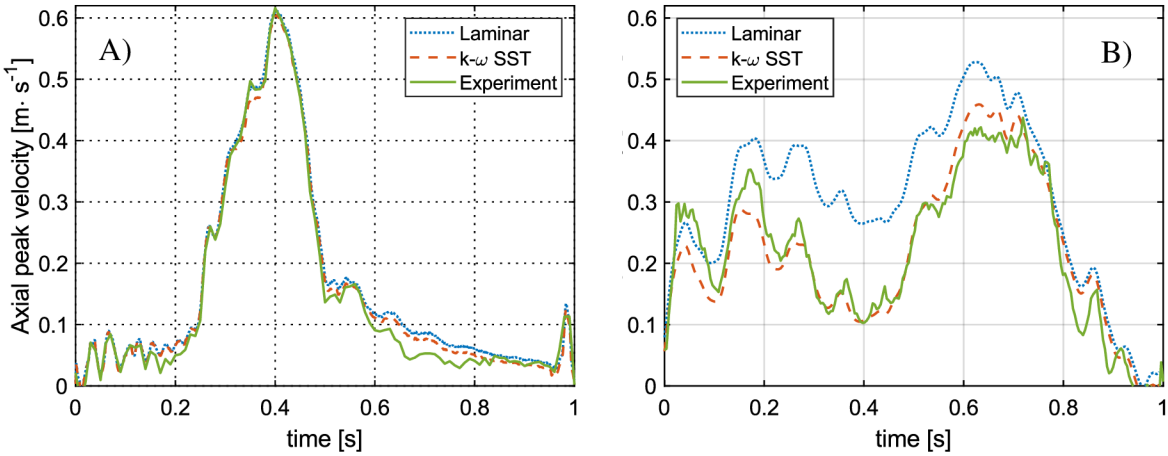

Figure 11 Shape of the velocity waveforms in the middle of the tube (center of the cross section at the half-tube length). The rigid (A) and the compliant (B) tube.

Comparison of Figure 11A and B shows significant differences in the shape of the peak velocities in the middle of the rigid and compliant tubes. As the experimental setup and dimensions are almost the same for both, this difference could be mistakenly attributed to the wall movement of the compliant tube. However, the interpretation cannot be so straightforward. The main reason for such a great discrepancy is the non-negligible time shift between the pressure waves at the inlet and the outlet (*i.e.*, in case of the rigid tube the time shift is negligible) resulting in totally different pressure gradients along the tube compared to a rigid tube. In addition, at least two locations exist in case of the compliant tube, where almost stepwise changes in the impedance occur being responsible for high portions of the reflected waves. They are located at the connections between the tested tube and the hydraulic circuit where the pressure sensors are embedded in metal (*i.e.*, nearly rigid) casings. This effect could be diminished by using materials with similar elastic modules for the whole circuit. Another source of the wave reflections and consequent oscillations, valves of the membrane pump, could be eliminated by using a peristaltic pump instead.

4.2. Comments on the main findings

The closed experimental circuit with its stepwise changes of stiffness is inconsistent with the arterial tree, which is characterized by a continuous distribution of parameters and terminates with a constant pressure in the capillary bed; thus it does not induce as many wave reflections as it was in the experimental circuit with its stepwise changes of stiffness. However, from the validation point of view, our conditions were harder (high frequency oscillations) than may occur in arterial blood flow. Therefore, the conclusions drawn on the basis of our simulations should be valid also for simulations of arterial flow, which can be, in addition, influenced also by the non-Newtonian blood properties and strain stiffening of the arterial wall.

In our study we worked with a rather well described tube (homogeneous, isotropic and hyperelastic) and also the BCs were recorded. However, for many computational studies which consider compliance of blood vessels (FSI analyses), such comprehensive inputs are not known. Number of the required inputs can be reduced by a lumped parameter model or structured tree model, usually used instead of the measured output pressure. For instance, in case of 3WK model used instead of the recorded transient pressure waveform at the outlet, only three unknown constants per each outlet have to be determined, *i.e.*, peripheral compliance, resistance and inertance. This approach was described in the chapter 3.4. Another option is to adopt representative BCs from the available literature [102–104] or from a validated 1D model of the whole arterial tree (1D [91] and/or 3D [105]). Regarding to these considerations, however, a synchronization between the input and outputs has to be done for correction of the time shift in the computational model because the time shift between the input and output BCs is PS and has significant influence on the flow. If not done, the pressure gradients along the domain can be highly different from their physiological values. It may result in a non-physiological flow in the simulations and, consequently, in incorrect results and conclusions.

4.3. Future work

For future CFD/FSI simulations of an idealized human arterial tree and PS carotid arteries, a special care will be devoted to BCs treatments. Regarding to idealized arterial tree with the BCs extracted from one healthy individual and implemented for all geometrical variant, the time shift correction based on the computed PWV will be implemented. Since we are using the same shape of BCs for all variants, the only variable is the time-shift between the inlet and outlets BCs. An idealized geometry allows us also to compute PWV and consequently the time-shift via Moens-Korteweg eq. with adjustment for thick wall or by P-U loop method [106]. As regards the PS carotid artery geometry with potential implementation of the PS BCs (*i.e.*, each geometry has a specific shape of the BCs), the multiscale 3D-0D modelling approach is chosen due to its effectivity in tuning its parameters to reach the required flow and pressure waveforms at the outlets. More details are presented in the following chapters.

5. Experimental and computational analysis of pulse wave propagation

5.1. Basis explanation of pulse wave propagation in an elastic tube

For better understanding of methods for determination of the PWV, I decided to elucidate the pressure waves propagation throughout a straight, cylindrical, compliant and elastic vessel in greater detail. The waves travel as transverse elastic waves because the fluid inside the tube is almost incompressible compared to the compliance of the wall. An incompressible fluid is considered also at rest. Although this is not the case of the blood flow in a real artery, propagation of the waves within such simplified case is, in principle, not so far from their real counterpart. When the pressure is elevated locally (point 1, Figure 12), the wall is also locally distended to store the elastic energy of the pulse. Consequently, the pressure gradient between points 1 and 2 causes that distension waves shift to the right. The same process is then repeated from point 2 to point 3 and so on. As a result, the pressure wave propagates down the tube.

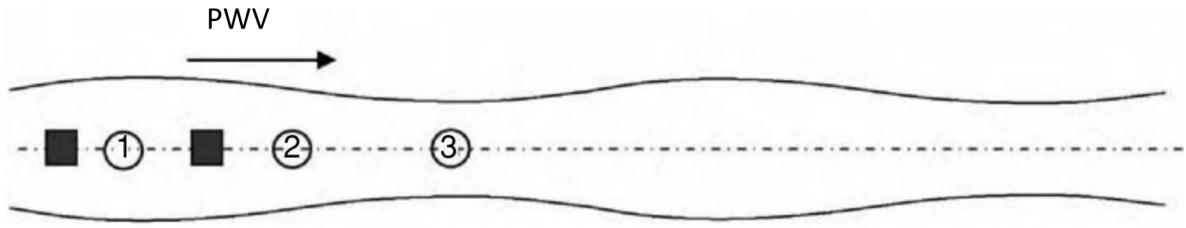

Figure 12 Schematic depiction how fluid elemets (represented by ■) move in a compliant tube. Adopted from [18].

5.2. Calculation of the PWV

The wave propagation phenomenon in an elastic tube can be mathematically described by Moens-Korteweg equation (5.1) [18]. This equation can be simplified into eq. (5.2), if compressibility of the fluid inside the tube is much lower than distensibility of the tube. For instance, compressibility modulus (*i.e.*, bulk modulus) of water at 20°C $\boldsymbol{K}$ is $2{,}03.10^{9}[Pa]$ while incremental (or secant) modulus of elasticity $\boldsymbol{E_{inc}}$ of a silicon tube used in experiment below equals to $4{,}55.10^{6}[Pa]$ (see Figure 15), *i.e.*, almost three orders lower. Moreover, the $\boldsymbol{E_{inc}}$ is even lower (by an order) in case of large arteries.

$$PWV_{fluid+solid} = \sqrt{\frac{\frac{K}{\rho}}{1+\frac{K \cdot d}{E_{inc} \cdot s}}} \tag{5.1}$$

$$PWV_{solid\ thin\ walled\ tube} = \sqrt{\frac{E_{inc} \cdot s}{\rho \cdot d}} \tag{5.2}$$

$$PWV_{solid\ thick\ walled\ tube} = \sqrt{\frac{E_{inc} \cdot s}{\rho \cdot d \cdot (1-\mu^2)}} \tag{5.3}$$

Here $\boldsymbol{\rho}$ represents mass density of the fluid [kg·m^{-3}], $\boldsymbol{s}$ and $\boldsymbol{d}$ are thickness and inner diameter of a tube, respectively [m], $\boldsymbol{\mu}$ Poisson's ratio [-].

Nevertheless, both of them represent an idealized wave velocity and are valid only under a number of simplifying assumptions for the tube: (i) thin-wall tube; (ii) it shows small

deformations; (iii) it is filled with a perfect incompressible inviscid liquid; (iv) its wall material can be considered as Hookean; v) it has (straight) cylindrical shape. Deviation due to the first assumption can be lowered by using corrected Moens-Korteweg eq. (5.3), which can be found within Bergel´s doctoral thesis [107]; it incorporates Poisson's ratio of the tube. In practice, eq. (5.3) represents an effective simplification [15]. Neglecting the dilatation of the tube (the second assumption) also means that inertial components due to the wall motion are not considered. However, these effects contribute only slightly to the overall error in case of real arteries [107]. The third assumption appears quite reasonable in case of larger arteries while a huge impact arise due to viscosity effect for smaller ones [15]. The fourth assumption is definitely not true for real arteries. They are highly non-linear, anisotropic, hyperelastic and non-homogeneous. However, non-linearity is compensated by using incremental Young modulus $\boldsymbol{E_{inc}}$ in eqs. (5.1, 5.2, 5.3), and the effect of anisotropy has shown no impact on the PWV if the tube length did not change [107]. The last set of assumptions have a major effect on PWV [18], since the arteries are tapered, curved and branched from the large aorta up to very small capillary beds. In general, we can see that arterial tree is a very complex branching network and every bifurcation has its own reflection characteristic. Nevertheless, it should be kept in mind that most of these bifurcation are well matched *in vivo* (consequently no significant reflection occurs) and reflections mostly occur at distal capillary beds [18,19]. Despite of these limitations, the Moens-Korteweg formula is still frequently used to calculate arterial stiffness (from the PVW) or PWV [15]. Its utilization is reasonable because the main focus of these studies is evaluation of relative differences in PWV (e.g., between young and old, or systolic and diastolic conditions) rather than finding its true absolute value.

5.3. Determination of the PWV in a clinical practice

The PWV can be obtained from the travel (or transit) time of a wave between two measuring sites, e.g. over a given distance or transit time between two sequentially measured waves using the electrocardiogram as a reference [15]. Many different waves have been used to determine the PWV, such as flow (or velocity), diameter or a pressure wave [15,108]. The distance is usually longer (e.g. carotid-femoral PWV – cfPWV, see Figure 13) to provide sufficient accuracy in the measured time delay, thus the resulting PWV is only an average over the measured arteries. Since the carotid and femoral arteries have different mechanical properties, such regional measurements of the PWV can mask potential arterial abnormalities [108,109]. Moreover, external measurement of the distance between two sites produces an additional error, especially for more curved and tortuous vessels [22,108].

However, the transit-time MRI method (*i.e.*, non-invasive method for the flow wave) was performed recently to obtain the PWV over short distance (< 10 cm) along the aortic arch [22]. One of the main outputs was that PWV increase in the aortic arch correlates better with pure arterial aging than the cfPWV. Such close proximity of two measuring sites pushes this approach towards local methods for determination of the PWV. The local methods, such as PU-loop, D^2P-loop, sum of squares or others have shown very good results but most of them are more or less sensitive to reflected waves [106][109][108]. Although in young healthy individuals the arterial tree is well matched and consequently the reflection coefficients at the bifurcation are very small [109][19], this is no longer true for older individuals neither those with CVD [109][110]. Nevertheless, if the measurement is performed far enough from the closest reflection point, the measured PWV appears reliable [109]. Finally, the last option is PWV calculation from measurements of the elastic properties and the dimensions of the artery

wall [106,109]. Such measurements are difficult and up to now, impossible to perform noninvasively [106,109].

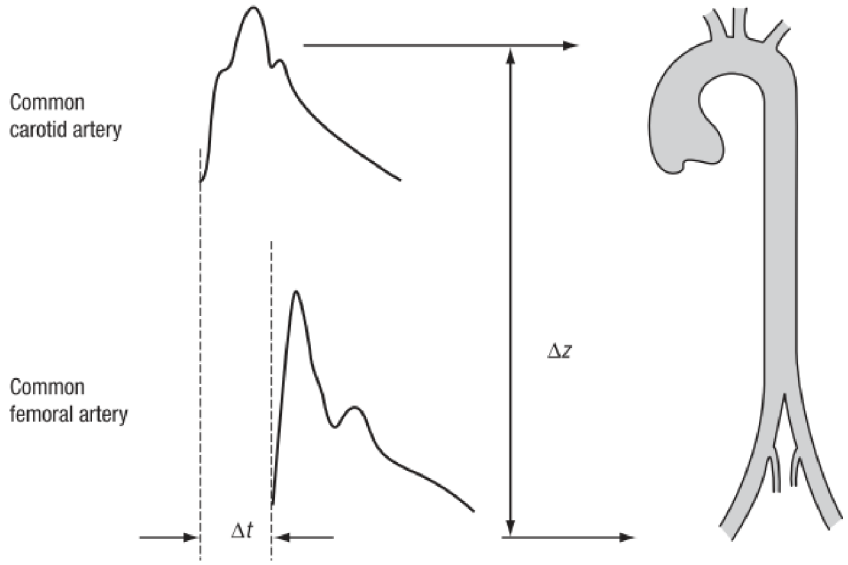

Figure 13 Schematic depiction of principle of the cfPWV evaluation by clinical measurement via time-to-foot method. Adopted from [15]

5.4. Experimental measurement of the PWV in a thick-walled hyperelastic tube

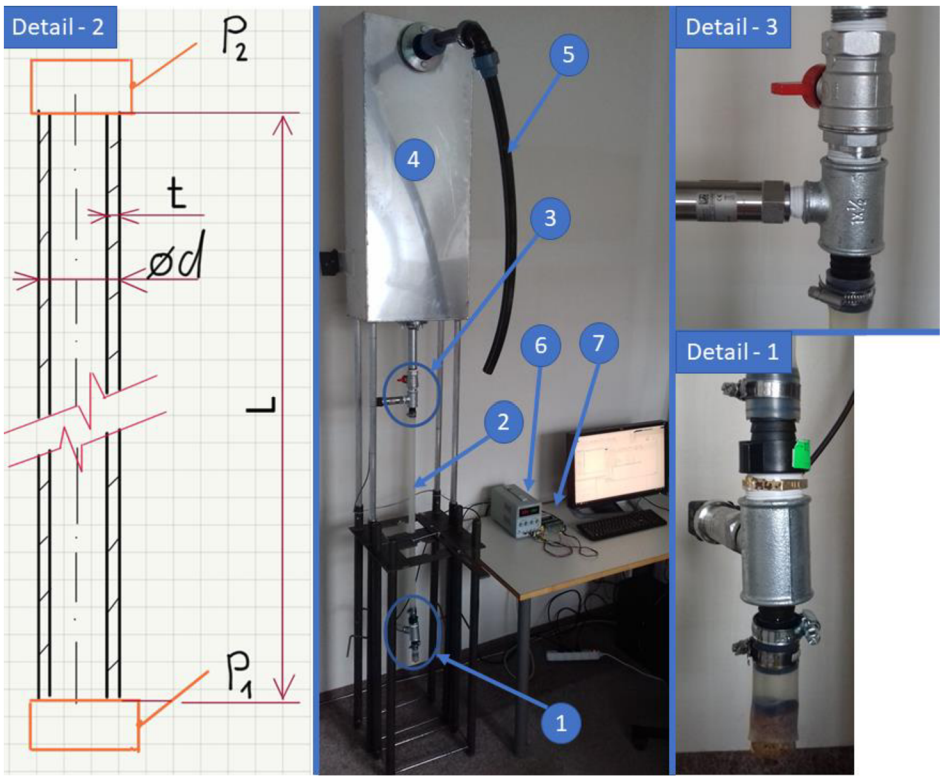

Figure 14 Experimental circuit simulating pulse wave propagation. (1) - lower pressure sensor with a source of a pressure wave; (2) – test section (compliant tube); (3) – upper pressure sensor with a ball valve; (4) - output water reservoir; (5) – an overflow (6) – source of the AC current with a terminal block (7)

The experimental circuit is presented in Figure 14, dimensions of the compliant (silicone) tube are: L = 1.33 m; t = 0.003 m; Ød = 0.026 m. Two samples were cut from the tube to perform uniaxial tests with our in-house testing machine. One in the circumferal and one in the longitudinal direction. Every sample was tested twice, thus four uniaxial tests were performed in total (see Figure 15 – left). Because the tube was thick-walled, the circumferal sample preserves significantly a circular shape. Although a preload was used before the testing procedure, it was quite hard to find a threshold between bending and pure tensile loading of the sample. Hence, only two tests from the longitudinal sample were used to identify the material model. Moreover, the deformations of the tube from the pressure pulse are small (between ~ 1 ÷ 3%) and thus, $\boldsymbol{E_{inc}}$ ~ 4.55 MPa (as an average from the slopes of two uniaxial tests, see Figure 15 - right) and $\boldsymbol{\mu}$ = 0.5 (*i.e.*, incompressible) were consider to fully describe the used Hookean material model. Furthermore, the tube was regarded as isotropic, incompressible and homogeneous.

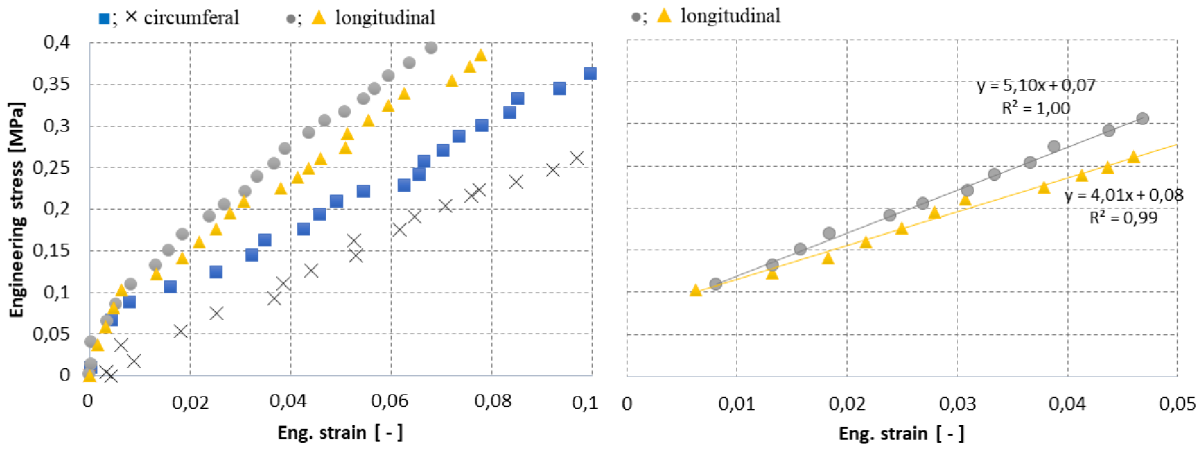

Figure 15 Experimental data from four uniaxial tests (left figure). Zoomed results for longitudinal samples approximated with a straight line, the slope of which defines the Young's modulus (right figure).

The working fluid of the circuit was water (at 20°C). Pressure sensors with sampling frequency of 200 Hz were located at the inlet and outlet of the test region (the measured tube). The pressure wave was actuated manually by pressing a short section of a tube right below the lower pressure sensor (see Figure 14, detail 1). The water reservoir (4) was connected to the circuit to set up the initial pressure in the circuit. Thus, a pressure difference between the lower and upper sensors corresponds to 1.33 m column of water (*i.e.*, hydrostatic pressure of 0.0133 MPa), see Figure 16. To ensure that amplitude of the pressure pulse will not be significantly attenuated as it spreads toward the upper pressure sensor within the compliant tube, the ball valve was installed right behind the upper pressure sensor. This allowed me to control the amplitude of the pressure pulse.

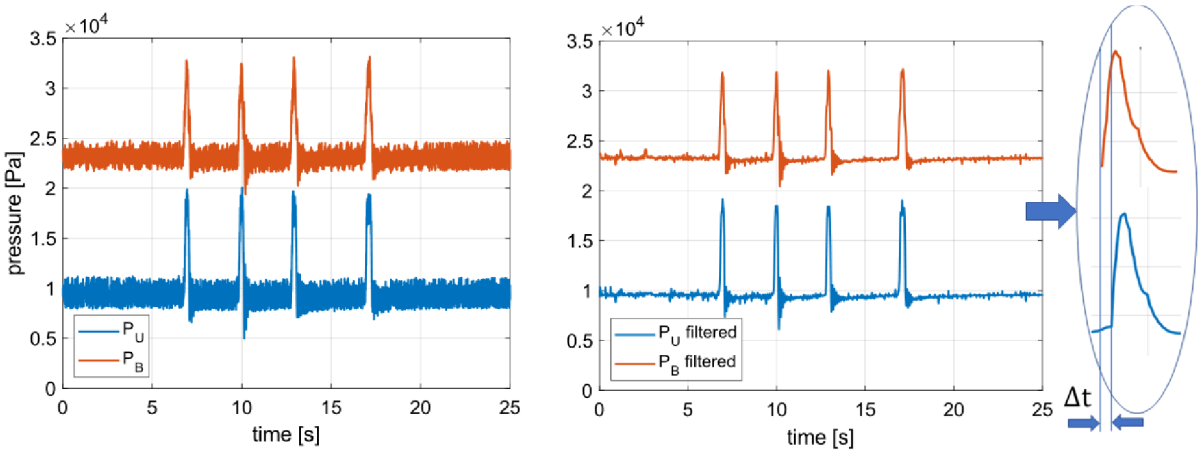

Figure 16 Pressure pulses recorded from the lower (blue) and upper (orange) pressure sensors. The left side depicts a non - filtered data while filtered data are on the right.

High frequency noise was filtered out by a low pass filter, consequently, the time-to-foot method was used to evaluate the time delay Δt between the pressure waves from the bottom and upper pressure sensors (see Figure 16). As a result, the PWV ~ 35 $m.s^{-1}$ was calculated as a ratio between the length of the tube L and the time delay Δt.

5.5. Experimental validation of the PWV calculation

The FSI simulation of the PWV propagation along the thick-walled tube (made of silicone) was performed in Ansys® by coupling Fluent® solver for the liquid phase with Ansys Structural solver (based on Finite Element Method) for the solid phase. Due to axial symmetry, only a quarter of the test region (detail 2 in Figure 14) was considered in the computational model. Acceleration of gravity was not taken into consideration.

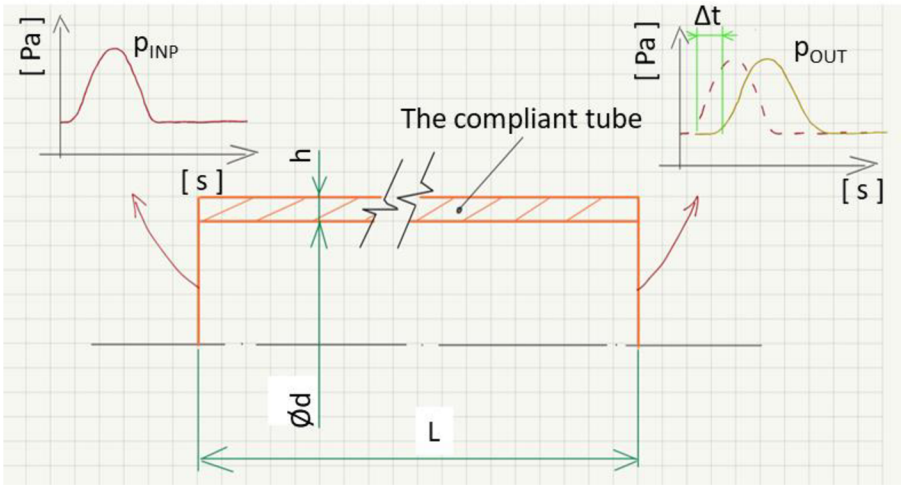

Figure 17 Boundary conditions

The idealized pressure waveforms represented by half-sine function were used as BCs at the inlet and outlet of the tube. Hovewer, the BC at the pressure outlet was shifted behind the BC at the pressure intlet by about Δt = 0.0166 s (see Figure 17). The time delay was calculated as a ratio of length of the tube L = 0.5 m to the PWV = 30.2 $m\cdot s^{-1}$ where the PWV was figured out from eq. 5.3 (*i.e.* Moens-Korteweg eq. for a thick-walled tube). Time step size was set to 0.004 s, which was sufficient to achieve the required convergence criteria for residuals. These criteria were set to 10^{-5} for velocity components and to 10^{-4} for continuity.

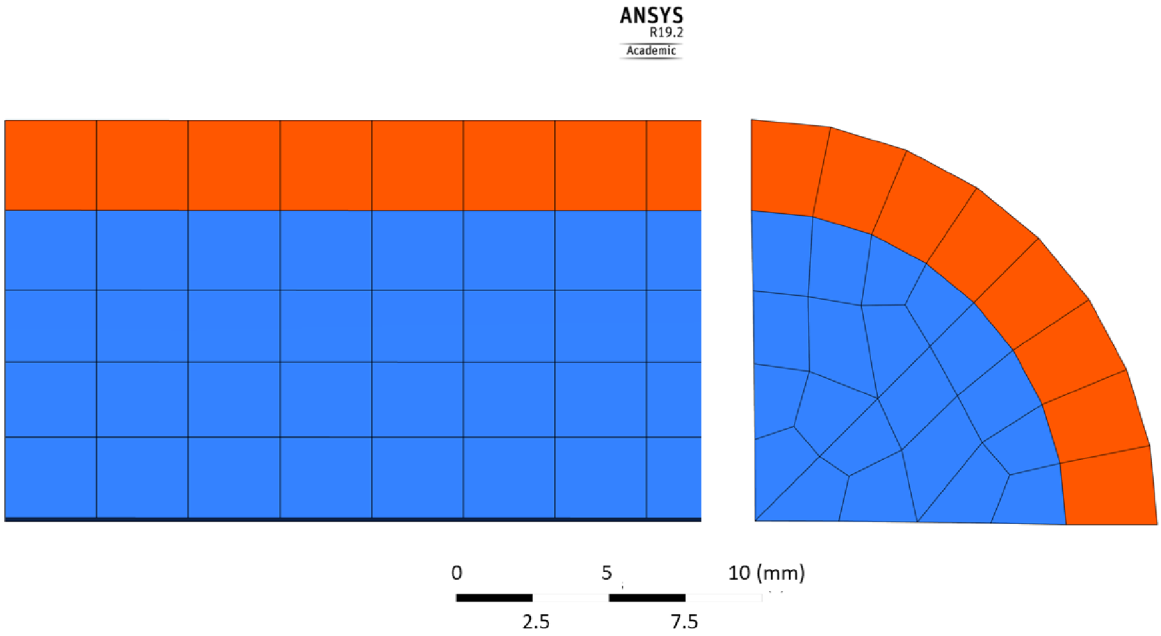

Figure 18 Mesh for the solid (orange) and fluid (blue) domains. Since an inviscid flow is considered, a relatively coarse mesh can be used.

Since I am interested in the PWV propagation only and not in the character of the flow, an inviscid assumption was chosen for a fluid domain which allows me to use a coarse mesh without BL (see Figure 18). A Hookean material model was used with E = 4.55 MPa and $\boldsymbol{\mu}$ = 0.5 (*i.e.*, incompressible) because of small deformations of the tube; the process of identifying the used material model for the solid domain, was described in the above chapter. The P-U loop method (eq. 5.4 [106]) was adopted as an alternative and more precise approach (in comparison to Moens-Korteweg eqs.) for the PWV evaluation. It is worth to note that its fundamental equation (eq. 5.4) also does not consider viscous flow.

$$PWV = \frac{1}{\rho} \cdot \frac{dP}{dU} = \frac{1}{\rho} \cdot \Delta \qquad (5.4)$$

Where $\boldsymbol{\rho}$ represents density of the fluid [kg·m^{-3}], $\boldsymbol{dP}$ and $\boldsymbol{dU}$ are instantaneous increments of pressure [Pa] and velocity [m· s^{-1}] at the same location, respectively.

To obtain the PWV from FSI simulation, we have to extract the transient velocity and pressure profile from the same location within the tube. Thus the plot pressure versus velocity should be linear (if there are only forward waves present, see Figure 19). Finally, the slope of the P-U line is equal to $\boldsymbol{\rho}$ PWV. Hence, it gives us the desired PWV = 34.7 m · s^{-1} when divided by $\boldsymbol{\rho}$. Comparison of different computational approaches with experimental measurement can be seen in Table 1.

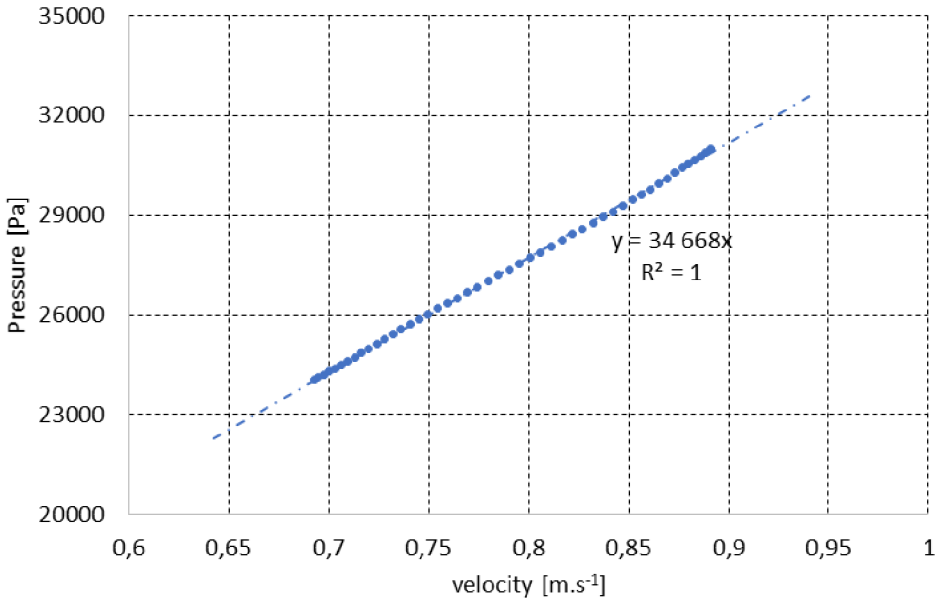

Figure 19 P-U dependence. Data extracted from the FSI simulation.

Table 1 Comparison of multiple approaches of the PWV evaluation.

	Used method			
	Time-to-foot method (experiment)	*K-M basis*	*K-M correction for thick wall*	*P-U loop*
PWV [m/s]	35.0	26.2	30.2	34.7
Relative error [%]	-	-25.3	-13.7	-0.9

6. Analysis of influence of arterial geometry and flow waveform shape on hemodynamics in arteries

6.1. FSI parametric study of idealized arterial tree: effect of geometry

This chapter is dealing with 3D two-way iteratively implicit (*i.e.*, *fluid and solid equations are solved separately. Solvers iterate within each time step to obtain an implicit solution*) fluid-structure interaction (FSI) simulations of eighteen idealized and one PS geometries of human aortic tree with common iliac and renal arteries with different iliac angles and aorto-iliac ratios. The main goal is to evaluate the influence of these geometric changes on blood pressure in the AA. The idea of this study has been initiated by Dr. Stanislav Polzer who also did some preliminary research. His doctoral student David Schwarz was responsible for geometry reconstruction and mesh creation. Prof. Jiří Burša, PhD. was responsible for review, editing and formal analysis. I, as the first author of the paper [111], have done most simulations, completed the preliminary research and proposed the methodology. I created also most parts of the paper which has been published in IF journal Medical Engineering & Physics.

6.1.1. Brief Introduction

As it was stated in chapter 1, it is not possible to scan regularly all this population in order to monitor if the aneurysms and/or atherosclerosis are developing or not. On the other hand, scanning only patients within a high-risk score is also not reliable. For this reason, there is still a need of further refinement of the risk factors to increase the reliability of scanning through the population in the risk group.

One of such factors influencing development of aneurysms and/or atherosclerosis might be iliac bifurcation geometry. For instance, some FSI studies showed that increasing angle ω between iliac arteries at the bifurcation (see Figure 20), as found often in clinical practice, is associated with increased BP and consequently stress within the AAA [102,104]. It has been shown experimentally that the ω angle increases and the area ratio AR (*i.e.* a sum of luminal cross sections of iliac arteries divided by the aortic luminal cross section) decreases with age [110,112], or could be modified through remodelling process due to haemodynamic changes caused by, for example, isolated common iliac artery aneurysms [113]. On the contrary, some experimental studies concluded that the effect of the bifurcation angle on the BP is small [112,114]. Regardless of the significance of these geometrical changes on the BP, the theory behind is that as the ω angle increases and the AR decreases, a higher-pressure wave reflection is induced at the bifurcation. The reflected wave may interfere with the forward pressure wave and result in a pressure increase in the AA where the elevated systolic blood pressure (SBP) affects the aorta in the same way as in case of hypertension. Unfortunately, this effect is hardly detectable for clinicians because the BP is commonly measured in brachial artery [15,40,46]. Moreover, AAA is often associated with significant stenosis of iliac and/or femoral arteries and it is not clear whether iliac stenosis may contribute to AAA formation by increasing the BP in the AA. Also, it is still not clear whether the pressure in AA may be significantly elevated in a healthy aortic tree compared to other large arteries. Therefore we focused on this question and analyzed computationally the effect of both aorto-iliac angles and AR on predisposition to AAA development by quantifying their effect on the pressure and peak wall stress (PWS) in the AA during a heart cycle. For this purpose, two-way weakly coupled FSI analyses with parametric idealized geometries of human aorta including renal arteries and iliac bifurcation were employed. A similar patient-specific (PS) geometry was added to the FSI analyses for validation.

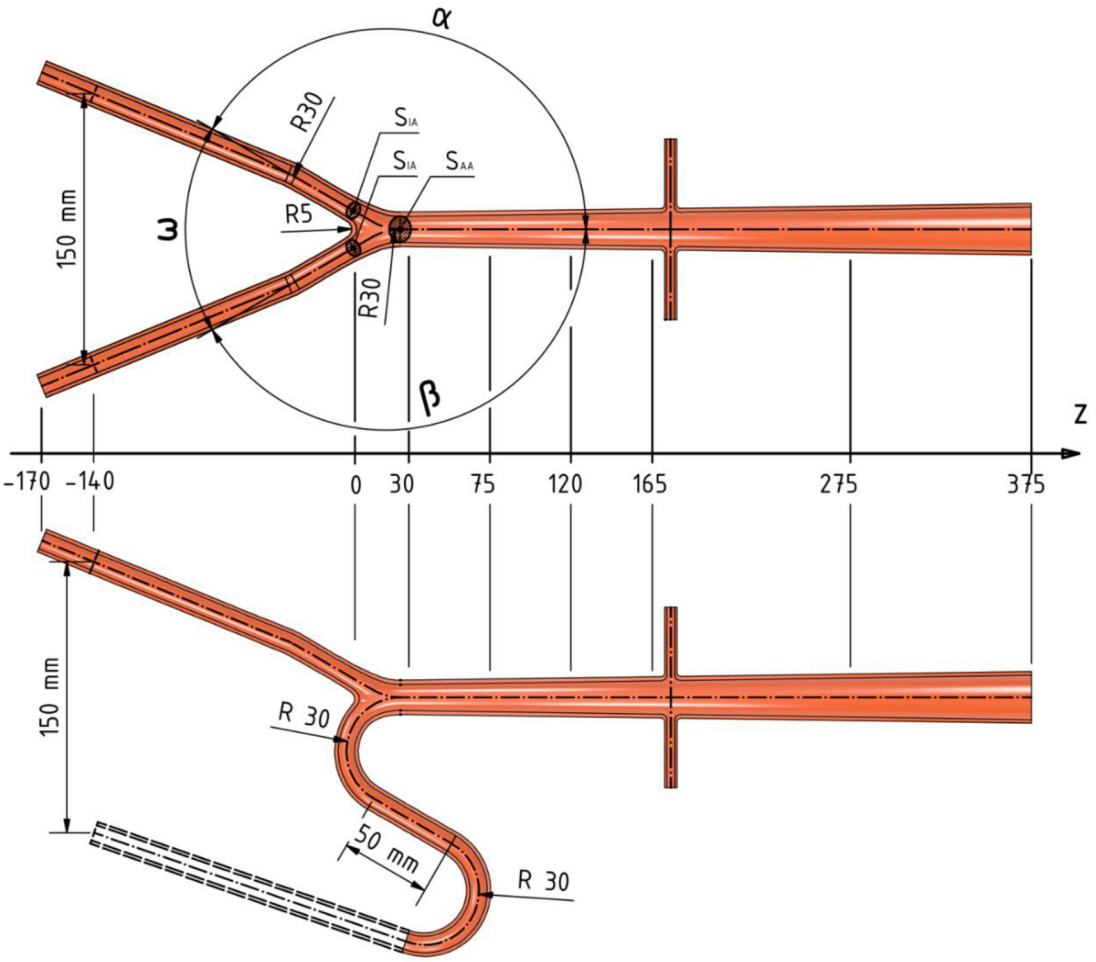

Figure 20 Dimensions of the geometrical model of aorta and iliac arteries for basis geometry (upper) and the most asymmetric geometry used in parametric analysis (lower). Angles $\boldsymbol{\alpha}$ *and* $\boldsymbol{\beta}$ *change in the parametric analysis, z coordinate defining the position of sections origins at the bifurcation apex. Geometries are constructed in a way that ensures the same 150mm distance of iliac arteries at the 140 mm distance from the bifurcation apex. Cross sections of the abdominal aorta (*S_{AA}*) and iliac arteries (*S_{IA}*) were used in evaluation of the area ratio AR.*

6.1.2. Methods

a) Geometry creation and mesh

As regards to idealized geometries and meshes, a 3D finite element model was created with diameters (changing linearly along the aorta) and wall thicknesses of individual arteries set according to available literature to represent 60 years old men [115,116] who is typically in risk for AAA and/or atherosclerosis development (see Figure 20). Since this study consider elasticity of arteries (FSI analysis) and dimensions are measured *in-vivo* (*i.e.*, under diastolic/systolic BP), we have to solve inverse problem to find out undeformed dimensions. Thus, diameters and wall thicknesses were iteratively changed to minimise deviation of the calculated deformed dimensions from the *in-vivo* (deformed) values measured under diastolic and systolic BP and axial prestretch. The same diameter of both iliac arteries was chosen to set the AR ratio to 1 in the basis variant. This ratio is validated with *in-vivo* measurements (for a healthy older individuals) [91,117]. Since the AR variability is considerable [112] so we extended our study by adding geometries with different AR to simulate various degree of iliac

stenosis or effect of aging. To cover an existing dispersion in geometry of aorto-iliac bifurcations, the shapes and ranges of their parameters in both symmetric and asymmetric variants follow the shapes observed in elder patients (see Figure 21), both healthy and suffering from iliac artery aneurysm [113]. A different aorto-iliac geometries were created from the basis geometry (see Figure 20 top) by changing the angles α and β and the AR. In accordance with anatomical reality, six combinations of different aorto-iliac angles between 30° and 150° were created and, for each of them, 3 variants with AR 1, 0.67 and 0.5.

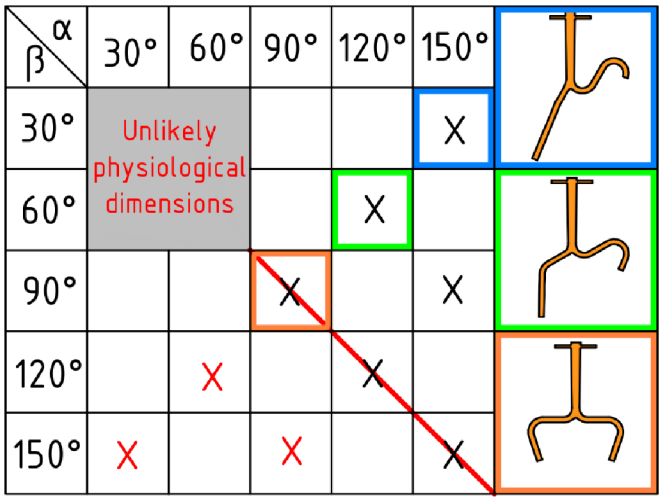

Figure 21 Overview of six analysed bifurcation geometries created by varying angles $\boldsymbol{\alpha}$ *and* $\boldsymbol{\beta}$ *of both iliacs for area ratio* $\boldsymbol{AR} = \mathbf{1}$ *with illustrations of three configurations. Three variants with* $\boldsymbol{AR}$ *= 1.0, 0.67 and 0.5 were created for each of these geometrical configurations, resulting in eighteen geometries in total. The red line highlights symmetrical geometries.*

Creation of the PS geometry of a 53-years-old man with no arterial pathology in aorta was reconstructed from computed tomography–angiography (CT-A) using software Blender 2.91. (Blender Foundation, Netherlands), which floods the volume portions having the same Hounsfield units (HU) with finite elements. The reconstruction was not straightforward but had to be done manually piecewise and then merged, smoothed, and validated using back projection of the reconstructed geometry to the original CT-A images. The aortic wall was assumed to be with constant thickness of 2 mm with local variation around bifurcations (necessary to prevent surface intersections). Altogether the reconstruction took 4 days of tedious work. The PS geometry had AR of 1.05 and aorto-iliac angles of 148°/149° which is practically identical with our basis variant.

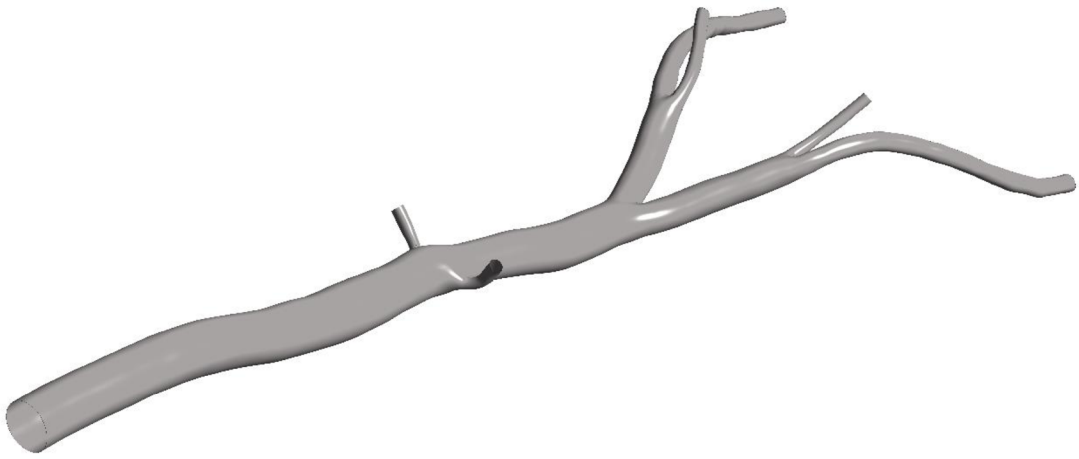

Figure 22 Isometric view on the reconstructed PS geometry used in the consequent FSI analysis.

A mapped pure hexahedral meshes of the lumen (*i.e.*, fluid) and the wall (*i.e.*, solid) were generated in Ansys ICEM CFD™. Detailed information regarding to mesh creation together with mesh sensitivity study can be found in [111].

b) Used boundary conditions and constitutive models

A hyperelastic 3rd Yeoh model (isotropic incompressible) was used for the arterial wall defined by strain energy density function [118].

$$\Psi = \sum_{i=1}^{3} c_{i0}(I_1 - 3)^i \tag{6.1}$$

where I_1 is the 1st invariant of right Cauchy-Green deformation tensor and c_{10}=78 kPa, c_{20}=0 and c_{30}=27 kPa are material constants, corresponding to the elastic modulus of aorta at circumferential stretch of 1.15 and axial stretch of 1.08 of some 400 kPa which matches the values observed *in-vivo* [15]. The solid part was solved using FE software Ansys®. The applied axial pre-stretch of λ_{ax}= 1.08 represents a typical value for 60 years old patients [119]. This was done by fixing the geometry at the apex of the bifurcation and by moving up the upper end of thoracic aorta axially by 30 mm. Circumferential displacements were constrained at this end, keeping thus only radial displacements free. An axial pre-stretch of $\lambda_{ax} = 1.16$ was prescribed in the same manner in renal arteries. In contrast, iliac arteries were not stretched but only fixed at their ends since it would cause their bending rather than stretching due to their curvature. The above values were introduced in the first loadstep and kept constant during all the simulation.
Blood was modelled as laminar flow of non-Newtonian liquid using Carreau model with viscosity being a function of shear rate $\dot{\gamma}$ as follows:

$$\eta = \eta_{inf} + (\eta_0 - \eta_{inf})[1 + \dot{\gamma}^2 t_0^2]^{\frac{n-1}{2}} \tag{6.2}$$

where n=0.3568 is a power law index, time constant $t_0 = 3.313\ s$, while $\eta_0 = 0.056\ Pa \cdot s$ and $\eta_{inf} = 0.0035\ Pa \cdot s$ refer to shear viscosities at zero and infinity strain rates, respectively [120]. The fluid part was solved using Ansys® Fluent® software applying finite volume method. The velocity waveforms for the thoracic aorta inlet and renal outlet BCs together with the pressure waveform for iliac outlets were adopted from literature [19,121]. We have applied the same BCs for all cases because it is known that the flow through severely stenosed arteries (carotid or iliac) is kept constant up to 65 - 85% area reduction [96,122]; probably it is thanks to distal adaptation of the vascular resistance. Thus, the same mass flow was preserved at the aorta inlet also for the cases with narrower iliac arteries. However, the input and output BCs

are shifted against each other (see Figure 23) and this time delay differs between young and older individuals to consider their different AA wall stiffness. Instead of highly simplified Moens-Korteweg equation assuming all parameters constant along the tube length, we considered also the tapered shape of arteries and the non-linear response of their wall by using the P - U loop method [106] for determination of the specific time delay. The method assumed that only forward waves are present which is true only for a phase right at the start of systole. Therefore, PWV was computed for particular parts of the arterial tree and shows an increasing trend towards the periphery (PWV ~ 7,3 and 8,8 m.s-1 for infrarenal aorta and iliac artery, respectively), which is in line with normotensive older (> 60 years old) individuals [123]. After this adaptation we reached the pressure and velocity waveforms along the abdominal aorta within their physiological ranges [124]. It is noted the same analysis was done also for the PS geometry. Finally, the problem was modelled as transient with time step size set to 0.003 *s* and 3 heart cycles were simulated; the data from the last cycle was considered as stable (see [111] for detailed fluid, solid and coupling setup).

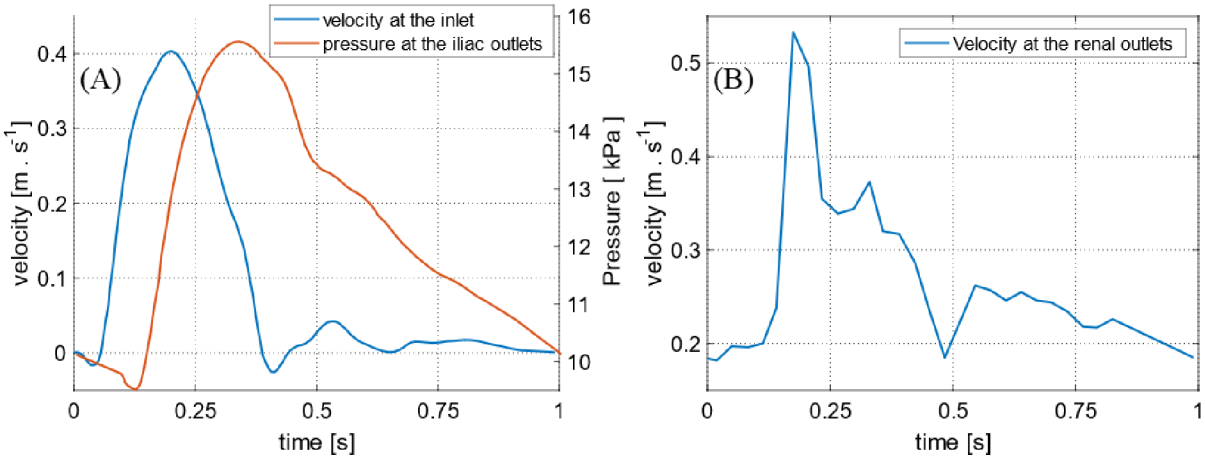

Figure 23 (A) - Pressure and velocity BCs adopted from a healthy young individual. (B) – Mean velocity waveform at renal arteries as a result of averaging over six healthy individuals.

6.1.3. Results

For each geometry, first principal stress (FPS) and pressures were recorded at three different locations along the AA (z = 30 mm, z = 75 mm and z = 120 mm). Relative change of circumferential strains was between 7.8% and 10.6% along the aorta, which is within the range reported in *in-vivo* measurements [115]. Further validation of the model via PWV, pressure and velocity waveforms can be found in [111].

a) Influence of bifurcation geometry on pressure and stresses

Pressure waves in the AA (z = 75 mm) are shown in for one extreme variant (150°/30° – see Figure 20 bottom) and for the basis (150°/150° – see Figure 20 top) with AR = 1, 0.67 and 0.5. The impact of aorto-iliac angles on the pressure wave and the SBP is negligible, in contrast to the more significant impact of the AR, increasing to + 0.67 kPa (*i.e.*, 4.1% of systolic and 10.2% of pulse pressure) and +1.22 kPa (*i.e.*, 7.5% of systolic and 18.8% of pulse pressure) for the ratios AR = 0.67 and AR = 0.5, respectively. The PS variant exhibited almost identical pressure waveforms as the basis (Figure 24, solid orange vs black dashed curve).

The resulting FPS in peak systole can be seen in Figure 25 for all the geometrical variants at three chosen positions along the AA. Again, variation along the AA is due to the changing dimensions while the results are practically independent of bifurcation angles (differences

below 2%). Conversely, significant increase of FPS along the AA can be seen with decreased AR ratio. The PS variant exhibits FPS along the AA between 60 and 93 kPa (see Figure 26) which is close to values for the basis variant.

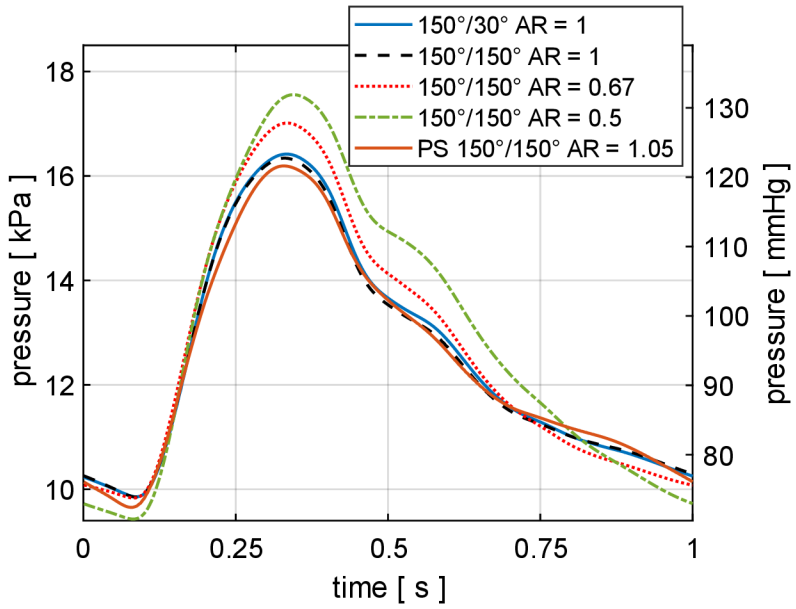

Figure 24 Evolution of pressure in time in abdominal aorta (AA) (z = 75 mm) for an extreme combination of angles (150°/30°) and for the basis (150°/150°) with AR = 1, 0.67 and 0.5. Moreover, results from the patient-specific variant similar to the basis is depicted (orange curve). We can see a negligible effect of aorto-iliac angle and a significant pressure increase with decreasing iliac diameters (AR).

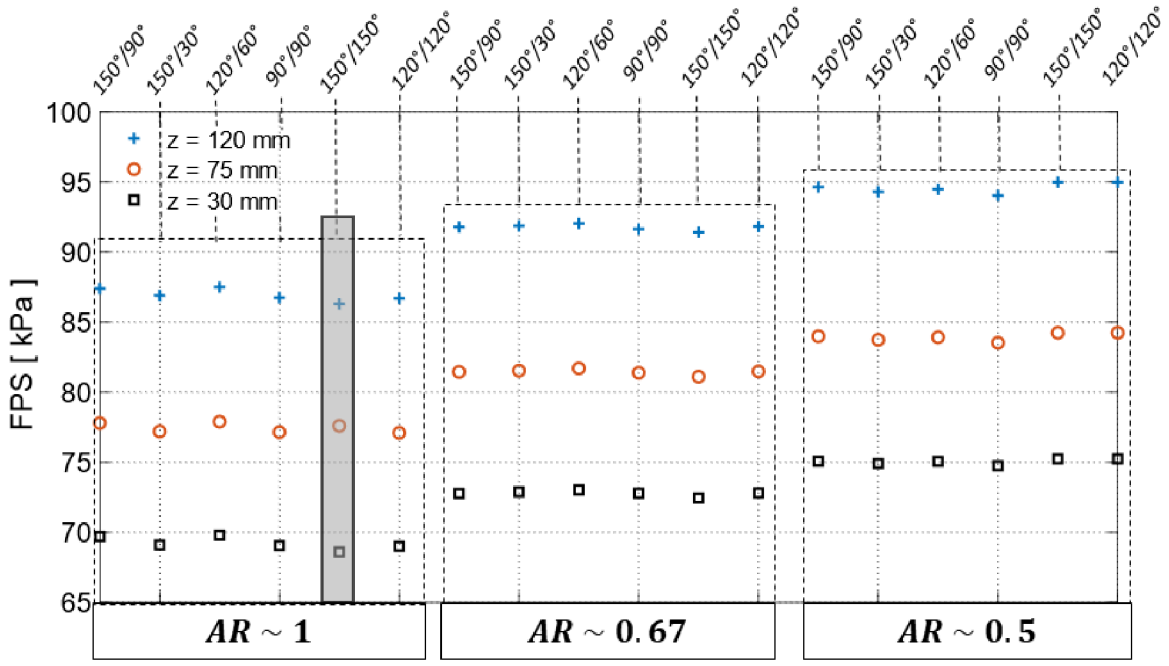

Figure 25 Effect of aorto-iliac angles and ratio on peak wall stress at three locations along the AA. We can see a negligible effect of aorto-iliac angle and a significant stress increase with decreasing AR (i.e., decreasing iliac diameters). The grey rectangle represents the span of FPS along the AA in the PS variant.

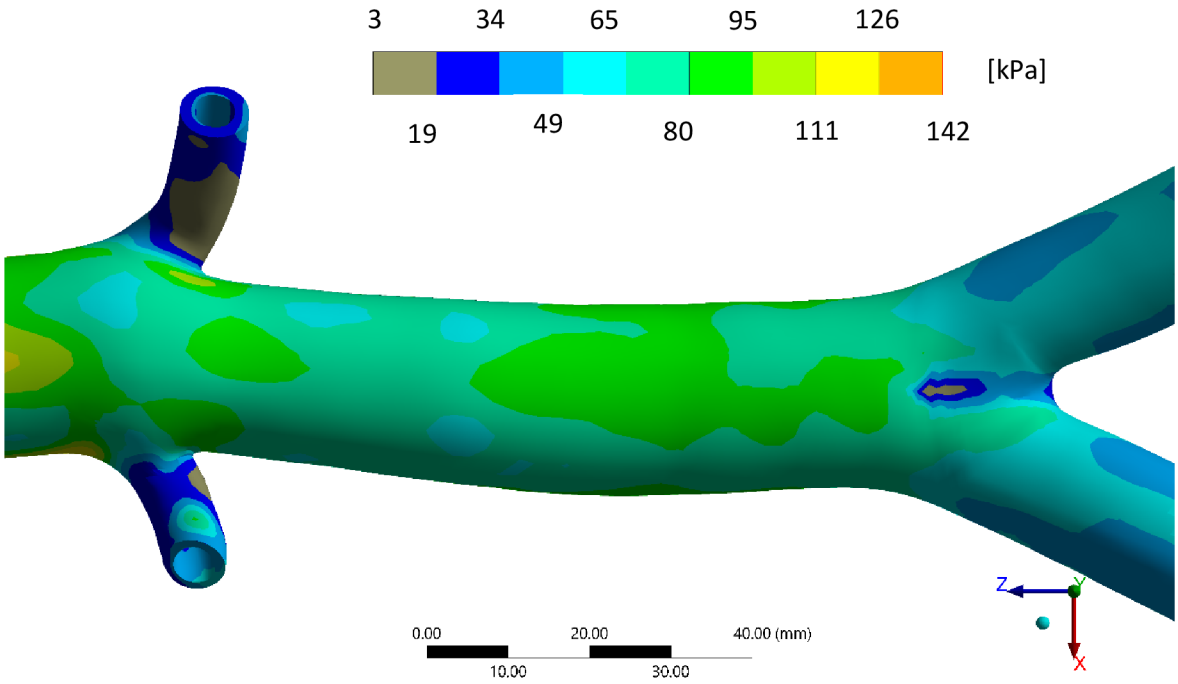

Figure 26 Map of FP stresses along the AA in the PS variant. The PS variant exhibits FPS along the AA between 60 and 93 kPa which is close to values for the basis variant.

6.1.4. Discussion

In this study we have investigated the effect of aorto-iliac geometry variations on the peak pressure and FPS in AA via two-way weakly coupled FSI parametric analyses using (i) realistic constitutive models for both arterial wall and blood, (ii) realistic axial prestretch of AA and (iii) realistic (deformed) arterial wall thicknesses and diameters. The idealized geometries were validated with a PS geometry confirming that the simplification necessary for parametric analyses did not affect the drawn conclusions and their applicability. Moreover, we have focused on a proper time shift between fluid phase boundary conditions which is not common in these analyses [102,104].

a) Aorto-iliac angles do not affect BP in AA

We have shown the effect of aorto-iliac angle on SBP and FPS is negligible across wide variety of considered geometries (see Figure 25). Our results are in agreement with previous experimental studies [112,114] while they seem to be in contradiction to previous computational studies [102,104] showing some increase in SBP and FPS in the wall. However, those studies analyzed an AA with aneurysm while we focused on stresses and BP in a non-dilated AA. Moreover, the discrepancy could be related to different boundary conditions for the solid phase. The mentioned studies have not applied any axial pre-stretch, thus the axial movement at the bifurcation was hardly constrained, especially in the cases with higher iliac angles. This resulted in higher PWS at the apex and on the sides of the bifurcation. Our model with axial pre-stretch applied on the AA does not show this dependence and we believe to be closer to reality.

The pressure elevation occurring proximally to the bifurcation might be also influenced by the pressure BCs on the output. To test this effect, we have switched the pressure BCs at iliac arteries to velocity BCs. Since the fluent solver would be unstable with only velocity inlet and outlets boundary conditions, a pressure waveform was imposed at the inlet and the analysis was

performed again; the impact of this BCs exchange was negligible, even smaller than that of the mesh density.
Another substantial difference is the time shift between BCs applied in our study. We have shown that unrealistic BC shifts lead to an increase or decrease of BP in the AA as shown in [111]. Unfortunately, studies [102,104] did not synchronized BCs which may explain the different conclusions.

b) *Decrease of iliac diameters increases BP in AA*

Contrary to the negligible effect of the aorto-iliac angle we observed significant dependence of BP on iliac diameters (*i.e.*, the AR ratio). In our simulations, the decreased dimensions of iliac arteries increase their resistance, which results in a higher pressure along the AA due to higher and earlier wave reflection. Thus the 50% iliac stenosis leads to FPS increase in the AA of some 8% (see Figure 25). Although this is certainly not enough to cause any immediate problems, its cumulative effect with other risk factors may accelerate a potential development of AAA. Moreover, for development of vascular diseases, not only the SBP but also pressure pulsations might be important and their relative magnitude increased by 19%. That would be in line with clinical observations showing the veterans with lower limb amputation (*i.e.*, occlusion of one iliac artery) have much higher prevalence of AAA [125]. Occlusion of one femoral artery due to amputation is similar to 50% stenosis of both iliac arteries simulated here. Comparison to other studies [102,104] is not possible because they did not vary the AR. This comparison confirms the novelty of our study, specifically in the variation of several geometric parameters and in the careful validation of the calculated velocity and pressure waveforms.

c) *Potential limitations*

Several limitations should be considered when interpreting our results. First, isotropic homogeneous material model of arterial wall was used, although it is known the mechanical properties of real arteries are anisotropic and they change along the arterial tree [126]. As the isotropic model was set to give realistic circumferential strains and axial stiffness may differ, we evaluated only circumferential stresses (FPS) while axial stresses were considered unrealistic. Second, we used idealized and simplified geometries for a parametric analysis. Although realistic geometries can be used already in FSI simulations [105,127], they are extremely demanding to manual reconstruction (9 days of manual work in our case)and computer time and thus not suitable for numerous simulations; moreover, they disable parametrization of the models needed for our study design focusing on impact of specific geometrical parameters. Also, it is expected that more PS geometries would increase the variability of obtained FPS in the AA due to local geometrical variations, thus even more cases would be needed to show the same effect. Nevertheless, the results of the PS variant were in excellent match (in terms of SBP) with the idealized results and have not evoked any doubts on falsified the validity of our study. Third, smaller arterial branches were neglected in the model because there is little information about their blood flow in the literature and their marginal effect on AA haemodynamic is expected [15].

6.2. CFD simulations on patient-specific carotid arteries: effect of flow waveform

The main goal of this computational study is to assess the influence of young versus old archetypal flow waveforms on hemodynamical conditions in PS human carotid artery bifurcation geometries. Based on the research performed, we pointed out that the shape of the flow waveform changes with age of the individual (similarly as arterial hypertension) and is closely related to stiffness of his/her arteries. It was also shown that physical exercising, healthy lifestyle or antihypertensive treatment can shift the shape of the flow wave close to a young and healthy one via lowering the arterial and peripheral stiffness. Taking these pieces together, a new mechanism how these factors attenuate the risk of atherosclerosis is shown below.

I am working on a manuscript to be submitted to an IF journal within a few months. I formulated its basic idea and concept and did also most of the research, simulations, and methodology proposal. Thus, I will be the first author of the manuscript. Nevertheless, since it is a greatly interdisciplinary problem, many other colleagues were involved. Dr. Petr Hájek was responsible for geometry reconstruction from CT-scans. MUDr. Tomáš Křivka had been searching within FNUSA database for suitable subjects with emphasis on variable carotid artery bifurcation geometry. MUDr. Tomáš Novotný, PhD. helped me a lot with the research regarding to the effect of antihypertensive drugs on compliance of (mainly peripheral) vessels. Jiří Kohút created the finite volume meshes for each geometry and also wrote a script for an instantaneous 3D parabolic velocity profile which was computed from volumetric flow BC. This script was used as input BC at the carotid artery inlet. Martin Formánek helped me with an estimation procedure used for determination of parameters needed for outlet BCs. Prof. Jiří Burša, PhD. was responsible for review, editing and formal analysis.

To understand properly this analysis, it is recommended to keep in mind the information written down in the chapters 3.3 and 3.4.

6.2.1. Introduction

Many similarities can be seen between the blood flow dynamics within subjects with the age-related elevation of arterial stiffness [84] and those with arterial hypertension [85]. In addition, the archetypal flow waveform shapes for young and old subjects can be found for the human carotid artery in the literature [84,128,129]. The most pronounced differences occur in presence of late systolic peak (see Figure 27, point V_2) which probably arise from the earlier return of the reflected waves (compared to young ones) from local upper-body sites and their interaction with later wave reflections returning from the opposite direction from sites in the lower part of the body in case of old waveform (see Figure 27, red triple arrow) [15,84]. Their earlier return is probably the result of increase in PWV due to increase in arterial stiffness with age. Contrary, only one systolic peak exists in case of the young flow waveform and wave reflection from the upper and lower body can be described separately (see Figure 27, early and later black triple arrow, respectively) [15]. Since arterial stiffness can be lowered through long-term application of all five basic groups of antihypertensives (angiotensin-converting enzyme inhibitors–ACEi, angiotensin receptor blockers–ARB, calcium channel blockers–CCB, beta-blockers, and diuretics) [40,45,46,130], possible benefits of such medical therapy could be not only in lowering the BP and peripheral resistance as mentioned in literature [40,46,130,131] but also in improving other hemodynamic conditions such as WSS.

Nevertheless, I and my co-workers have found only one comprehensive hemodynamic analysis of this phenomenon [132]. This numerical study reported negligible hemodynamic differences

between representative young and elderly waveforms for the human carotid artery. Although the conclusions stated in [132] were formulated on the basis of nine PS geometrical models, their inter-subject variability was quite low. Moreover, they used archetypal waveform referenced as young from [133] where 17 young, normal volunteers were measured, despite of existence of a more statistically significant study [129], where the authors recorded and analysed 3560 cardiac cycles in total (with the same number of volunteers) to assess inter- and intra-subject variability. Above that, we decided to extract the flow waveform from the latter study for two more reasons: (i) the instantaneous velocities were measured with temporal resolution three times shorter (*i.e.*, of ~ 12 ms for the [129] while ~ 36 ms in case of the [133]); (ii) the flow archetypal waveform are in line with that reported in [128] where also detailed reasoning of such shape is introduced on the basis of aortic valve closure and reflected waves from the upper and lower part of the body.

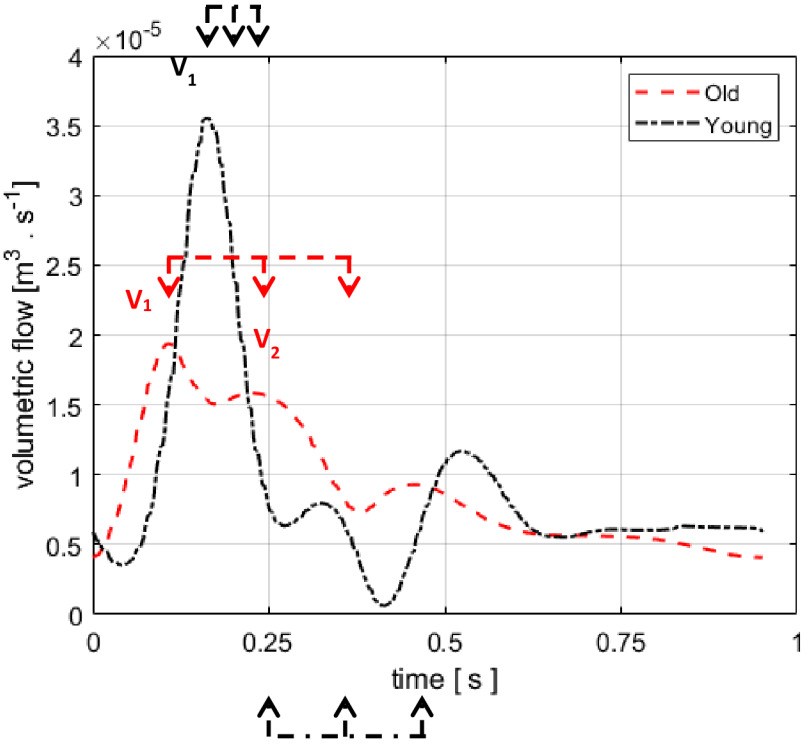

Figure 27 Comparison of the young and old flow waveforms (black and red curves, respectively). The most pronounced difference occurs in presence of late systolic peak (point V2) in the old waveform while only one systolic peak exists within the young flow waveform.

In the current study, we aim to assess the hypothesis stated in [132], that the differences between young and elderly archetypal waveforms have a negligible impact on hemodynamics and thus on elevated risk of the atherosclerosis development. This is done via 3D transient computational fluid dynamics (CFD) analysis of five PS geometries of human carotid arteries with archetypal flow waveform shapes corresponding to healthy young and elderly individuals extracted from the two most relevant *in-vivo* studies [84,129]. The geometries have been selected with emphasis on a pronounced inter-subject variability and thus we believe our results can further strengthen or dispute the conclusions in [132]. Moreover, this is the first study trying to quantify the influence of hypertension or true aging process on hemodynamics in a carotid artery and to elucidate possible mechanisms for secondary benefits of the anti-hypertensive drugs therapy within these groups.

6.2.2. Methods

a) Study subjects and imaging protocols

The carotid arteries with characteristic shapes of the bifurcation were chosen from a set of 89 patients supplied from St. Anne´s University Hospital Brno deposit. A CT imaging protocol was performed using a Brilliance iCT 256 scanner (Phillips Medical Systems, Eindhoven, the Netherlands). All patients underwent the CT protocol including a non-contrast CT (nCT) of the brain and a multiphase CT angiography (mCTA) of the head and neck. The mCTA scanning was performed from the aortic arch to the vertex. The mCTA images were acquired with the following scan parameters: slice thickness of 0.9 mm, spacing between slices of 0.45 mm, field-of-view of 250 mm and acquisition matrix of 512 pixels with in-plane resolution of 2.048 pixels per mm (thus, pixel spacing 0.489/0.489). Five healthy subjects (61±27 years old) without known coronary, cerebral, or peripheral artery disease and without carotid artery stenosis were selected for the current study, with an emphasis on heterogeneous carotid anatomy such as a diverse bifurcation geometry (angle, curvature). A written informed consent was obtained from all participants to the use of their health records for scientific and research purpose.

b) Lumen geometry extraction

Typical provided raw data originated from CTA scans with the in-plane resolution of 2.048 pixels per mm and with the slice spacing of 0.45 mm. Thresholding and segmentation were done manually in the open-source ImageJ software (https://imagej.net/software/fiji/downloads) and the proprietary licensed Medical 3D Image modeling software [134], respectively. Subsequently, the obtained stereolithography (STL) models were smoothed and regularized in the GOM Inspect software (https://www.gom.com/en/products/zeiss-quality-suite/gom-inspect-pro) with the surface tolerance below 0.2 mm, which lied safely below the mCTA scan resolution. The STL meshes were interpolated by the non-uniform rational base spline (NURBS) surfaces in Catia V5R21 (https://www.3ds.com/products-services/catia/). The final surface body of the carotid artery was equipped with a circular inlet situated one millimeter below the caudal plane of the artery. The inlet is located at least in a distance equal five times the diameter of the artery upstream to carotid bifurcation. Outlets from the internal (ICA) and external carotid artery (ECA) were cut just before a next bifurcation.

c) CFD simulations and boundary conditions

Five finite volume models of PS geometries of human carotid bifurcations were created based on mCTA scans. Laminar blood flow was modeled in Ansys® Fluent® using Carreau model of non-Newtonian incompressible liquid with viscosity being a function of shear rate $\dot{\gamma}$ as presented in chapter 6.1.2.

To avoid an unrealistic piston profile at the inlet, an instantaneous 3D parabolic velocity profile was computed from volumetric flow BC and implemented (via user-defined function - UDF) in Ansys Fluent. In total, two different (old [84] and young [129]) archetypal flow waveforms were used. In order to create the 3D parabolic velocity profile, the mean velocity obtained from the archetypal waveform was inserted into the analytical solution of a parabolic profile. Such a profile (either old or young) could be applied to the circular inlet of the CCA. Even though the Womersley velocity profile is more credible (unsteady term is included), the results of individual solutions are almost identical for both young and old flow waveforms (see Figure 28A and B for comparison of velocity profiles computed from the old and young flow waveforms for Womersley and paraboloid solution depicted every 0.05s within the cardiac cycle – orange vs blue curves, respectively). The preference of the pulsatile paraboloid velocity

profile over the Womersley profile is also supported by the study [135]. For both young and old waveforms, the periods were set to 65 bpm and the cycle-averaged flow rate for the CCA was allometrically scaled by the ratio of the CCA area to the average CCA area over all the subjects, as recommended in [136]. Moreover, young flow waveform was scaled by factor 1.08 to ensure the same cycle-average flow as the old one.

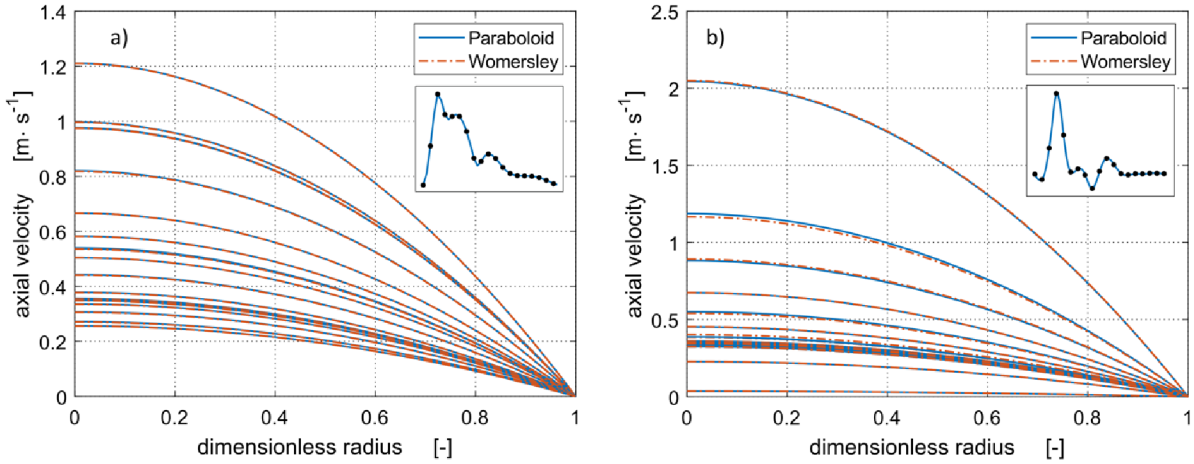

Figure 28 A comparison of velocity profiles computed from the old (A) and young (B) flow waveforms for Womersley (orange dash-dotted curves) and paraboloid (blue curves) solution depicted every 0.05s within the cardiac cycle. Since the curves are almost identical (hardly distinguishable in the figure), an easy-to-solve/implement paraboloidal profile was used in 3D-0D simulations.

A 3-parameter Windkessel model (3WK) was imposed at each outlet via UDF to create a complete 3D-0D model of the carotid artery (3D model) and its periphery (0D model). To estimate its parameters efficiently, a lumped-parameter (*i.e.*, 0D only) model of the whole carotid arterial tree (from CCA to periphery) was created in MATLAB® Simulink® 2022b (the Simulink file with the lumped-parameter model of carotid artery can be found in the supplementary material). The lumped-parameter model consists of:

- two 3WKs connected to the ICA and ECA outlets representing the periphery (see Figure 29 - blue box). Its suitability for such purpose was proved elsewhere [57,94,97].
- three 2WKs representing each segment of carotid artery (*i.e.*, CCA, ECA and ICA). Each 2WK consists of one resistance term (R_{CC}, R_{IC}, R_{EC}) and one inductance term (L_{CC}, L_{IC}, L_{EC}) connected in a serio-parallel manner (see Figure 29 – red boxes). Since we are interested in the old patients having commonly stiffer arteries, the compliances C of individual segments were not considered.

The initial values of the resistance R and inductance L (i.e., 2WKs) for the CCA, ICA and ECA segments with length l and inner radius R_0 were computed from equations (6.3 and 6.4) based on averaged dimensions and steady and Newtonian flow assumptions [57]:

$$R = \frac{8l\eta}{\pi R_0^4} \qquad [\text{N s m}^{-5}] \qquad (6.3)$$

i.e., Hagen-Poiseuille eq. where η is dynamic viscosity.

$$L = \frac{\rho l}{\pi R_0^2} \qquad [\text{kg m}^{-4}] \qquad (6.4)$$

where ρ represents blood density.

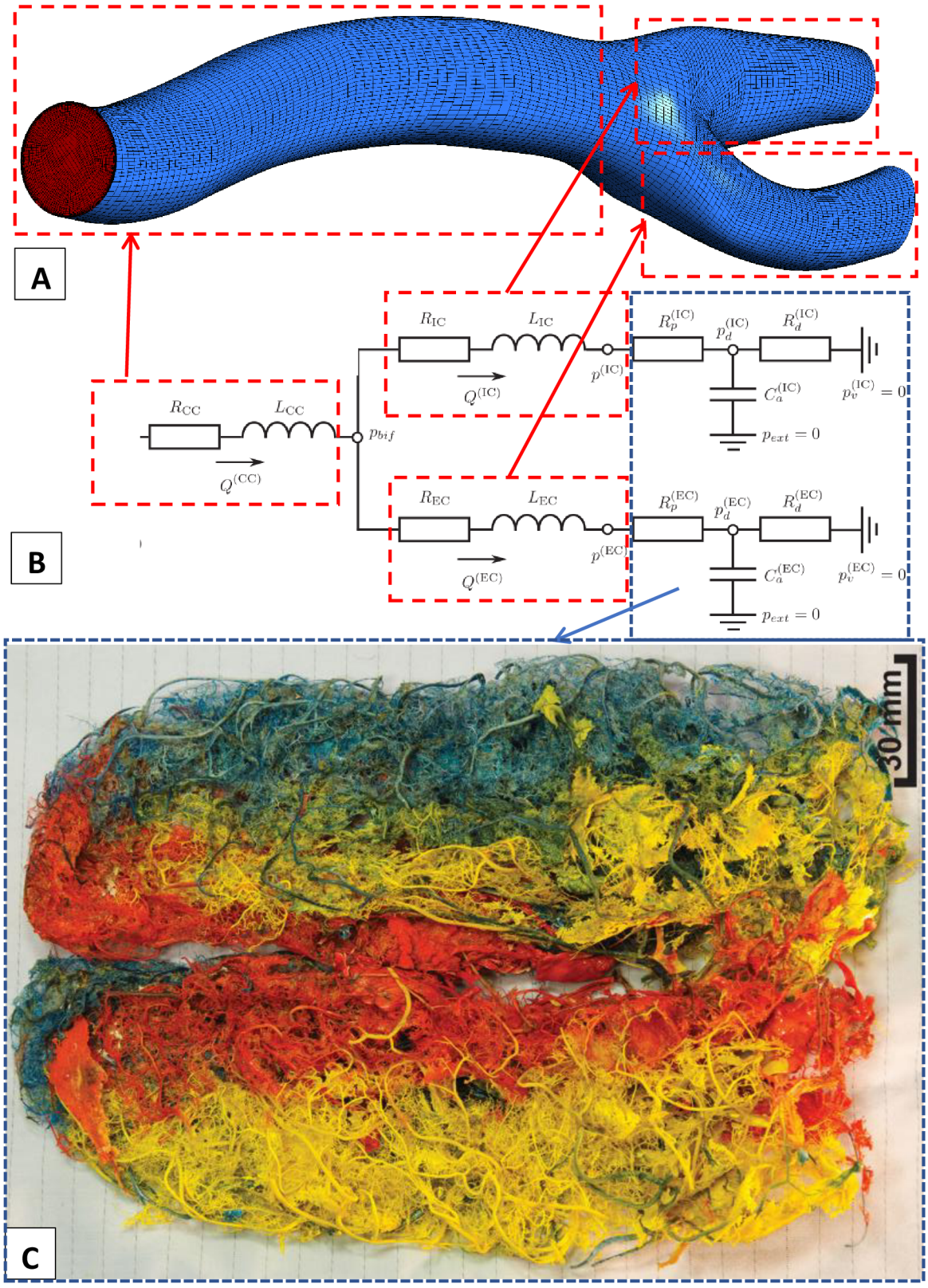

Figure 29 (A) A 3D model of patient-specific carotid artery and (B) its corresponding reduced-order model representation (Modified from [57]*). (C) The plastic cast of the full cerebral arterial circulation used here as an example of the cerebral periphery downstream to the carotid artery (Modified from* [17]*)*

Then, the initial values for the periphery (i.e., 3WK) were extracted from [57].
Since an initial parameter guess is known, the parameter estimation procedure was used to obtain an estimate of the 3WK parameters of the periphery while the other parameters were fixed. The flow waveform at the CCA [84] was used as input to the lumped model while the flow waveforms measurements at the ECA and ICA outlets [84] were used as reference signals. The unknown parameters (*i.e.*, R_p^{IC}; R_p^{EC}; R_d^{IC}; R_d^{EC}; C_a^{IC}; C_a^{EC}) were estimated by minimizing the error between outputs from the model and the reference signals via nonlinear least-square method. This system of differential and algebraic equations (DAE) was implemented into Simulink environment. The solution of these equations was obtained from Simscape™ DAE solver with a default configuration.
Thereafter, the parameter estimates (R_p^{IC}; R_p^{EC}; R_d^{IC}; R_d^{EC}; C_a^{IC}; C_a^{EC}) were used to start the 3D-0D (multiscale) simulation. Only two iteration cycles based on the results from 3D-0D simulation were needed to satisfy the root-mean-square-error < $3.5e^{-7}$ between the reference signals (*i.e.*, measurements) and the 3D-0D model (see Figure 30). However, it can be anticipated that more iterations will be needed as the number of outlets increases. A general methodology (independent of the estimation algorithm) was described in chapter 3.4 (see Figure 10). A detailed description of the methodology can be found in Figure 31.

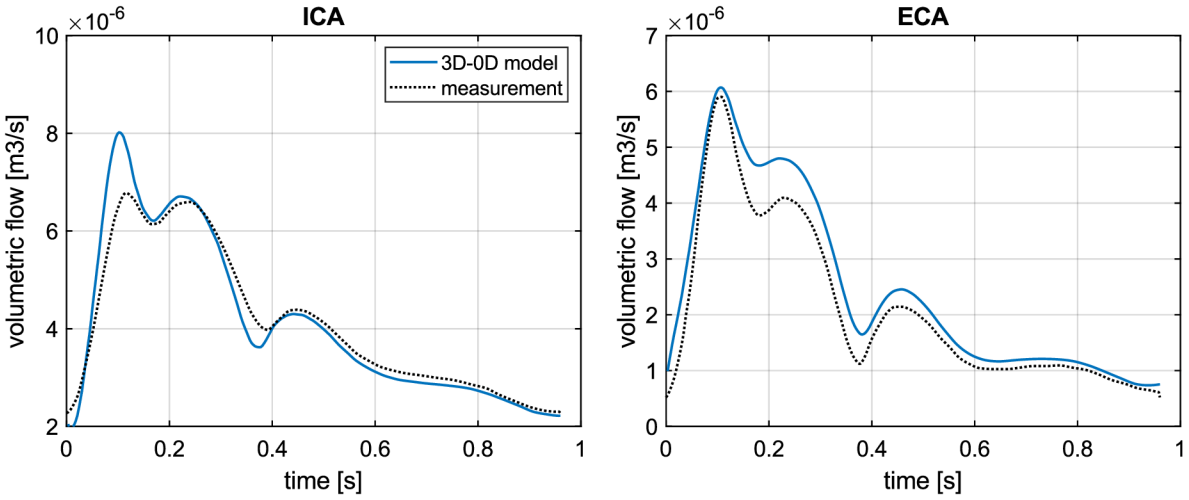

Figure 30 Comparison of the reference signals (measurements) and flow waveforms from 3D-0D simulation at the outlets from internal (left) and external (right) carotid artery after second (final) iteration cycle. Root-mean-square-errors are < $3.5e^{-7}$.

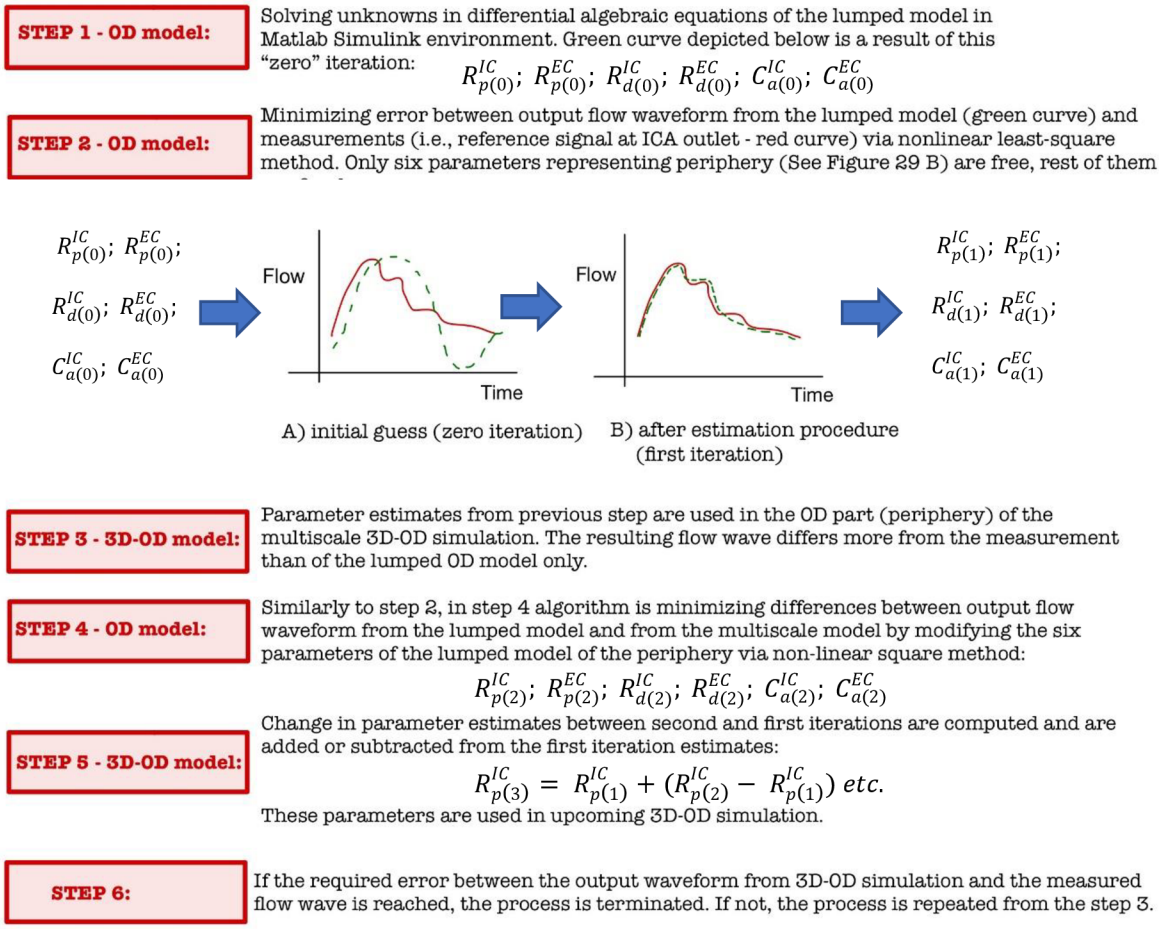

Figure 31 Step-by-step procedure for finding parameters which represent a periphery downstream the carotid artery while the required flow waveforms in the ECA and ICA are achieved. The symbols are introduced in Figure 29.

d) Mesh and model validation

A mapped pure hexahedral mesh of the carotid lumen was generated in Ansys ICEM CFD™ (see Figure 32). Around 48 elements across the CCA diameter were used with their axial length of ~ 0.8 mm and radial size changing from ~ 0.015 mm to ~ 0.14 mm between the wall and the central region (see Figure 32B) to capture the steep changes in the boundary layer. The axial direction is not so prone to changes as radial, nor the circumferential, so the discretization in these directions is not so strict and is mostly set to default. Lower limit of number elements was set to 300k, since it is important to satisfy the requirements of the computational viscous model (e.g., $y+$ values) and also to preserve the good quality metrics at the same time (i.e., maximal aspect ratio and minimal skewness were 65 and 0.33 whereas their average values were 12.4 and 0.93, respectively). For a mesh sensitivity study, this basic variant was compared with a mesh refined to 1000k; the velocity profiles matched well and differences remained < 2% for most of the cardiac cycle. The computational domain was discretized in time with a step size of 0.003 s. To meet the required convergence criteria, the solver iterated until the residuals were less than 10^{-4} for continuity equation and 10^{-6} for velocity components at the end of each time step. When the quantitative differences in velocities between the 2nd and 3rd period were < 1%, the 2nd cycle was considered as stabilized. It is worth to note that mesh sensitivity study was performed with k - ω SST model of turbulence with low-RE corrections to verify laminar flow assumption. Some minor changes between k - ω SST and laminar model were observed.

Despite of this, we chose laminar model since the main purpose of this study is primarily a relative comparison between two archetypal flow waveforms.

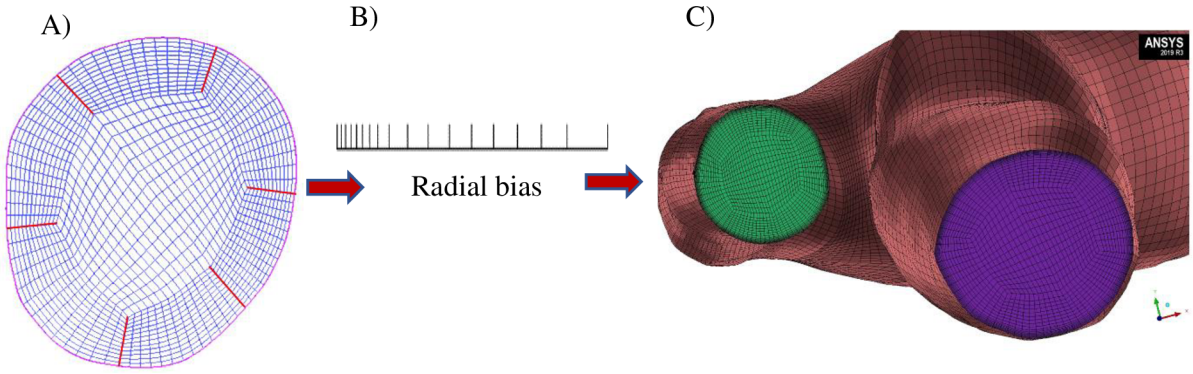

Figure 32 Pre-meshing and its feature for radial discretization. A) Hexahedral mesh of the outlet from ICA. B) Changes in element size with distance from the wall along each radial edge (red lines in fig. A). C) – Final mesh of the PS carotid artery respecting linear law discretization in radial direction.

e) Scalar metrics of disturbed flow

A time-averaged wall shear stress (TAWSS) together with a relative residence time (RRT) were used as hemodynamic indicators for the risk of atherosclerosis development. The former has high sensitivity and low positive predictive value (PPV) while the latter has the opposite [137]. Regions are classified as atheroprone (from a merely fluid dynamic point of view) if TAWSS is < 0.48 Pa and RRT > 2.9 Pa^{-1} [132]. TAWSS and RRT were derived from the calculated wall shear stress field using MATLAB® and Ansys CFD Post™. In order to calculate RRT, oscillatory shear stress (OSI) was defined where zero value corresponds to purely unidirectional flow while 0.5 represents purely oscillatory flow. All of these parameters are defined according to [137]:

$$TAWSS = \frac{1}{T}\int |\boldsymbol{\tau}|\, dt \tag{6.5}$$

$$OSI = \frac{1}{2}\left(1 - \frac{\left|\int_0^T \boldsymbol{\tau} dt\right|}{\int_0^T |\boldsymbol{\tau}| dt}\right) \tag{6.6}$$

Here $|\boldsymbol{\tau}|$ is magnitude of the instantaneous wall shear stress vector τ (*i.e.,* tangential component of the traction vector) and T is the duration of one cardiac cycle. Finally, RRT can be defined through TAWS and OSI:

$$RRT \sim [(1 - 2\, OSI)\, TAWSS]^{-1} \tag{6.7}$$

6.2.3. Results

Results were extracted from the 2nd cycle of the transient 3D CFD simulations in which a stabilized cyclic response was reached. They show a significant reduction of the TAWSS risk areas (*i.e.,* areas showing TAWSS below its threshold value of 0.48 Pa) for the young archetypal waveform (see Figure 33 and Table 2). Moreover, TAWSS risk areas are totally missing in the patients 2 and 5 thanks to the favourable influence of the young waveform (see Table 2, second row). The RRT risk areas (i.e., areas with RRT above the threshold value 2.9 Pa^{-1}) are not depicted. Only their quantitative evaluation can be found in the Table 2. When RRT risk areas from old and young cases are compared, only minor changes with unclear trend can be observed.

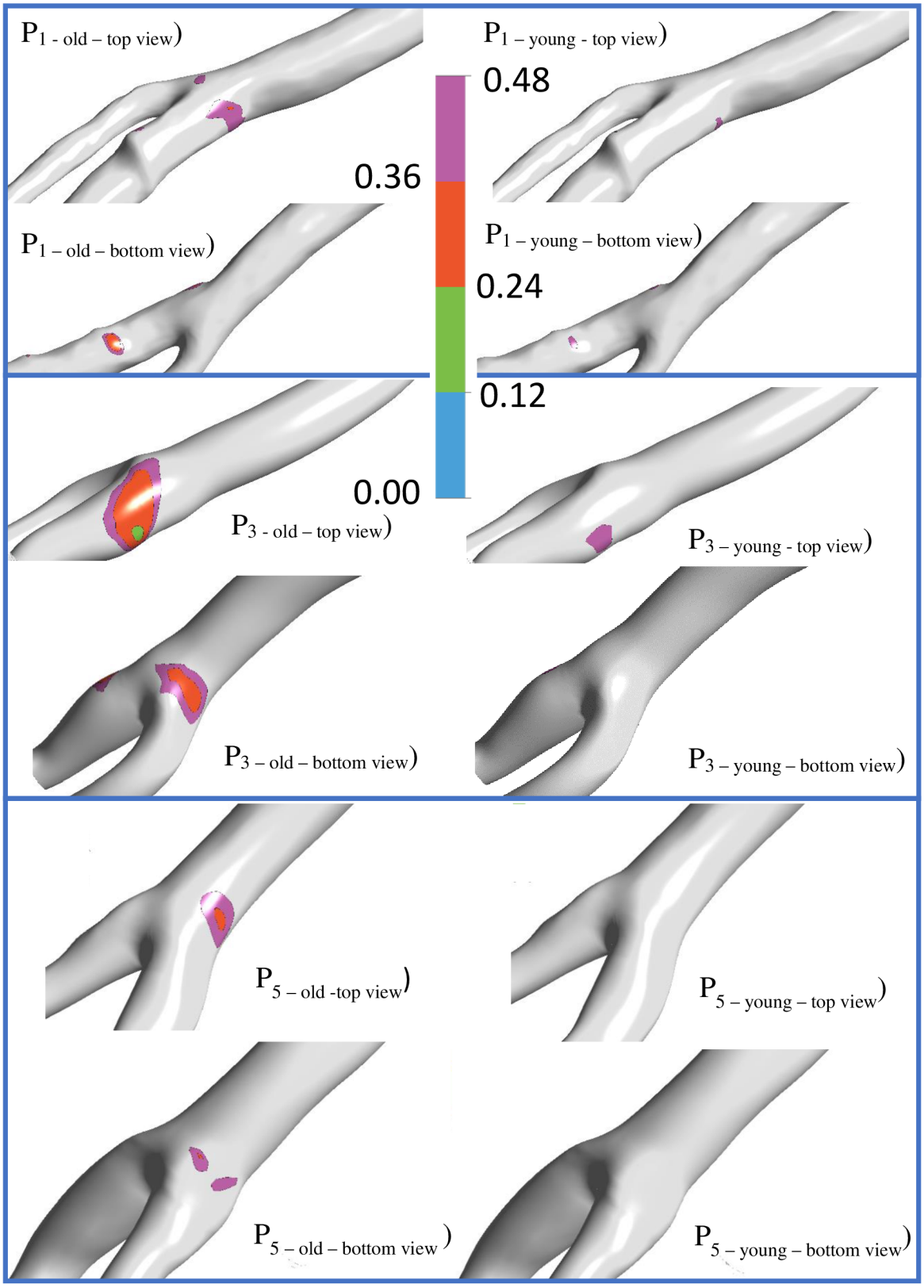

Figure 33 Maps of the time-averaged wall shear stress for patients 1, 3 and 5, respectively. Results for the old (left) vs young (right) archetypal flow waveforms and in top(upper) and bottom (lower) views show significant reduction of the risk factor for the young flow wave form. Three representative geometries were selected for qualitative comparison.

Table 2 Δ_1 represents a relative change of the TAWSS and RRT risk areas due to application of the young flow waveform against the old one.

	TAWSS risk area [m^2]		Δ_1 [-]	RRT risk area [m^2]		Δ_1 [-]
	Old	Young		Old	Young	
P1	2,17E-05	1,99E-06	-91%	2,18E-05	2,59E-05	19%
P2	4,43E-05	0,00E+00	-100%	4,53E-05	4,32E-05	-5%
P3	8,67E-05	8,78E-06	-90%	8,00E-05	7,12E-05	-11%
P4	1,11E-04	3,36E-05	-70%	1,08E-04	9,65E-05	-11%
P5	1,88E-05	0,00E+00	-100%	2,76E-05	2,13E-05	-23%

To compare our results with clinical outcomes from [138][139], we have evaluated that the area-averaged TAWSS decreases on the straight CCA segment if the young flow waveform is used instead of the old one. Moreover, we added similar comparison in the risk areas (*i.e.,* areas showing TAWSS below its threshold value of 0.48 Pa). For the old flow waveform, the area-averaged TAWSS over straight CCA segments is by 11 – 18% lower (*i.e.,* more risky) than for the young waveform while these percentage of decrease is 2.5 – 4.5 times higher in the risk areas (see Table 3).

Table 3 Δ_2 represents a relative change of area-averaged TAWSS due to application of the old flow waveform against the young one.

	straight CCA segment			risk area		
	area-averaged TAWSS [Pa]					
	Old	Young	Δ_2 [-]	Old	Young	Δ_2 [-]
P1	1,73	1,98	-13%	0,51	0,74	-32%
P2	1,75	2,05	-15%	0,71	1,19	-41%
P3	1,19	1,45	-18%	0,44	0,77	-43%
P4	1,11	1,28	-13%	0,39	0,64	-39%
P5	1,14	1,28	-11%	0,64	1,27	-50%

The instantaneous ICA:CCA flow division varied significantly throughout the cardiac cycle. Moreover, very high values (~ 4) of ICA:CCA ratio could be observed for the young case within some 40 ms during the diastolic phase (see Figure 34B and D, extreme at time t ~ 2.3 s). This results from a nearly zero instantaneous flow at the CCA inlet. Only the results from patient 5 are depicted in Figure 34 because flow waveforms and instantaneous ICA:CCA flow divisions follow similar shape through all patients. The ICA:CCA ratios of cycle-averaged volumetric flows for all the patients are ~ 0.68 and ~ 0.64 for old and young waveforms, respectively. This represents a very good agreement with the measured value of 0.66 for an old volunteers [84].

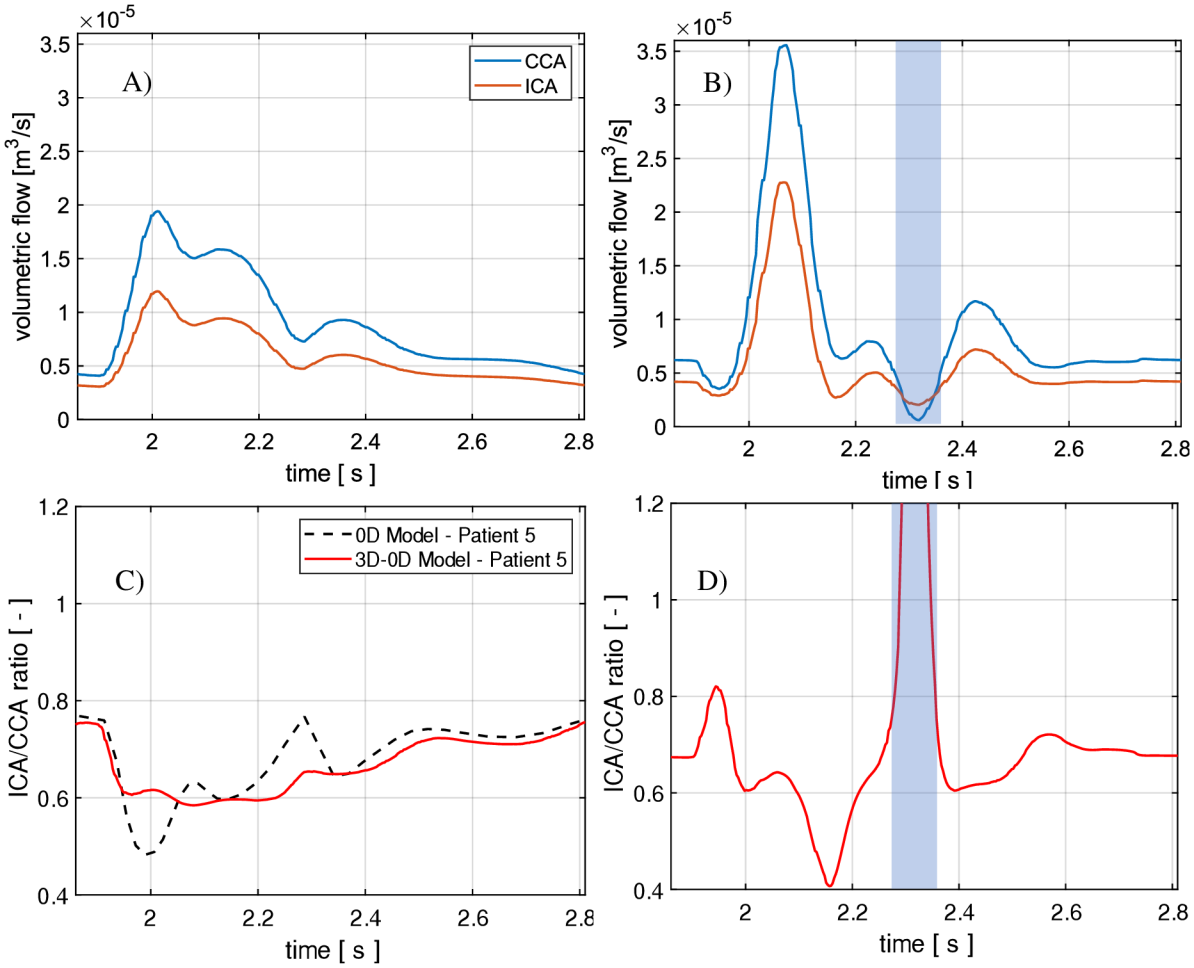

Figure 34 The representative results from patient P5 for old (left column) and young (right column) flow waveforms: volumetric flow at the CCA inlet (blue curve) and ICA outlet (orange curve), respectively (A) and (B). Instantaneous ICA:CCA flow division. In case of the young waveform, the ICA:CCA ratio shows a significant peak (~ 4) in time ~ 2.3s due to a nearly zero instantaneous flow at the CCA inlet (transparent blue rectangle).

6.2.4. Discussion

Our results are in contrast to those reported in the only one existing study on this topic [132]. They reported negligible hemodynamic differences between young and old waveforms in nine carotid arteries used in their simulations. Although the same old flow waveform was employed in our study, a substantial difference arises when the young archetypal waveforms are compared. As far as we understand the influence of aging process (as clearly reported in fundamental literature [15,84,128]), we believe that the archetypal young flow waveform [129] used in our simulations is more representative in term of young vs old typical hemodynamic differences than that measured in [133] and employed in the computational study [132]. It should be classified rather as "intermediate" than a young one. Nevertheless, the mean age of the subjects involved in these studies is identical (i.e., 28±7 vs 28±3 years for [133] and [129], respectively). Another reason for such obvious differences between these young archetypal flow waveforms might be the three times higher temporal resolution in case of [129] (12 *ms* vs 36 *ms*), which were used also in our study, enabling thus to capture high dynamics in the young flow waveform. Moreover, the study [132] computed the flow waveform at the CCA inlet on the basis of time-varying ICA:CCA flow division data (reported in [140]). The data was

recorded with even coarser temporal resolution (~ 50 ms) leading thus to further temporal distortion.

Clinical studies [138,139] reported a significant decrease (~ 15% within a 12-years period and ~ 34 – 46% within a 60-years period, respectively) in the area-averaged TAWSS within neck vessels with age. We used young and old waveforms corresponding to 28±3 and 68±8 years old subjects, respectively, and our results showing the area-averaged TAWSS are lowered by 13 – 18% (see Table 3), for the old flow waveform falling close to observed range. It is worth noting that the lower decrease in our simulations is reasonable due to the fact, that we fixed other potential contributors to the TAWSS decrease observed in those *in-vivo* studies (i.e., luminal diameter, arterial stiffness and SBP increase while blood flow decrease with age). In addition, we have shown that the area averaged TAWSS decrease is much more pronounced in the risk areas in comparison to the straight CCA artery segment (see Table 3). Nevertheless, some discrepancies regarding the cause of the area averaged TAWSS decrease have to be discussed here. Within the clinical studies [138,139] many other factors do also change, making thus almost impossible to distinct the most important contributor to the TAWSS decrease. Notwithstanding, both the clinical studies point out the main contributors are probably the increased luminal diameter together with the decreasing blood flow. The former study with older patients is longitudinal (i.e., the same patients are evaluated after 12 years from the baseline measurement) and includes 48 patients only. Although their data show very marked increase in arterial stiffness during this 12-years follow-up period (+74.5% in women and +28% in men), the authors do not discuss its potential effect on the TAWSS decrease. The latter study has 301 patients and investigates the cross-sectional area changes with the age ranging between 18-84 years. The authors are somewhat less confident in this conclusion because the most pronounced drop in TAWSS does not correspond with a significant drop in flow but do correspond with increase in luminal diameter and SBP. Unfortunately, arterial stiffness is not evaluated here. However, it is broadly recognized, that the SBP correlates positively very well with arterial stiffness. Thus, both studies show significant increases in arterial stiffness and SBP followed by a decrease in TAWSS. The results of our computational study shed some light on the potential contribution of the elevated arterial stiffness or SBP to the TAWSS decrease with arterial aging, when all the parameters were kept identical except for the flow waveform boundary condition (which represents increased arterial stiffness). Moreover, it shows that the area-averaged TAWSS decrease with the old flow waveform is much more pronounced when evaluated at risk areas instead of the straight CCA segments as commonly done in clinical studies (see Table 3).

In conclusion, as although the low TAWSS is a necessary indicator of plaque formation, it is not sufficient for reliable prediction of the future plaque location [137]. Since the low TAWSS region overlaps the region with oscillatory flow and high RRT, it seems that the significant decrease (especially in the risk areas) of the TAWSS related to the old archetypal flow waveform may increase the risk of future atherosclerosis development. This important mechanism accelerating the atherosclerotic process may be mitigated by antihypertensives or regular aerobic exercise. Both reduce the wall stiffness, transforming thus the flow waveform to a younger one and consequently decelerating the atherosclerotic process through increase of the TAWSS and decrease of the RRT in the risk regions.

- *Potential Limitations*

Although it is well reported that aging influences the flow waveform analogous to the arterial hypertension mainly due to the elevated arterial stiffness and to the consequent early return of the reflected waves, we have not found any *in-vivo* study related to the influence of antihypertensives on the flow waveform. One study [85] measured the flow waveform on 286 medically treated (calcium channel blocker mainly) patients with hypertension. They reported that the late systolic peak in velocity waveforms (see Figure 27, V_2 on the black curve) increases with age. Moreover, when the flow waveforms of subjects under antihypertensive treatment are compared with those observed in healthy elderly individuals [84] the peak V_2 is rather lower. However, it can be caused by a lower mean age (58 ± 13 years in [85] vs 68 ± 8 years in [84]). Unfortunately, flow waveforms recorded before starting the antihypertensive treatment are not available, thus it is impossible to evaluate its influence. Due to paucity of the data on the effect of antihypertensives on blood flow in carotid artery, an assumption was stated that antihypertensives shift the shape of the flow waveform typical for old or hypertensive individuals towards the young one. Although such assumption might be too optimistic, our results contribute to the strong evidence that the hypertension is a leading risk factor for major CVDs, such as heart attack, stroke, chronic kidney disease, heart failure, cognitive impairment and [15,66]. These late complications of hypertension are closely associated with the process of atherosclerosis. Even though this process is still generally poorly understood, an important mechanism playing a role in its development seems to be endothelial dysfunction [141]. Wall shear stress related to vascular hemodynamics is proven to affect endothelial dysfunction [142]. Antihypertensive drugs may improve or restore endothelial function through multiple mechanisms (direct effect on endothelial cells, hemodynamic effects, wall shear stress changes, etc.) [82]. The exact mechanisms, however, need to be elucidated in the future.

We have stated that regular aerobic exercise can lower the arterial stiffness offering thus and alternative option to antihypertensives. This statement is definitely true but data on this subject are biased by a numbers of factors with the most pronounced is that people who are ill for any reason, or have subclinical arterial stiffening or hypertension are usually not comfortable with exercise and probably will not last long with it. They are thus under-represent in group of people who engage in regular exercise [15].

Further enlargement of this study will be possible as soon as some representative flow waveforms at the carotid artery will be available on patients with hypertension before and after a medical treatment reducing the blood flow resistance and arterial stiffness.

7. Outputs of the dissertation thesis

7.1. Methodological

- Validation of FSI methodology and CFD model suitable for pulsatile flow in aorta-like tube against velocity profiles extracted every 0.001s from 2D PIV.

- Description and practical implementation of two alternative approaches for utilizing of physiological BCs mimicking periphery of arterial circulation:

    1. Evaluation of the PWV and consequent correction in time shift between inlet and outlets BCs extracted from the literature. This method is proper for idealized arterial segment, nevertheless, its feasibility was successfully tested also on PS arterial tree with six outlets. However, this approach has little predictive capabilities because pressure or velocities are prescribed at the outlets (for further details see chapter 6.1.2).

    2. Estimation of the parameters of periphery via iterative process between multiscale 3D-0D model and reduced order (0D) model until required flow and pressure waveforms are achieved in the multiscale model. This approach has very good predictive capabilities over certain range of physiological conditions since pressure or velocities are not prescribed at the outlets whereas a relationship between them is imposed (for further details see chapters 3.4 and 6.2.2).

- The second methodology has a great potential to be, at least, semi-automated since Matlab/Simulink can be linked with Ansys Fluent creating thus a closed-loop system in terms of parameter updates.

7.2. Proposed syllabus of a new course

The results of this thesis and the related work of other doctoral students (J. Kohút, M. Formánek) created a basis for a potential new course in MSc studies of biomechanics. The title of this porposed course is "Simulations of blood flow in arteries" and its syllabus includes the following topics:

1. Introduction to blood flow modelling in arteries.
   - Motivation
   - Inputs we can receive from the non-invasive screening in hospital.
   - Which outputs from us are anticipated by surgeons and what we can provide for now?
   - Examples of cooperation between biomechanicians and surgeons in this field.
2. Theory: Soft tissue imaging methods (revision - already included in BIO I)
   - Workshop: carotid artery lumen reconstruction from the CT-scans
3. Theory: Derivation of Moens-Korteweg eq. and non-reflective BC
   - Workshop: PWV propagation in thick and thin-walled hyperelastic tube (experiment)
4. Theory: Derivation of parabolic and Womersley velocity profiles
   - Workshop: computational simulation of PWV propagation with non-reflective BC (the UDF script will be prepared by teacher) with consequent validation against the experiment performed in Workshop 3
5. Theory: *The previous lecture continued*
   - Workshop: Meshing of a PS carotid artery in ICEM software
6. Theory: Derivation of lumped parameter (0D) models – two and three element Windkessel models (2 and 3 WKs)
   - Workshop: *continuing from the previous workshop*
7. Theory: *The previous lecture continued*
   - Workshop: implementation of the 3WK model in Ansys Fluent via UDF
8. Theory: Derivation of 1D structured tree model
   - Workshop: implementation of the 1D structured tree model in Ansys Fluent via UDF
9. Theory: *The previous lecture continued*
   - Workshop: *continuing from the previous workshop*
10. Theory: WK´s parameter estimation process to achieve an agreement with measured data
    - Workshop: Creation of the lumped parameter model in Matlab Simulink and estimating of its parameter to achieve an agreement with measured data
11. Theory: *The previous lecture continued*
    - Workshop: Creation of the 1D structured tree model in Matlab Simulink and estimating of its parameter to achieve an agreement with measured data. Comparison of the results and effectivity of lumped and 1D structured tree models.
12. Theory: Atherosclerosis process indicators and its mechanobiological meaning – WSS, TAWSS, OSI and RRT
    - Workshop: Example of evaluation of these indicators in Ansys CFD Post and Matlab

7.3. Clinical

- Impact of the aorto-iliac angles on hemodynamic parameters (i.e., pressure and stresses) within the AA was negligible while significant sensitivity was found to AR. Nevertheless, the geometry-related changes of hemodynamic parameters in healthy individuals (i.e., AR ~ 1) do not exceed their limits for atherosclerosis inception. However, pressure is significantly increased by some 1.2 kPa (19% of pulse pressure) for AR = 0.5 representing 50% iliac stenosis. Iliac stenosis might be therefore a risk factor for AAA formation. In addition, similar effect can be expected due to a natural decrease of the AR with aging.

- Among broadly reported SBP-lowering effect of five basic group of antihypertensives (ACEi, ARB, CCB, beta-blockers, and diuretics), we hypotheses (based on literature review and high-fidelity computational simulations) their potential secondary benefit. Their favorable effect lies in significant increase of TAWSS as a result of decreasing the arterial stiffness and relating PWV. Such TAWSS increase (especially in atheroprone region, see Table 3) is probably one of the possible mechanisms how the risk of atherosclerosis is attenuated.

7.4. Effect of shear forces on an attached cell

During my PhD studies, I got an opportunity to contribute to the paper [143] dealing with a cell behaviour. Since the mechanical response of cells is affected by the cell cycle (i.e., events which include the duplication of its DNA and some of its organelles, and subsequently the partitioning of its cytoplasm, chromosomes and other components into two daughter cells), differentiation, and pathological processes such as malignant transformation, cardiovascular diseases, aging, etc., the evaluation of its mechanical properties is of a great interest. Hence, main goals of this paper were: a) proposal of a fast, reliable, and minimally invasive methodology for measurement of the cell´s shear modulus during live-cell experiments (i.e., the methods widely established so far induce mostly non-physiological stresses in the cell which can unnaturally affect the results); b) testing of the proposed methodology in several experiments investigating cell types of different shear modulus and treated also with cytochalasin D or docetaxel. Movement of the center of mass (*CoM*) of an attached cell in liquid flow was used in shear strain calculation and consequently in derivation of the shear modulus. Ing. Tomas Vicar, PhD, as the first author, together with doc. MUDr. Jaromir Gumulec, PhD were struggling with two crucial questions: (i) how the alteration of cell shape affects the *CoM* displacement (and thus whether it is important to reflect the cell shape in the model) and (ii) to show, how the wall shear stress is altered by the presence of the cells in the chamber.

The *CoM* displacement of the cell was computed as the difference between its actual $CoM(t)$ and initial $CoM(t_0)$ position, where the displacement was considered in the direction of the applied flow only (z-axis – see Figure 35). The displacement of the *CoM* is 0.709, 0.706 and 0.729 μm for a spherical dome, block and cylinder with the same median height (median of all z-values of the top surface of the spherical dome) of H_{med} = 5.81 μm, respectively. The displacement values are almost the same for all geometric variants.

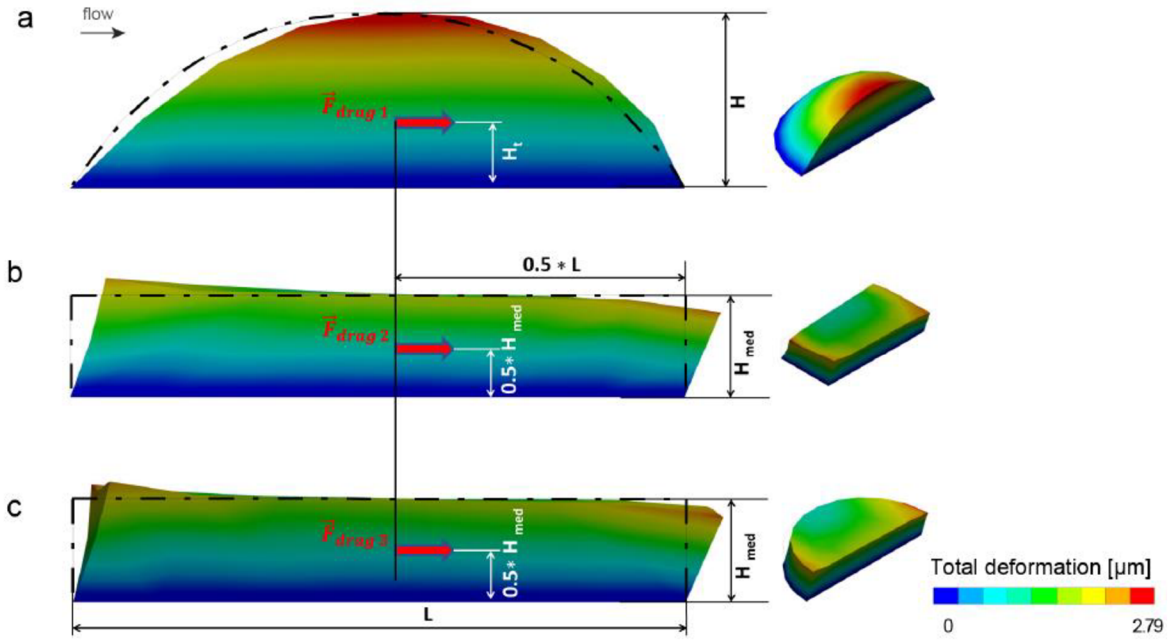

Figure 35 Deformed shapes of 3D idealized isotropic cells with different geometry (only half geometry was considered due to symmetry): (a) – spherical dome with maximum height H = 10 μm, median height H_{med} = 5.81 μm and L (diameter) = 34.64 μm; (b) – block with H_{med} = 5.81 μm and L = 34.64 μm and (c) cylinder with H_{med} = 5.81 μm and diameter = 34.64 μm. Neo-Hookean hyperelastic constitutive model was used for all variants (with initial shear modulus G = 51.4 Pa). The cells were loaded by drag force from the surrounding flow computed from CFD analysis.

Furthermore, the influence of different densities of cell population on the total drag force acting on particular cells was investigated via CFD simulations. Figure 36 shows that the wall shear stress (WSS) is almost equally distributed over the population of cells where only the first row of cells upstream shows elevated values of WSS and consequently, elevated drag forces. With increasing confluence (i.e., cell seeding density, percentage of substrate surface covered with the cells), the relative change of drag force of the cells is observable just in confluences 20 % and higher (3.8 % force decrease in a center of the cell population).

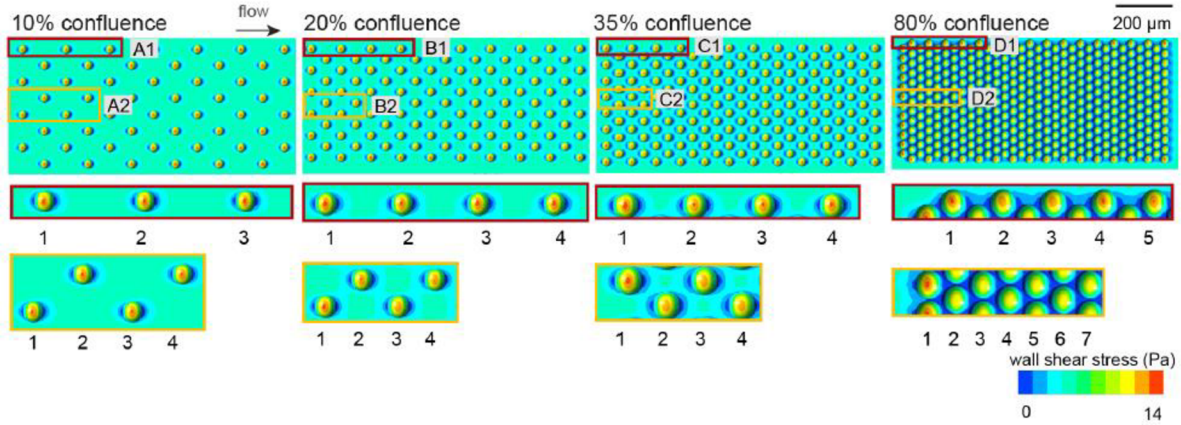

Figure 36 Maps of wall shear stress for different densities of cell population used in CFD analysis. Differences in the drag forces for individual cells (modelled as spherical domes) seeded on the area 840 x 400 μm in increasing confluence (details on center area and periphery shown in yellow and red frames, respectively).

Taken together, given the negligible differences in a *CoM* displacement between various geometric structures made of a homogeneous material, the usage of rectangular block was considered sufficient. Furthermore, for the modelling of the confluence (further experimentally verified in [143]) within the values ranging approx. 5-15 % (values used in this paper), the presence of cells does affect the overall chamber wall shear stress minimally.

7.5. Peristaltic pump

Although a peristaltic pump seems to be far from my research area, this project has been developing since the beginning of 2020 (one-year project FV 20-13) and was not primarily focused on the pump. Main goals were design and construction of the experimental circuit for PWV measurements in hyperelastic tubes. To make the circuit more universal, the pump was used as a source of pulses.

Next year, I and my colleagues from the institute of fluid engineering (Ing. Jiří Kohút, my former master student) and from the institute of mechatronics (Ing. Martin Formánek) proposed some modifications of the existing circuit. This was done within another one-year university project FV 21-13. Once the changes were implemented, the circuit allowed us to mimic hemodynamic conditions observed in humans (i.e., in terms of the pressure and flow waveforms shape), mainly thanks to a structured tree made of hyperelastic tubes which was fitted at the outlet of the circuit. The structured tree was designed and consequently manufactured according to 1D linear model theory [19] and its main purpose is to mimic the periphery of arterial network. We summarized its proposal in an extended abstract published and presented at *36th conference of Computational Mechanics in Srní* [144]. Nevertheless, shape of the waveforms was tuned using "trial and error" approach which was time-consuming and highly operator dependent.

To overcome this issue, we decided to use a neural network. It was trained with approx. 500 datasets (i.e., one dataset is represented by one period of pressure waveform and rotational speed profile of the pump´s rotor). After the training phase, a neural network was able to create/find rotational speed profile which corresponds a required pressure waveform. One-year interfaculty project no. FIT/FSI-J-22-7952 was used for funding and cooperation with faculty of informatics (Ing. Jan Kohút) was established. As regards to the outputs, one extended abstract was published and presented at the *7th International Conference on Computational & Mathematical Biomedical Engineering in Milano* [145], one at *20th International Conference on Mechatronics in Plzeň* (indexed in WoS) [146] and one manuscript is in final phase of preparation for submition to an IF journal.

Moreover, another valuable cooperation was established during the year 2022 with doc.MUDr. Pavel Suk, PhD. from the Saint Anne hospital in Brno who is experienced in veno-arterial extracorporeal oxygenation (VA-ECMO) support. In the previous project, we have observed significant changes in pressure oscillation during our measurements with variable rotational speed profile of the pump´s rotor. In some cases, undesired pressure oscillations resulting from quick release/compression of the pump´s tube were significantly attenuated, or almost diminished. Since these undesired pressure oscillations can be related to red blood cell damage (i.e., hemolysis), we created a CFD model of the pump to evaluate its influence. Significant reduction (approx. 70%) in hemolysis index was observed between the configuration of the pump with constant rotational speed (conventionally used in clinics) and variable rotational speed (i.e., lower speed was enforced during release/compression phase while higher speed was used during the rest of the pump´s cycle). The above-mentioned prepared manuscript summarises these results in detail.

Based on this promising results, GAČR project no. 24-10918S was submitted in cooperation with doc.MUDr. Pavel Suk, PhD and with my supervisor, prof. Jiří Burša, as a leader of the project. One of the main goals of this project is to validate the hypothesis on significant hemolysis reduction in the peristaltic pump on the real blood. Moreover, one master student from India (Prerak P Bharadwaj) is involved within validation of CFD simulations of the pump. Based on the quality of his bachelor´s thesis and future plans, it is probable that he will become a valuable member of the team.

8. Conclusions

- Creation of a credible computational model of pulsatile blood flow in arteries, including its BCs, and its validation with experiments.

The results of the computational and experimental study have been published in [99]. I am the first author, and this work fulfils the first goal completely. On the top of that, a very high-quality master thesis was the output which laid down the foundation for the long-term enriching cooperation with Ing. Jiří Kohút and fluid engineering department.

- Design and creation of an experimental circuit simulating pulse wave propagation (PWV) in a compliant tube.

The experimental circuit was designed and created; however, any publication or conference contribution have not been published so far. For this reason, the methodology is briefly described in section 4. Nevertheless, this circuit together with the related computational methodology for PWV evaluation have been implemented into the biomechanical lectures. Moreover, the proposed circuit serves as a basis for consequent projects focused on the peristaltic pump described in section 7.5. It is worth to note that these projects established new cooperations (doc. MUDr. Pavel Suk, PhD., Ing. Martin Formánek and his modified doctoral topic in mechatronics).

- Exploitation of the created model for FSI analyses of human aortic tree and evaluation of impact of some of its geometrical parameters on the risk of development of aneurysms and atheromas in critical regions.

The results of the computational study regarding FSI analyses of human aortic tree have been published in IF journal Medical Engineering & Physics [111]. *This study showed an insignificant impact of aorto-iliac angle on the haemodynamic parameters but a significant increase of aortic pressure and consequently of AAA risk for lower area* ratio (i.e., a sum of luminal cross sections of iliac arteries divided by the aortic luminal cross section). *I am the first author, and this work fulfills the third goal completely.*

- Creation of a 3D CFD PS model of human carotid arteries with lumped parameters BCs. Analysis of influence of diastolic phase length on hemodynamic parameters.

This is the last, and probably the most interdisciplinary goal. Many surgeons from Saint Anne hospital were involved together with other colleagues from Brno University of Technology. Now, I am working on the manuscript which is planned to be submitted to an IF journal at the end of the august 2023. Since it is not published yet, the actual state (including methodology, partial results and discussion) is described in section 6.2 in detail. The only difference between the final manuscript and the work described here is a number of PS geometries. In the final manuscript is it planned to include 10 geometries, so far we have only 5. The proposed methodology for a blood flow modelling in PS carotid arteries will be used also in the actual GAČR project dealing with assessment of stenosis severity in carotid artery with tandem (double) stenosis. Since the methodology contains multiple steps which need to be done manually, some level of automation would be useful in the future.

9. List of author´s publications

- **Conference papers related to dissertation:**
  - Jagoš, J., Jašíková, D., Knotek, M., Burša, J., Simulation and experimental validation of pulsatile flow in a compliant tube, *VIIIth International Conference on Computational Bioengineering*, 4-6 September, 2019, Belgrade, Serbia
  - J. ŠVANCARA, P.; LISICKÝ, O.; JAGOŠ, J.; BURŠA, Computational Modeling of Blood Flow in the Bifurcation of Human Carotid Artery, in: *26th Int. Conf. Eng. Mech.*, 2020: pp. 480–483. https://doi.org/10.21495/5896-3-480.
  - J. Kohut, J. Jagos, M. Formanek, J. Burša, In vitro structured tree model of the peripheral vascular network, in: *Comput. Mech.,* Srní, 2021: pp. 118–121.
  - J. Jagoš, J. Kohút, J. Kohút, M. Formánek, J. Burša, Roller pump controlled by neural network: experimental study under physiological conditions, *7 th International Conference on Computational & Mathematical Biomedical Engineering*, 27-29 June, 2022, Milano, Italy, pp. 389 – 392. ISBN: 978-0-9562914-6-2
  - M. Formánek, M. Appel, J. Jagoš, J. Kohút, M. Rajchl, Dynamic model of peristaltic pump with arterial tree for real-time pressure waveform control, *in: Proc. 2022 20th Int. Conf. Mechatronics*, IEEE, Plzeň, 2022. https://doi.org/10.1109/ME54704.2022.9982882.
- **IF papers related to disseration:**
  - J. Jagos, J. Kohut, M. Kotek, P. Skacel, J. Bursa, Influence of Turbulence in Aorta-like Tube: Computational and Experimental Study, J. Appl. Fluid Mech. 14 (2021) 1411–1420. https://doi.org/10.47176/jafm.14.05.32291.
  - Jagos, J., Schwarz, D., Polzer, S., & Bursa, J. (2023). Effect of aortic bifurcation geometry on pressure and peak wall stress in abdominal aorta : Fluid-structure interaction study. *Medical Engineering and Physics*, *118*(June), 1–8. https://doi.org/10.1016/j.medengphy.2023.104014
- **Other conference papers**
  - ZUMBERG, I.; ČMIEL, V.; ORLOVÁ, L.; HASHEMI, A.; JAGOŠ, J. Monitoring the endothelial cell behavior during flow stress induction using digital holographic microscopy. *16th Multinational Congress on Microscopy* 16MCM: BOOK OF ABSTRACTS. Brno: Czechoslovak Microscopy Society, 2022. s. 304-305. ISBN: 978-80-11-02253-2 (https://www.16mcm.cz/wp-content/uploads/2022/09/16MCM-abstract-book.pdf
- **Other IF papers:**
  - T. Vicar, J. Gumulec, J. Chmelik, J. Navratil, R. Kolar, L. Chmelikova, V. Cmiel, I. Provaznik, J. Jagos, M. Masarik, Cancer Cells Viscoelasticity Measurement by Quantitative Phase and Flow Stress Induction, Biophys. J. 121 (2022) 1632–1642. https://doi.org/10.1016/j.bpj.2022.04.002.

10. References

[1] D.A. Sinclair, Lifespan: the revolutionary science of why we age and why we don't have to, Atria Books, New York, 2019.

[2] J.C. Riley, Estimates of regional and global life expectancy, 1800-2001, Popul. Dev. Rev. 31 (2005) 537–543. https://doi.org/10.1111/j.1728-4457.2005.00083.x.

[3] H. Rosling, R.A. Ronnlund, O. Rosling, Factfulness: Ten Reasons We're Wrong about the World - and Why Things Are Better than You Think, Sceptre, London, 2019.

[4] S.L. Murphy, J. Xu, K.D. Kochanek, E. Arias, B. Tejada-Vera, Deaths: Final Data for 2018, Natl. Vital Stat. Reports. 69 (2021).

[5] B. Keisler, C. Carter, Abdominal aortic aneurysm, Am. Fam. Physician. 91 (2015) 538–543.

[6] S.P. Glasser, A.P. Selwyn, P. Ganz, Atherosclerosis: Risk factors and the vascular endothelium, Am. Heart J. 131 (1996) 379–384. https://doi.org/10.1016/S0002-8703(96)90370-1.

[7] K.C. Kent, R.M. Zwolak, N.N. Egorova, T.S. Riles, A. Manganaro, A.J. Moskowitz, A.C. Gelijns, G. Greco, Analysis of risk factors for abdominal aortic aneurysm in a cohort of more than 3 million individuals, J. Vasc. Surg. 52 (2010) 539–548. https://doi.org/10.1016/j.jvs.2010.05.090.

[8] H. Sillesen, E. Falk, Why not screen for subclinical atherosclerosis?, Lancet. 378 (2011) 645–646. https://doi.org/10.1016/S0140-6736(11)60059-7.

[9] C. Rutledge, S. Jonzzon, E.A. Winkler, D. Raper, M.T. Lawton, A.A. Abla, Small Aneurysms with Low PHASES Scores Account for Most Subarachnoid Hemorrhage Cases, World Neurosurg. 139 (2020) e580–e584. https://doi.org/10.1016/j.wneu.2020.04.074.

[10] J. Morgan, What's The Difference Between Invention And Innovation?, Forbes. (2015). https://www.forbes.com/sites/jacobmorgan/2015/09/10/whats-the-difference-between-invention-and-innovation/?sh=3c67b86770f4.

[11] E. Brynjolfsson, A. McAfee, The Second Machine Age: Work, Progress, and Prosperity in a Time of Brilliant Technologies, W. W. Norton & Company, New York, 2016.

[12] S. Payne, Cerebral Flow in the Brain Control of Blood Autoregulation, Springer Nature, Switzerland, 2016. https://doi.org/10.1007/978-3-319-31784-7.

[13] P.R. Hoskins, P. V. Lawford, B.J. Doyle, Cardiovascular Biomechanics, 2017. https://doi.org/10.1007/978-3-319-46407-7.

[14] J. Alastruey, K.H. Parker, S.J. Sherwin, Arterial pulse wave haemodynamics, in: BHR Gr. - 11th Int. Conf. Press. Surges, 2012: pp. 401–442.

[15] W.W. Nichols, M.F. O'Rourke, C. Vlachopoulos, A.P. Hoeks, R.S. Reneman, McDonald's blood flow in arteries theoretical, experimental and clinical principles, Sixth Edit, Hodder and Stoughton Ltd, a division of Hachette UK,

London, 2011. https://doi.org/10.1111/j.1540-8175.1991.tb01207.x.

[16] J.T. Ottesen, M.S. Olufsen, J.K. Larsen, Applied Mathematical Models in Human Physiology, 2004. https://doi.org/10.1137/1.9780898718287.

[17] J.H.G. Helthuis, T.P.C.V.A.N. Doormaal, B. Hillen, R.L.A.W. Bleys, A.A. Harteveld, J. Hendrikse, A.V.A.N.D.E.R. Toorn, M. Brozici, J.J.M. Zwanenburg, A.V.A.N.D.E.R. Zwan, Branching Pattern of the Cerebral Arterial Tree, Anat. Rec. 302 (2018) 1434–1446. https://doi.org/10.1002/ar.23994.

[18] C. R. Ethier and C. A. Simmons, Introductory Biomechanics From Cells to Organisms, 2007.

[19] M.S. Olufsen, C.S. Peskin, W.Y. Kim, E.M. Pedersen, A. Nadim, J. Larsen, Numerical simulation and experimental validation of blood flow in arteries with structured-tree outflow conditions, Ann. Biomed. Eng. 28 (2000) 1281–1299. https://doi.org/10.1114/1.1326031.

[20] N. Stergiopulos, P. Segers, N. Westerhof, Use of pulse pressure method for estimating total arterial compliance in vivo, Am. J. Physiol. - Hear. Circ. Physiol. 276 (1999). https://doi.org/10.1152/ajpheart.1999.276.2.h424.

[21] R.D. Latham, N. Westerhof, P. Sipkema, B.J. Rubal, P. Reuderink, J.P. Murgo, Regional wave travel and reflections along the human aorta: A study with six simultaneous micromanometric pressures, Circulation. 72 (1985) 1257–1269. https://doi.org/10.1161/01.CIR.72.6.1257.

[22] A. Redheuil, W.C. Yu, C.O. Wu, E. Mousseaux, A. De Cesare, R. Yan, N. Kachenoura, D. Bluemke, J.A.C. Lima, Reduced ascending aortic strain and distensibility: Earliest manifestations of vascular aging in humans, Hypertension. 55 (2010) 319–326. https://doi.org/10.1161/HYPERTENSIONAHA.109.141275.

[23] N. Westerhof, J.W. Lankhaar, B.E. Westerhof, The arterial windkessel, Med. Biol. Eng. Comput. 47 (2009) 131–141. https://doi.org/10.1007/s11517-008-0359-2.

[24] J.D. Humphrey, C.A. Taylor, Intracranial and abdominal aortic aneurysms: Similarities, differences, and need for a new class of computational models, Annu. Rev. Biomed. Eng. 10 (2008) 221–246. https://doi.org/10.1146/annurev.bioeng.10.061807.160439.

[25] P.A. Cahill, E.M. Redmond, Vascular endothelium - Gatekeeper of vessel health, Atherosclerosis. 248 (2016) 97–109. https://doi.org/10.1016/j.atherosclerosis.2016.03.007.

[26] A.M. Malek, S.L. Alper, Heamodynamics Shear stress and Its Role in Atherosclerosis, Stress Int. J. Biol. Stress. 282 (1999) 2035–2042.

[27] J.M. Dolan, J. Kolega, H. Meng, High wall shear stress and spatial gradients in vascular pathology: A review, Ann. Biomed. Eng. (2013). https://doi.org/10.1007/s10439-012-0695-0.

[28] J.J. Chiu, S. Chien, Effects of disturbed flow on vascular endothelium: Pathophysiological basis and clinical perspectives, Physiol. Rev. 91 (2011) 327–387. https://doi.org/10.1152/physrev.00047.2009.

[29] A.E. Murphy SL, Xu JQ, Kochanek KD, Mortality in the United States, 2017 Key

findings Data from the National Vital Statistics System, NCHS Data Brief. (2018) 1–8.

[30] K.D. Kochanek, S.L. Murphy, J. Xu, E. Arias, Deaths: Final data for 2014, Natl. Vital Stat. Reports. 68 (2016) 1–18.

[31] M. Nichols, N. Townsend, M. Rayner, European cardiovascular disease statistics, 2012.

[32] K.D. Kochanek, S.L. Murphy, J. Xu, E. Arias, D. Ph, Deaths : Final Data for 2017, Natl. Vital Stat. Reports. 68 (2019).

[33] H.J. Carpenter, A. Gholipour, M.H. Ghayesh, A.C. Zander, P.J. Psaltis, A review on the biomechanics of coronary arteries, Int. J. Eng. Sci. 147 (2020) 103201. https://doi.org/10.1016/j.ijengsci.2019.103201.

[34] M.R. Nehler, S. Duval, L. Diao, B.H. Annex, W.R. Hiatt, K. Rogers, A. Zakharyan, A.T. Hirsch, Epidemiology of peripheral arterial disease and critical limb ischemia in an insured national population, J. Vasc. Surg. 60 (2014) 686-695.e2. https://doi.org/10.1016/j.jvs.2014.03.290.

[35] S.L. Murphy, J. Xu, K.D. Kochanek, S.C. Curtin, E. Arias, Deaths: Final data for 2015, Natl. Vital Stat. Reports. 66 (2017). https://doi.org/10.1136/vr.h753.

[36] J. Golledge, Abdominal aortic aneurysm: update on pathogenesis and medical treatments, Nat. Rev. Cardiol. 16 (2019) 225–242. https://doi.org/10.1038/s41569-018-0114-9.

[37] H. Meng, V.M. Tutino, J. Xiang, A. Siddiqui, High WSS or Low WSS? Complex interactions of hemodynamics with intracranial aneurysm initiation, growth, and rupture: Toward a unifying hypothesis, Am. J. Neuroradiol. 35 (2014) 1254–1262. https://doi.org/10.3174/ajnr.A3558.

[38] N. Ajiboye, N. Chalouhi, R.M. Starke, M. Zanaty, R. Bell, Unruptured Cerebral Aneurysms: Evaluation and Management, Sci. World J. 2015 (2015). https://doi.org/10.1155/2015/954954.

[39] O. Tanweer, T.A. Wilson, E. Metaxa, H.A. Riina, H. Meng, A Comparative Review of the Hemodynamics and Pathogenesis of Cerebral and Abdominal Aortic Aneurysms: Lessons to Learn From Each Other, J. Cerebrovasc. Endovasc. Neurosurg. 16 (2014) 335. https://doi.org/10.7461/jcen.2014.16.4.335.

[40] B. Williams, G. Mancia, W. Spiering, E.A. et al. Rosei, 2018 ESC/ESH Guidelines for the management of arterial hypertension, Eur. Heart J. 39 (2018) 3021–3104. https://doi.org/10.1093/eurheartj/ehy339.

[41] H. Scott, M.J. Barton, A.N.B. Johnston, Isolated systolic hypertension in young males: a scoping review, Clin. Hypertens. 27 (2021) 1–12. https://doi.org/10.1186/s40885-021-00169-z.

[42] K.I. Paraskevas, D.P. Mikhailidis, F.J. Veith, J.D. Spence, Definition of Best Medical Treatment in Asymptomatic and Symptomatic Carotid Artery Stenosis, Angiology. 67 (2016) 411–419. https://doi.org/10.1177/0003319715624526.

[43] R. Noiphithak, A. Liengudom, Recent update on carotid endarterectomy versus carotid artery stenting, Cerebrovasc. Dis. 43 (2017) 68–75.

https://doi.org/10.1159/000453282.

[44] G. Montalescot et al., 2013 ESC guidelines on the management of stable coronary artery disease, Eur. Heart J. 34 (2013) 2949–3003. https://doi.org/10.1093/eurheartj/eht296.

[45] K.T. Ong, S. Delerme, B. Pannier, M.E. Safar, A. Benetos, S. Laurent, P. Boutouyrie, Aortic stiffness is reduced beyond blood pressure lowering by short-term and long-term antihypertensive treatment: A meta-analysis of individual data in 294 patients, J. Hypertens. 29 (2011) 1034–1042. https://doi.org/10.1016/S0140-6736(16)31134-5.

[46] F.H. Messerli, B. Williams, E. Ritz, Essential hypertension, Lancet. 370 (2007) 591–603. https://doi.org/10.1016/S0140-6736(07)61299-9.

[47] A. R. Naylor et al., Editor's Choice – Management of Atherosclerotic Carotid and Vertebral Artery Disease: 2017 Clinical Practice Guidelines of the European Society for Vascular Surgery (ESVS), Eur. J. Vasc. Endovasc. Surg. 55 (2018) 3–81. https://doi.org/10.1016/j.ejvs.2017.06.021.

[48] H. Ota, K. Takase, H. Rikimaru, M. Tsuboi, T. Yamada, A. Sato, S. Higano, T. Ishibashi, S. Takahashi, Quantitative vascular measurements in arterial occlusive disease, Radiographics. 25 (2005) 1141–1158. https://doi.org/10.1148/rg.255055014.

[49] H.R. Underhill, T.S. Hatsukami, Z.A. Fayad, V. Fuster, C. Yuan, MRI of carotid atherosclerosis: Clinical implications and future directions, Nat. Rev. Cardiol. 7 (2010) 165–173. https://doi.org/10.1038/nrcardio.2009.246.

[50] N.H.J. Pijls, J.A.M. Van Son, R.L. Kirkeeide, B. De Bruyne, K.L. Gould, Experimental basis of determining maximum coronary, myocardial, and collateral blood flow by pressure measurements for assessing functional stenosis severity before and after percutaneous transluminal coronary angioplasty, Circulation. 87 (1993) 1354–1367. https://doi.org/10.1161/01.cir.87.4.1354.

[51] N.H.J. Pijls, B. De Bruyne, G.J.W. Bech, F. Liistro, G.R. Heyndrickx, H.J.R.M. Bonnier, J.J. Koolen, Coronary pressure measurement to assess the hemodynamic significance of serial stenoses within one coronary artery: Validation in humans, Circulation. 102 (2000) 2371–2377. https://doi.org/10.1161/01.CIR.102.19.2371.

[52] Pim A.L. et al., Fractional Flow Reserve versus Angiography for Guiding Percutaneous Coronary Intervention, N. Engl. J. Med. 360 (2009) 2605–2615.

[53] P.D. Morris, D. Ryan, A.C. Morton, R. Lycett, P. V. Lawford, D.R. Hose, J.P. Gunn, Virtual fractional flow reserve from coronary angiography: Modeling the significance of coronary lesions. Results from the VIRTU-1 (VIRTUal fractional flow reserve from coronary angiography) study, JACC Cardiovasc. Interv. 6 (2013) 149–157. https://doi.org/10.1016/j.jcin.2012.08.024.

[54] P.D. Morris, D.A. Silva Soto, J.F.A. Feher, D. Rafiroiu, A. Lungu, S. Varma, P. V. Lawford, D.R. Hose, J.P. Gunn, Fast Virtual Fractional Flow Reserve Based Upon Steady-State Computational Fluid Dynamics Analysis: Results From the VIRTU-

Fast Study, J Am Coll Cardiol Basic Trans Sci. 2 (2017) 434–446. https://doi.org/10.1016/j.jacbts.2017.04.003.

[55] I.Y. Elgendy, C.R. Conti, A.A. Bavry, Fractional fow reserve: An updated review, Clin. Cardiol. 37 (2014) 371–380. https://doi.org/10.1002/clc.22273.

[56] C.A. Taylor, T.A. Fonte, J.K. Min, Computational fluid dynamics applied to cardiac computed tomography for noninvasive quantification of fractional flow reserve: Scientific basis, J. Am. Coll. Cardiol. 61 (2013) 2233–2241. https://doi.org/10.1016/j.jacc.2012.11.083.

[57] A. Jonášová, J. Vimmr, Noninvasive assessment of carotid artery stenoses by the principle of multiscale modelling of non-Newtonian blood flow in patient-specific models, Appl. Math. Comput. 319 (2018) 598–616. https://doi.org/10.1016/j.amc.2017.07.032.

[58] N. Murata, H. Aihara, Y. Soga, Y. Tomoi, S. Hiramori, Y. Kobayashi, K. Ichihashi, N. Tanaka, Validation of pressure gradient and peripheral fractional flow reserve measured by a pressure wire for diagnosis of iliofemoral artery disease with intermediate stenosis, Med. Devices Evid. Res. 8 (2015) 467–472. https://doi.org/10.2147/MDER.S83768.

[59] P. Libby, P.M. Ridker, A. Maseri, Inflammation and atherosclerosis, Circulation. 105 (2002) 1135–1143. https://doi.org/10.1161/hc0902.104353.

[60] P. Libby, Y. Okamoto, V.Z. Rocha, E. Folco, Inflammation in atherosclerosis: Transition from theory to practice, Circ. J. 74 (2010) 213–220. https://doi.org/10.1253/circj.CJ-09-0706.

[61] J. Moriya, Critical roles of inflammation in atherosclerosis, J. Cardiol. 73 (2019) 22–27. https://doi.org/10.1016/j.jjcc.2018.05.010.

[62] D.N. Ku, D.P. Giddens, C.K. Zarins, S. Glagov, Pulsatile flow and atherosclerosis in the human carotid bifurcation. Positive correlation between plaque location and low and oscillating shear stress, Arteriosclerosis. 5 (1985) 293–302. https://doi.org/10.1161/01.atv.5.3.293.

[63] N Sakalihasan, R Limet, OD Defawe, Abdominal aortic aneurysm, Lancet. 365 (2005) 1577–89. https://doi.org/https://doi.org/10.1016/S0140-6736(05)66459-8.

[64] S. Jana, M. Hu, M. Shen, Z. Kassiri, Extracellular matrix, regional heterogeneity of the aorta, and aortic aneurysm, Exp. Mol. Med. 51 (2019). https://doi.org/10.1038/s12276-019-0286-3.

[65] P.E. Norman, J.T. Powell, Site specificity of aneurysmal disease, Circulation. 121 (2010) 560–568. https://doi.org/10.1161/CIRCULATIONAHA.109.880724.

[66] G.R. Drummond, A. Vinh, T.J. Guzik, C.G. Sobey, Immune mechanisms of hypertension, Nat. Rev. Immunol. 19 (2019) 517–532. https://doi.org/10.1038/s41577-019-0160-5.

[67] P.B. Dobrin, Pathophysiology and pathogenesis of aortic aneurysms, Surg. Clin. North Am. 69 (1989) 687–703. https://doi.org/10.1016/S0039-6109(16)44876-0.

[68] A. V. Sterpetti, R.J. Feldhaus, R.D. Schultz, E.A. Blair, Identification of abdominal aortic aneurysm patients with different clinical features and clinical outcomes, Am. J. Surg. 156 (1988) 466–469. https://doi.org/10.1016/S0002-9610(88)80530-0.

[69] J.M. Reilly, M.D. Tilson, Incidence and etiology of abdominal aortic aneurysms, Surg. Clin. North Am. 69 (1989) 705–711. https://doi.org/10.1016/S0039-6109(16)44877-2.

[70] D. Reed, C. Reed, Are Aortic Aneurysms Caused by Atherosclerosis?, Circulation. 85 (1992) 205–211. https://doi.org/https://doi.org/10.1161/01.CIR.85.1.205.

[71] S.H. Johnsen, S.H. Forsdahl, K. Singh, B.K. Jacobsen, Atherosclerosis in abdominal aortic aneurysms: A causal event or a process running in parallel? the tromsø study, Arterioscler. Thromb. Vasc. Biol. 30 (2010) 1263–1268. https://doi.org/10.1161/ATVBAHA.110.203588.

[72] B.J. Toghill, A. Saratzis, M.J. Bown, Abdominal aortic aneurysm—an independent disease to atherosclerosis?, Cardiovasc. Pathol. 27 (2017) 71–75. https://doi.org/10.1016/j.carpath.2017.01.008.

[73] S. Ito, K. Akutsu, Y. Tamori, S. Sakamoto, T. Yoshimuta, H. Hashimoto, S. Takeshita, Differences in Atherosclerotic Profiles Between Patients With Thoracic and Abdominal Aortic Aneurysms, Am. J. Cardiol. 101 (2008) 696–699. https://doi.org/10.1016/j.amjcard.2007.10.039.

[74] E. Kobeissi, M. Hibino, H. Pan, D. Aune, Blood pressure, hypertension and the risk of abdominal aortic aneurysms: a systematic review and meta-analysis of cohort studies, Eur. J. Epidemiol. 34 (2019) 547–555. https://doi.org/10.1007/s10654-019-00510-9.

[75] S. Lewington, R. Clarke, N. Qizilbash, R. Peto, R. Collins, Age-specific relevance of usual blood pressure to vascular mortality: A meta-analysis of individual data for one million adults in 61 prospective studies, Lancet. 360 (2002) 1903–1913. https://doi.org/10.1016/S0140-6736(02)11911-8.

[76] C. Vlachopoulos, K. Aznaouridis, M.F. O'Rourke et al., Prediction of cardiovascular events and all-cause mortality with central haemodynamics: A systematic review and meta-analysis, Eur. Heart J. 31 (2010). https://doi.org/10.1093/eurheartj/ehq024.

[77] Y. Ben-Shlomo, M. Spears, C. et al. Boustred, Aortic pulse wave velocity improves cardiovascular event prediction: An individual participant meta-analysis of prospective observational data from 17,635 subjects, J. Am. Coll. Cardiol. 63 (2014) 636–646. https://doi.org/10.1016/j.jacc.2013.09.063.

[78] M.H. Olsen, S.Y. Angell et al., A call to action and a lifecourse strategy to address the global burden of raised blood pressure on current and future generations: the Lancet Commission on hypertension, Lancet. 388 (2016) 2665–2712. https://doi.org/10.1016/S0140-6736(16)31134-5.

[79] P.H. Stone, Systemic Arterial Hypertension: Innovative Methods to Elucidate Mechanisms of Atherosclerosis and Arterial Restructuring, J. Am. Coll. Cardiol.

77 (2021) 590–592. https://doi.org/10.1016/j.jacc.2020.12.007.

[80] D.L. Penn, R.J. Komotar, E. Sander Connolly, Hemodynamic mechanisms underlying cerebral aneurysm pathogenesis, J. Clin. Neurosci. 18 (2011) 1435–1438. https://doi.org/10.1016/j.jocn.2011.05.001.

[81] S. Xu, I. Ilyas, P.J. Little et al., Endothelial dysfunction in atherosclerotic cardiovascular diseases and beyond: From mechanism to pharmacotherapies, Pharmacol. Rev. 73 (2021) 924–967. https://doi.org/10.1124/PHARMREV.120.000096.

[82] A. Virdis, L. Ghiadoni, S. Taddei, Effects of antihypertensive treatment on endothelial function, Curr. Hypertens. Rep. 13 (2011) 267–281. https://doi.org/10.1007/s11906-011-0207-x.

[83] D. Vinereanu, R. Dulgheru, S. Magda et al., The effect of indapamide versus hydrochlorothiazide on ventricular and arterial function in patients with hypertension and diabetes: Results of a randomized trial, Am. Heart J. 168 (2014) 446–456. https://doi.org/10.1016/j.ahj.2014.06.010.

[84] Y. Hoi, B.A. Wasserman, Y.J. Xie, S.S. Najjar, L. Ferruci, E.G. Lakatta, G. Gerstenblith, D.A. Steinman, Characterization of volumetric flow rate waveforms at the carotid bifurcations of older adults, Physiol. Meas. 31 (2010) 291–302. https://doi.org/10.1088/0967-3334/31/3/002.

[85] J. Hashimoto, B.E. Westerhof, S. Ito, Carotid Flow Augmentation, Arterial Aging, and Cerebral White Matter Hyperintensities: Comparison with Pressure Augmentation, Arterioscler. Thromb. Vasc. Biol. 38 (2018) 2843–2853. https://doi.org/10.1161/ATVBAHA.118.311873.

[86] Westerhof, Nicolaas, Stergiopulos, Nikolaos, Noble M. I. Mark, B.E. Westerhof, Snapshots of hemodynamics: an aid for clinical research and graduate education, Third Edit, Springer, 2019. https://doi.org/10.1007/978-3-319-91932-4.

[87] A. Noordergraaf, P.D. Verdouw, H.B.K. Boom, The use of an analog computer in a circulation model, Prog. Cardiovasc. Dis. 5 (1963) 419–439. https://doi.org/10.1016/S0033-0620(63)80009-2.

[88] N. Westerhof, F. Bosman, C.J. De Vries, A. Noordergraaf, Analog studies of the human systemic arterial tree, J. Biomech. 2 (1969) 121–143. https://doi.org/10.1016/0021-9290(69)90024-4.

[89] Y. Shi, P. Lawford, R. Hose, Review of Zero-D and 1-D Models of Blood Flow in the Cardiovascular System, Biomed. Eng. Online. 10 (2011). https://doi.org/10.1186/1475-925X-10-33.

[90] P. Reymond, F. Merenda, F. Perren, D. Rüfenacht, N. Stergiopulos, Validation of a one-dimensional model of the systemic arterial tree, Am. J. Physiol. - Hear. Circ. Physiol. 297 (2009) 208–222. https://doi.org/10.1152/ajpheart.00037.2009.

[91] P. Reymond, Y. Bohraus, F. Perren, F. Lazeyras, N. Stergiopulos, Validation of a patient-specific one-dimensional model of the systemic arterial tree, Am. J.

Physiol. - Hear. Circ. Physiol. 301 (2011) 1173–1182. https://doi.org/10.1152/ajpheart.00821.2010.

[92] A. Quarteroni, L. Formaggia, A. Veneziani, Cardiovascular Mathematics: Modeling and simulation of the circulatory system, Springer, 2009.

[93] R.L. Spilker, C.A. Taylor, Tuning multidomain hemodynamic simulations to match physiological measurements, Ann. Biomed. Eng. 38 (2010) 2635–2648. https://doi.org/10.1007/s10439-010-0011-9.

[94] J.-F.G. and I.E.V.-C. S. Pant, B.Fabrèges, A methodological paradigm for patient-specific multi-scale CFD simulations: from clinical measurements to parameter estimates for individual analysis, Int. J. Numer. Meth. Biomed. Engng. 30 (2014) 1614–1648. https://doi.org/10.1002/cnm.

[95] A. Jonášová, J. Vimmr, On the relevance of boundary conditions and viscosity models in blood flow simulations in patient-specific aorto-coronary bypass models, Int. j. Numer. Method. Biomed. Eng. (2021) 1–30. https://doi.org/10.1002/cnm.3439.

[96] I.E. Vignon-Clementel, C. Alberto Figueroa, K.E. Jansen, C.A. Taylor, Outflow boundary conditions for three-dimensional finite element modeling of blood flow and pressure in arteries, Comput. Methods Appl. Mech. Eng. 195 (2006) 3776–3796. https://doi.org/10.1016/j.cma.2005.04.014.

[97] L. Grinberg, G.E. Karniadakis, Outflow boundary conditions for arterial networks with multiple outlets, Ann. Biomed. Eng. 36 (2008) 1496–1514. https://doi.org/10.1007/s10439-008-9527-7.

[98] S.H. Attaran, H. Niroomand-oscuii, F. Ghalichi, A novel, simple 3D/2D outflow boundary model for blood flow simulations in compliant arteries, Comput. Fluids. 174 (2018) 229–240. https://doi.org/10.1016/j.compfluid.2018.08.006.

[99] J. Jagos, J. Kohut, M. Kotek, P. Skacel, J. Bursa, Influence of Turbulence in Aorta-like Tube: Computational and Experimental Study, J. Appl. Fluid Mech. 14 (2021) 1411–1420. https://doi.org/10.47176/jafm.14.05.32291.

[100] M.C. Brindise, P.P. Vlachos, Pulsatile pipe flow transition: Flow waveform effects, Phys. Fluids. 30 (2018). https://doi.org/10.1063/1.5021472.

[101] E. Özahi, M.Ö. Çarpınlıoğlu, A non-dimensional oscillation parameter describing interactive influence of oscillation frequency and velocity amplitude ratio for use in pulsatile flows, Meas. J. Int. Meas. Confed. 99 (2017) 36–43. https://doi.org/10.1016/j.measurement.2016.12.018.

[102] M. Xenos, Y. Alemu, D. Zamfir, S. Einav, J.J. Ricotta, N. Labropoulos, A. Tassiopoulos, D. Bluestein, The effect of angulation in abdominal aortic aneurysms: Fluid-structure interaction simulations of idealized geometries, Med. Biol. Eng. Comput. 48 (2010) 1175–1190. https://doi.org/10.1007/s11517-010-0714-y.

[103] F. Gao, H. Ueda, L. Gang, H. Okada, Fluid structure interaction simulation in three-layered aortic aneurysm model under pulsatile flow: Comparison of wrapping and stenting, J. Biomech. 46 (2013) 1335–1342.

https://doi.org/10.1016/j.jbiomech.2013.02.002.
[104] C.J. Drewe, L.P. Parker, L.J. Kelsey, P.E. Norman, J.T. Powell, B.J. Doyle, Haemodynamics and stresses in abdominal aortic aneurysms: A fluid-structure interaction study into the effect of proximal neck and iliac bifurcation angle, J. Biomech. 60 (2017) 150–156. https://doi.org/10.1016/j.jbiomech.2017.06.029.
[105] P. Reymond, P. Crosetto, S. Deparis, A. Quarteroni, N. Stergiopulos, Physiological simulation of blood flow in the aorta: Comparison of hemodynamic indices as predicted by 3-D FSI, 3-D rigid wall and 1-D models, Med. Eng. Phys. 35 (2013) 784–791. https://doi.org/10.1016/j.medengphy.2012.08.009.
[106] K.H. Parker, An introduction to wave intensity analysis, Med. Biol. Eng. Comput. 47 (2009) 175–188. https://doi.org/10.1007/s11517-009-0439-y.
[107] D.H. Bergel, Viscoelastic properties of the arterial wall, Queen Mary University of London, 1960.
[108] T. Pereira, C. Correia, J. Cardoso, Novel methods for pulse wave velocity measurement, J. Med. Biol. Eng. 35 (2015) 555–565. https://doi.org/10.1007/s40846-015-0086-8.
[109] A. Borlotti, Y. Li, K.H. Parker, A.W. Khir, Experimental evaluation of local wave speed in the presence of reflected waves, J. Biomech. 47 (2014) 87–95. https://doi.org/10.1016/j.jbiomech.2013.10.007.
[110] R.G. Gosling, D.L. Newman, N.L. Bowden, K.W. Twinn, The area ratio of normal aortic junctions. Aortic configuration and pulse-wave reflection., Br. J. Radiol. 44 (1971) 850–853. https://doi.org/10.1259/0007-1285-44-527-850.
[111] J. Jagos, D. Schwarz, S. Polzer, J. Bursa, Effect of aortic bifurcation geometry on pressure and peak wall stress in abdominal aorta : Fluid-structure interaction study, Med. Eng. Phys. 118 (2023) 1–8. https://doi.org/10.1016/j.medengphy.2023.104014.
[112] S.E. Greenwald, A.C. Carter, C.L. Berry, Effect of age on the in vitro reflection coefficient of the aortoiliac bifurcation in humans, Circulation. 82 (1990) 114–123. https://doi.org/10.1161/01.CIR.82.1.114.
[113] L.P. Parker, J.T. Powell, L.J. Kelsey, B. Lim, R. Ashleigh, M. Venermo, I. Koncar, P.E. Norman, B.J. Doyle, Morphology and Hemodynamics in Isolated Common Iliac Artery Aneurysms Impacts Proximal Aortic Remodeling, Arterioscler. Thromb. Vasc. Biol. 39 (2019) 1125–1136. https://doi.org/10.1161/ATVBAHA.119.312687.
[114] J.K.J. Li, Dominance of geometric over elastic factors in pulse transmission through arterial branching, Bull. Math. Biol. 48 (1986) 97–103. https://doi.org/10.1016/s0092-8240(86)90023-6.
[115] S. Roccabianca, C.A. Figueroa, G. Tellides, J.D. Humphrey, Quantification of regional differences in aortic stiffness in the aging human, J. Mech. Behav. Biomed. Mater. 29 (2014) 618–634. https://doi.org/10.1016/j.jmbbm.2013.01.026.
[116] S.K. Aytac, H. Yigit, T. Sancak, H. Ozcan, Correlation between the diameter of the

main renal artery and the presence of an accessory renal artery: Sonographic and angiographic evaluation, J. Ultrasound Med. 22 (2003) 433–439. https://doi.org/10.7863/jum.2003.22.5.433.

[117] P.M. O'Flynn, G. O'Sullivan, A.S. Pandit, Geometric variability of the abdominal aorta and its major peripheral branches, Ann. Biomed. Eng. 38 (2010) 824–840. https://doi.org/10.1007/s10439-010-9925-5.

[118] O.H. Yeoh, Some forms of the strain energy function for rubber, Rubber Chem. Technol. 66 (1993) 754–771. https://doi.org/10.5254/1.3538343.

[119] L. Horny, T. Adamek, E. Gultova, R. Zitny, J. Vesely, H. Chlup, S. Konvickova, Correlations between age, prestrain, diameter and atherosclerosis in the male abdominal aorta, J. Mech. Behav. Biomed. Mater. 4 (2011) 2128–2132. https://doi.org/10.1016/j.jmbbm.2011.07.011.

[120] M.W. Siebert, P.S. Fodor, Newtonian and Non-Newtonian Blood Flow over a Backward- Facing Step – A Case Study, Excerpt from Proc. COMSOL Conf. 2009 Bost. (2009) 5.

[121] S.E. Maier, M.B. Scheidegger, K. Liu, E. Schneider, A. Bellinger, P. Boesiger, Renal artery velocity mapping with MR imaging, J. Magn. Reson. Imaging. 5 (1995) 669–676. https://doi.org/10.1002/jmri.1880050609.

[122] H.C. Groen, L. Simons, Q.J.A. van den Bouwhuijsen, E.M.H. Bosboom, F.J.H. Gijsen, A.G. van der Giessen, F.N. van de Vosse, A. Hofman, A.F.W. van der Steen, J.C.M. Witteman, A. van der Lugt, J.J. Wentzel, MRI-based quantification of outflow boundary conditions for computational fluid dynamics of stenosed human carotid arteries, J. Biomech. 43 (2010) 2332–2338. https://doi.org/10.1016/j.jbiomech.2010.04.039.

[123] C.M. McEniery, Yasmin, I.R. Hall, A. Qasem, I.B. Wilkinson, J.R. Cockcroft, Normal vascular aging: Differential effects on wave reflection and aortic pulse wave velocity - The Anglo-Cardiff Collaborative Trial (ACCT), J. Am. Coll. Cardiol. 46 (2005) 1753–1760. https://doi.org/10.1016/j.jacc.2005.07.037.

[124] A.Vieli U.Moser S.Maier D.Meier P.Boesiger, Velocity profiles in the normal human abdominal aorta: A comparison between ultrasound and magnetic resonance data, Ultrasound Med. Biol. 15 (1989) 113–119.

[125] J.F. Vollmar, P. Pauschinger, E. Paes, E. Henze, A. Friesch, Aortic Aneurysms As Late Sequelae of Above-Knee Amputation, Lancet. 334 (1989) 834–835. https://doi.org/10.1016/S0140-6736(89)92999-1.

[126] A. V. Kamenskiy, I.I. Pipinos, Y.A. Dzenis, C.S. Lomneth, S.A.J. Kazmi, N.Y. Phillips, J.N. MacTaggart, Passive biaxial mechanical properties and in vivo axial pre-stretch of the diseased human femoropopliteal and tibial arteries, Acta Biomater. 10 (2014) 1301–1313. https://doi.org/10.1016/j.actbio.2013.12.027.

[127] J. Lantz, J. Renner, M. Karlsson, Wall shear stress in a subject specific human aorta - Influence of fluid-structure interaction, Int. J. Appl. Mech. 3 (2011) 759–778. https://doi.org/10.1142/S1758825111001226.

[128] K. Hirata, T. Yaginuma, M.F. O'Rourke, M. Kawakami, Age-related changes in

carotid artery flow and pressure pulses: Possible implications for cerebral microvascular disease, Stroke. 37 (2006) 2552–2556. https://doi.org/10.1161/01.STR.0000242289.20381.f4.

[129] D.W. Holdsworth, C.J.D. Norley, R. Frayne, D.A. Steinman, B.K. Rutt, Characterization of common carotid artery blood-flow waveforms in normal human subjects, Physiol. Meas. 20 (1999) 219–240. https://doi.org/10.1088/0967-3334/20/3/301.

[130] M.E. Safar, Arterial aging-hemodynamic changes and therapeutic options, Nat. Rev. Cardiol. 7 (2010) 442–449. https://doi.org/10.1038/nrcardio.2010.96.

[131] M.J. Mulvany, Small artery remodelling in hypertension: Causes, consequences and therapeutic implications, Med. Biol. Eng. Comput. 46 (2008) 461–467. https://doi.org/10.1007/s11517-008-0305-3.

[132] Y. Hoi, B.A. Wasserman, E.G. Lakatta, D.A. Steinman, Carotid bifurcation hemodynamics in older adults: Effect of measured versus assumed flow waveform, J. Biomech. Eng. 132 (2010) 1–6. https://doi.org/10.1115/1.4001265.

[133] M.D. Ford, N. Alperin, H.L. Sung, D.W. Holdsworth, D.A. Steinman, Characterization of volumetric flow rate waveforms in the normal internal carotid and vertebral arteries, Physiol. Meas. 26 (2005) 477–488. https://doi.org/10.1088/0967-3334/26/4/013.

[134] P. MARCIÁN, O. KONEČNÝ, L. BORÁK et al., On the Level of Computational Models in Biomechanics Depending on Gained Data from Ct/Mri and Micro- Ct, in: MENDEL 2011 - 17th Int. Conf. Soft Comput., Brno University of Technology, Brno, 2011: pp. 455–462.

[135] I.C. Campbell, J. Ries, S.S. Dhawan, A.A. Quyyumi, W.R. Taylor, J.N. Oshinski, Effect of inlet velocity profiles on patient-specific computational fluid dynamics simulations of the carotid bifurcation, J. Biomech. Eng. 134 (2012) 1–8. https://doi.org/10.1115/1.4006681.

[136] S.W. Lee, L. Antiga, J.D. Spence, D.A. Steinman, Geometry of the carotid bifurcation predicts its exposure to disturbed flow, Stroke. 39 (2008) 2341–2347. https://doi.org/10.1161/STROKEAHA.107.510644.

[137] F. Rikhtegar, J.A. Knight, U. Olgac, S.C. Saur, D. Poulikakos, W. Marshall, P.C. Cattin, H. Alkadhi, V. Kurtcuoglu, Choosing the optimal wall shear parameter for the prediction of plaque location-A patient-specific computational study in human left coronary arteries, Atherosclerosis. 221 (2012) 432–437. https://doi.org/10.1016/j.atherosclerosis.2012.01.018.

[138] C. Irace, C. Carallo, M.S. De Franceschi, F. Scicchitano, M. Milano, C. Tripolino, F. Scavelli, A. Gnasso, Human common carotid wall shear stress as a function of age and gender: A 12-year follow-up study, Age (Omaha). 34 (2012) 1553–1562. https://doi.org/10.1007/s11357-011-9318-1.

[139] X. Zhao, M. Zhao, S. Amin-Hanjani, X. Du, S. Ruland, F.T. Charbel, Wall Shear Stress in Major Cerebral Arteries as a Function of Age and Gender-A Study of 301 Healthy Volunteers, J. Neuroimaging. 25 (2015) 403–407.

https://doi.org/10.1111/jon.12133.

[140] I. Marshall, P. Papathanasopoulou, K. Wartolowska, Carotid flow rates and flow division at the bifurcation in healthy volunteers, Physiol. Meas. 25 (2004) 691–697. https://doi.org/10.1088/0967-3334/25/3/009.

[141] G. Gallo, M. Volpe, C. Savoia, Endothelial Dysfunction in Hypertension: Current Concepts and Clinical Implications, Front. Med. 8 (2022) 1–8. https://doi.org/10.3389/fmed.2021.798958.

[142] J. Malik, L. Novakova, A. Valerianova, E. Chytilova, V. Lejsek, K. Buryskova Salajova, L. Lambert, T. Grus, M. Porizka, P. Michalek, Wall Shear Stress Alteration: a Local Risk Factor of Atherosclerosis, Curr. Atheroscler. Rep. 24 (2022) 143–151. https://doi.org/10.1007/s11883-022-00993-0.

[143] T. Vicar, J. Chmelik, J. Navratil, R. Kolar, L. Chmelikova, V. Cmiel, J. Jagos, I. Provaznik, M. Masarik, J. Gumulec, Cancer cell viscoelasticity measurement by quantitative phase and flow stress induction, Biophys. J. 121 (2022) 1632–1642. https://doi.org/10.1016/j.bpj.2022.04.002.

[144] J. Kohut, J. Jagos, M. Formanek, J. Burša, In vitro structured tree model of the peripheral vascular network, in: Comput. Mech., Srní, 2021: pp. 118–121.

[145] J. Jagoš, J. Kohút, J. Kohút, M. Formánek, J. Burša, Roller pump controlled by neural network: experimental study under physiological conditions, in: P. Nithiarasu, C. Vergara (Eds.), 7th Int. Conf. Comput. Math. Biomed. Eng., Milano, 2022: pp. 389 – 392.

[146] M. Formánek, M. Appel, J. Jagoš, J. Kohút, M. Rajchl, Dynamic model of peristaltic pump with arterial tree for real-time pressure waveform control, in: 20th Int. Conf. Mechatronics, IEEE, Plzeň, 2022. https://doi.org/10.1109/ME54704.2022.9982882.